From spiking neurons to brain waves

Sid Visser

FROM SPIKING NEURONS TO BRAIN WAVES

SID VISSER

De promotiecommissie:

Voorzitter en secretaris:

Prof. dr. ir. A.J. Mouthaan	Universiteit Twente

Promotoren:

Prof. dr. S.A. van Gils	Universiteit Twente
Prof. dr. ir. M.J.A.M. van Putten	Universiteit Twente

Leden:

Prof. dr. S. Coombes	University of Nottingham
Prof. dr. O. Diekmann	Universiteit Utrecht
Prof. dr. ir. B.J. Geurts	Universiteit Twente
Prof. dr. C.C.A.M. Gielen	Radboud Universiteit Nijmegen
Prof. dr. Yu.A. Kuznetsov	Universiteit Twente
Prof. dr. F.H. Lopes da Silva	Universiteit van Amsterdam

NWO
Nederlandse Organisatie voor
Wetenschappelijk Onderzoek

UNIVERSITY OF TWENTE.

MIRA
BIOMEDICAL TECHNOLOGY
AND TECHNICAL MEDICINE

The research presented in this thesis was done in the group Applied Analysis and Mathematical Physics, Faculty Electrical Engineering Mathematics and Computer Science (EEMCS), University of Twente, The Netherlands.

Financial support from the Dutch Organization for Scientific Research (NWO), on grant 635.100.019, *From spiking neurons to brain waves*.

Printed by: Gildeprint Drukkerijen - www.gildeprint.nl

ISBN : 978-90-365-3508-3 DOI : 10.3990/1.9789036535083

FROM SPIKING NEURONS TO BRAIN WAVES

PROEFSCHRIFT

ter verkrijging van
de graad van doctor aan de Universiteit Twente,
op gezag van de rector magnificus,
prof. dr. H. Brinksma,
volgens besluit van het College voor Promoties
in het openbaar te verdedigen
op donderdag 28 maart 2013 om 14:45 uur

door

Sid Visser
geboren op 13 juli 1987
te Amsterdam

Dit proefschrift is goedgekeurd door de beide promotoren:

Prof. dr. S.A. van Gils en Prof. dr. ir. M.J.A.M. van Putten

To my parents

ταῦτα μὲν ἐς τοὺς οἰκηίους ὁ Καμβύσης ἐξεμάνη, εἴτε δὴ διὰ τὸν Ἄπιν εἴτε καὶ ἄλλως, οἷα πολλὰ ἔωθε ἀνθρώπους κακὰ καταλαμβάνειν: καὶ γὰρ τινὰ ἐκ γενεῆς νοῦσον μεγάλην λέγεται ἔχειν ὁ Καμβύσης, τὴν ἱρὴν ὀνομάζουσι τινές. οὔ νύν τοι ἀεικὲς οὐδὲν ἦν τοῦ σώματος νοῦσον μεγάλην νοσέοντος μηδὲ τὰς φρένας ὑγιαίνειν.

Herodotus, Histories, book 3:33.

Contents

Chapter 1
Introduction

"Isn't it remarkable," I occasionally think, "that the human brain is too complex to be fully captured by our own minds? Doesn't that explain why all of our current insights on its functioning are expressed as extensive simplifications? Is our language even capable of articulating the vast amount of neurons and their numerous interactions?" In this last question lies, I believe, the main motivation for conducting mathematical neuroscience: by identifying processes with symbols and equations, one becomes less dependent on their imagination to overcome difficulties — one can rely on mathematical identities instead.

As a second thought, it seems that neither the number of processes, nor the spatial and temporal scales on which these act, render the brain more complex than many other systems, but rather the number of scales at which a *single* process acts. A sole neuron, for instance, might connect to both a neighboring neuron, having a separation of only several micrometers, and to a distant neuron in the spinal cord, about one meter away. Contrast this, for example, to an atmospheric model: although the model extends over many more scales, from jet streams of thousands of kilometers down to properties of gases and fluids at a molecular level, the majority of processes interacts only with others at a similar scale[1].

Since no single model would be able to capture all scales of the brain simultaneously — from ions and proteins to the whole body and from microsceconds to a life's span — a collection of models is required instead: models which represent a caricature of a certain process or phenomenom. Here, the concept of 'model' should be interpreted in its widest sense, since the model hierarchy should, next to mathematical models, also include animal, *in vivo* and *in vitro* models. By developing such a framework of models, one would ideally be able to select, depending on the interest one has, a subset of relevant processes and combine the corresponding models to study the phenomenon at hand.

The multiscale nature of the system, however, is likely to interfere with the merging of models. A prevalent method for incorporating processes occuring at smaller or faster

[1] In this respect, it becomes apparent why the phenomenon of lightning is still poorly understood: its scales range from quantum effects of plasma formation to the kilometers of height.

scales in a model is called *averaging*, or *lumping*: only the global properties of a large number of underlying processes are considered, rather than all the individual processes. It appears that numerous processes in the brain are particularly suitable for lumping, like the thermodynamic limits which are widely used to describe the voltage-gated ion channels on the cell membrane, but many others, especially those involving multiple scales, are not. Unfortunately, not only is lumping impracticable at every scale, also data acquisition and imaging techniques are hampered by the multiscale nature of the system. The lack of data with respect to a specific scale inhibits the validation of the lumping at that scale, resulting in a 'gap' in the multiscale framework, i.e. a scale for which neither appropriate models nor data are available that adequately characterize the phenomena at that level. In order to narrow this 'gap,' new techniques have to be developed that exploit principal properties of the multiscale system.

Over the past decades, the lumping of neural networks, which would provide a basic understanding on the influence of key features of individual neurons on the rhythms they collectively produce, has proven to be a persistent challenge. In order to improve our basic understanding of the generation of both physiological and pathological brain rhythms, it is valuable to gain a better insight into these procedures.

In this thesis, I present an overview of the current efforts for obtaining such a reduction, that is *from spiking neurons to brain waves*, primarily in relation to epileptic seizures. In particular, I show how lumped models can be constructed qualitatively from the analysis of highly complex network models, how existing procedures can be extended to incorporate additional features of the underlying neurons, and how new results in dynamical systems' theory are necessary to analyze particular models in full detail.

Models, networks, and noise

Networks of spiking neurons can be created which may incorporate many of the known physiological aspects. These models accurately describe the interactions of a large collection of individual neurons connected with chemical or electrical synapses, henceforth they are referred to as *detailed models*.

A natural questions arising for these models is how the neurons in the network synchronize (at least partially) such that they exhibit the physiological rhythms that are observed in both experimental and clinical settings. What are the dominant mechanisms in the system responsible for the emergent behavior?

Given the fact that detailed models appear to be a natural approach to modeling tissue, one should be wary for the conclusions drawn from them. First of all, models of this type, since they capture a large part of the physiology, tend to rapidly grow in complexity as the size of the network increases. Combined with the (typically) non-linear dynamics of the individual neurons and the pulse-coupled nature of the connections, conventional types of

analysis, such as dynamical systems' theory, are often unsuitable to answer the previously posed questions. Another impediment of detailed models is the fact that the many parameters of the system, particularly those relating to the connectivity, are only limitedly available from experiments. Although one can make an educated guess for these parameters, the results of the model might be critically dependent on these values. Theoretically, this could be resolved by a sensitivity analysis, but the number of parameters is often too large and this type of analysis might not be feasible if evaluation of the model already demands supercomputing, such as [114, 110, 86, 69]. Finally, because detailed models are predominantly studied using simulations only, one can, in general, neither ascertain whether the model has converged to its limiting attractor, nor exclude the presence of other attractors. This impedes the possibility to draw conclusions at a global, or system-wide, scale.

Though it might seem that, given this summation of pitfalls, detailed modeling is not particularly valuable for obtaining insights in the behavior of a spiking neuron network, the contrary is true: rather than drawing far-reaching conclusions from these models, they should be considered as an experimental setting instead, leading to *in silico* experiments. Careful analysis of the large data sets, which often result from these simulations, could assist in the identification of novel mechanisms underlying a particular feature. Ideally, one would isolate and characterize this feature such that it assists in the formulation of new hypotheses. This, in its turn, would stimulate the development of new models and experiments to validate these premises.

A comment by Von Neumann, on the processing of information in networks, is the following "*[...] without randomness, situations may arise where errors tend to be amplified instead of canceled out*" [126]. At a time when data from the nervous system were only scarcely available, he already reasoned that the local redundancy of networks, due to a disorderly organization, is required for a reliable functioning of the (brain) network. Although the randomness might be necessary to ensure a reliable execution of a specific task, performing a similar task will likely involve the same general mechanism. Following this train of thought, one might conclude that, for capturing these basic features of the system, a precise computation of all neurons in the network, i.e. the detailed modeling approach, is not a necessity.

By making extensive assumptions on the neurons and their connections in the network, the randomness can be averaged such that a smoothed, or lumped, model remains, which describes the net behavior. Depending on the assumptions one makes, different reductions can be made, but each typically revolves around the following quantities: mean membrane potential [53, 80], average firing rate [97, 99], or fraction of active neurons [132, 133] in the population. At a closer look, the majority of the lumping procdedures takes into account two types of averaging. First, temporal averaging is used to smooth the spiketrain, a series of discrete-time events, replacing it either with a firing rate, i.e. the rate at which action potentials are generated, or with an effective synaptic current produced by the neuron.

Secondly, the network connectivity is simplified, which occasionally takes into account a spatial structure of some sort. Common assumptions made on the connectivity include all-to-all and completely random.

Despite the fact that the compact formulation of lumped models qualifies them for a thorough mathematical analysis, the results obtained from these models should be interpreted with care. Indeed, the averaging procedures, on which the reductions are based, require many assumptions about the neurons and their connections, which might not all be supported by physiology. Since not every parameter of the spiking neuron network has a representative in the reduced model, or, vice versa, the lumping introduces new parameters which often have no physiological meaning, it is, therefore, not trivial to translate results obtained from lumped models back to biophysical properties of the neural network.

In addition, it is relevant to mention that understanding a single diseased state of the brain does not only assist in unraveling the pathology at hand, it also provides principal insights into the functioning of a healthy brain. Due to the multiscale nature of the system, a complete comprehension of any disorder will essentially involve the majority of temporal and spatial scales in the brain, rendering it almost as complex as the brain itself.

In this light, I believe that epileptic seizures provide a favorable testing ground for studying both the effectiveness of lumping procedure and the conditions which might be required. For that reason, I give an overview of the pathology related to epilepsy, together with a motivation for modeling particular aspects of the malady.

Epilepsy, seizures, and synchrony

Epilepsy is a neurological disorder, characterized by an increased risk of recurring seizures, which affects nearly 1% of world population. Seizures typically last for several seconds up to a few minutes, although they can persist for days in exceptional cases. During ictal events neural activity hypersynchronizes, thereby inducing an abnormally large electric field, which can be distinguished from regular activity by a variety of imaging techniques, such as electroencephalography (EEG), electrocorticography (ECoG), and magnetoencephalography (MEG). A typical example of a seizure is depicted in Figure 1.1.

Considering seizures merely a symptom of epilepsy, the presence of this symptom can be determined more or less objectively from these data, especially compared with other disorders, whose symptoms are often dependent on behavioral examinations or psychological assessments. Although the seizures are objectively identifiable, reliable diagnosis of epilepsy is often severely impeded by the low incidence of seizures, or other electrophysiological markers related to the disease, such as interictal discharges. Indeed, due to the episodic nature of the disease, it is considered a *dynamic disease* [90, 91].

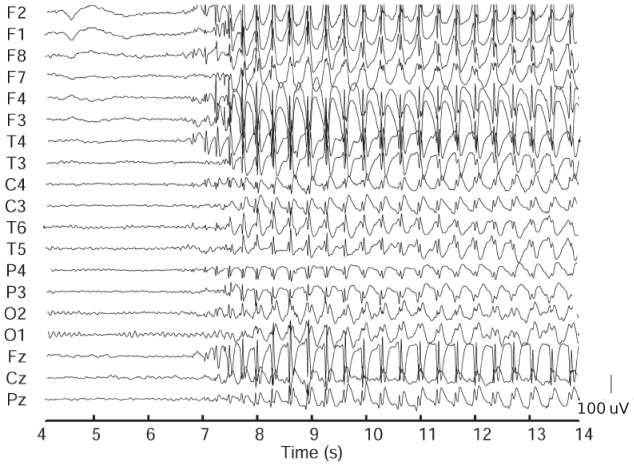

Fig. 1.1 EEG of a generalized seizure which is typical for absence epilepsy. At $t = 7s$, there is a sudden transition to abnormal bilateral synchronization, showing characteristic 3Hz spike-wave complexes. Courtesy of Medisch Spectrum Twente.

Bearing in mind that the causes for epilepsy are numerous, ranging from conditions as cortical deformations, traumatic brain injury and stroke, to subtle traits, like channel mutations and genetic factors, suggests that epilepsy is a multiscale disease [43]. Often, it is an interplay of many circumstances that results in *epileptogenesis*, i.e. the acquisition of epilepsy, which has lead to the metaphor of a 'river of epilepsy' [78, 84]: small changes 'upstream' can result in devastating effects 'downstream.' As a matter of fact, the majority of the factors involved in the disorder are likely to vary slowly over time and it is therefore important to stress the fact that a seizure model, e.g. a neural network that generates seizures, is not the same as a model for epilepsy. The latter would particularly focus on characterizing the evolution of the disease in terms of the slow factors, like pharmacoresistance and aging effects. Keeping in mind that the focus of this thesis is primarily on the characterization of collective behavior in neural networks, I will particularly concentrate on the generation of epileptiform activity within networks.

It is common practice to classify seizures by their clinical and behavioral manifestations, leading to about 40 different types of epilepsy recognized by the International League against Epilepsy (ILAE) [3, 44]. An intelligible distinction is made between partial seizures, which prevail only in a part of the brain, and generalized seizures, in which the whole brain is involved. Abnormal activity during a partial seizure has in some cases a negative effect on connected brain areas, causing the seizure to expand in size by spreading to these areas; eventually this can lead to a generalized seizure.

The prevalent cause for seizure generation is thought to be hyperexcitability of the network, either caused by an excess of excitatory drive or due to lacking inhibitory control.

Consequently, most anti-epileptic drugs (AED) focus on amending this imbalance by reducing excitation or enhancing inhibition. It should therefore be no surprise that these drugs may have a significant impact on both brain and body, such that side effects like drowsiness, dizziness, and nausea are inevitable [55, 131]. Furthermore, it is not uncommon for patients to have their seizures unadequately controlled by such medication. Indeed, despite the introduction of many novel drugs, the fraction of patients whose condition is not properly controlled with AEDs has remained near 30% for several decades already [77].

It does not seem surprising that especially patients suffering from partial seizures are less responsive to drugs. After all the medication can only be administered to the full brain [35]. Lack of the ability to target the epileptic focus with AED has led to a seemingly crude intervention: during so-called epilepsy resective surgery, the alleged epileptogenic zone is surgically removed from the brain. Despite the fact that this type of surgery is quite successful, it is only performed limited since the procedure is neither free of risk and nor does every patient have a discernible focus [106].

Interest in focal partial seizures is twofold. Not only due to the fact that epileptic foci are relatively small networks, making them more accesible for modeling than the whole brain, also the availability of data is convincing: resective surgery for focal seizures often follows after a long-term electrocorticogram which assists pinpointing the focus. Recordings obtained from these invasively placed electrodes capture the neural activity at a much higher spatial scale than a scalp EEG would and, furthermore, without interference of the skull. These data are, since they constitute the mean electric potential of the underlying cortical area, very well suited to be related to lumped models of the corresponding network.

For that reason, several detailed models have been put forward that study the epileptiform activity and spike-wave discharges in focal seizures. For instance, a model of neocortex, which incorporates the layered anatomical organization, has been used to devise a counterintuitive hypothesis that weak excitatory synapses could result in epileptiform activity [115, 112]. Consequently, supportive evidence for this hypothesis has been obtained from *in vitro* mouse experiments [113]. Another model suggests that especially the electrical synapses, i.e. gap junctions, between axons are important for the generation of high frequency oscillations (HFO) in conjunction with interictal discharges [42, 111, 93]. Development of epileptiform activity after (partial) isolation of cortical networks, as might result from stroke or traumatic brain injury, is characterized in [109, 62, 8, 108] using *in vivo*, *in vitro* and *in silico* models. Epileptogenesis, following upon slight network damage in hippocampal networks, is modeled in [92] as caused by mossy fiber sprouting. This might be a prevalent mechanism for mesial temporal lobe epilepsy.

Since even an epileptic brain functions almost flawlessly for 99% of the time, detailed models would have to be simulated for prolonged durations to exclude the possibility of generating epileptiform activity. Detailed models, for that reason, are also affected by the

low incidence of insults, just as the diagnosis in patients. Hence, the above described studies often force the model into a regime where seizures are more likely to be observed. In that respect, these *in silico* experiments are much like *in vitro* and *in vivo* experiments, where conditions are often enhanced in favor of the pathology — for instance with pharmacological interventions or electrical stimulation.

Due to their concise formulation, lumped models of neural networks often allow, by using results from dynamical systems' theory, a more global analysis of the dynamics, such that qualitative changes in the behavior can be characterized. This, combined with the fact that the majority of the neurons behaves very similarly during epileptic insults, suggests that lumped models are very suitable for modeling seizures. Indeed, long-standing work by Lopes da Silva focuses on lumped models of the thalamocortical loops [82, 81]. Driven by a noisy input, these models for absence epilepsy can switch from one attractor, corresponding with regular background activity, to another, which is characterized by a spike-wave complex. A comparable model, c.f. [99, 98], is subjected to a thorough bifurcation analysis to identify the mechanisms underlying transitions of spike-waves to poly-spike complex [100]. Furthermore, it has been shown that use of particular anesthetics could, in some cases, also result in epileptiform activity [79].

The fact that some of these models are able to mimic clinical data accurately is, at least in my opinion, rather surprising. It appears particularly ambiguous how these models capture, for instance, the properties of thalamocortical loop with the neocortex represented by only two populations — one containing excitatory neurons, the other inhibitory — while signals in the actual system pass through several layers of neocortex before projecting back to thalamus. Furthermore, by condensing the entire structure, many of the intrinsic properties are lost, too. It is, for instance, unclear what the spatial arrangement of the synchrony looks like, or how bilateral synchronous activity, as is common in generalized seizures, can persist in the presence of delays. The latter effect, though, is often neglected since the transmission delay of action potentials propagating through the myelinated axons in the corpus callosum is commonly thought to be several milliseconds only. Small diameters of the axons, however, might significantly increase the delays of particular fibers. Indeed, it is suggested that 40–60% of the fibers in corpus callosum may introduce 100–200ms conduction delay between the hemispheres [89, 91]. Naturally, these late pulses will have some effect on the synchrony in the network.

The role of delays in brain networks appears to be underestimated. Indeed, analysis of dynamical systems which incorporate time delays becomes more complicated, particularly due to the fact that these system are infinite-dimensional. However, since delays seem to have an impact on both synchrony and temporal pattern formation in the network, they will play an important role in the work described in this thesis.

Space, time, and delays

In the next chapter I discuss **a qualitative reduction of a detailed model**. Here, studying simulation results of the detailed model of neocortex, originally proposed by Van Drongelen and coworkers [115, 113, 112], reveals that pyramidal neurons in layers II/III and V/VI have comparable firing patterns. Further analysis shows that the alternating activation of either population is primarily caused by the delays due to both action potential propagation and synaptic activation. Essential features of this phenomenon are shown to be well-captured by a two-node Hopfield network, with delayed, reciprocal connections. The inhibitory processes in the network are mainly of a local nature, such that these can be condensed into the excitatory nodes as an intrinsic property. Both simulations and numerical bifurcation analysis in one parameter bring to light that the reduced model mimics the qualitative behavioral transitions seen in the detailed model, albeit in a fairly simplistic manner.

Thereafter, I focus **on stability and bifurcations in a lumped model of neocortex**, where the previously proposed model is subjected to a thorough mathematical analysis. Local dynamics near equilibria are determined by studying the characteristic equation and bifurcations resulting in non-local behavior — such as limit cycles — are first classified analytically and numerically investigated afterwards. The chapter concludes with the observation that the two-parameter bifurcation diagram of the lumped model shares essential features with a brute-force exploration of the parameter space of the corresponding detailed model [113].

Seeing that this reduction illustrates the fact that delays due to the *laminar* organization are key for the generation of temporal patterns, it is natural to question how delays due to the *columnar* organization affect pattern formation. Therefore, I concentrate **on neural fields with transmission delay** next. Indeed, the laminar structure introduces only a limited number of delays in the lumped model, corresponding with the intra– and interlayer connections, while the columnar arrangement gives rise to a distance-dependent form in the delay. The spatiotemporal dynamics in such models have received considerable attention [80, 67, 65, 102, 123, 66, 64, 32, 30, 29], but analysis is often hampered by the lack of a proper mathematical setting. In this chapter it is shown that neural field models with transmission delay may be cast as abstract delay differential equations. Theory of dual semigroups (also called sun-star calculus) provides a natural framework for the analysis of such models, such that stability of equilibria and normal forms of bifurcations can be determined. Consequently, spatiotemporal patterns anticipated by theory correspond with numerical approximations of the system.

The availability of such a functional analytic setting for the analysis of neural fields encourages the development of more advanced neural fields. Indeed, the majority of the lumping procedures considers the neurons in the network as (leaky) integrators, such that

a clear relation exists between the current arriving at the soma and the corresponding firing rate. Although some models incorporate an additional state variable, which results in spike frequency adaptation (SFA), more advanced spiking behaviors, like bursting and rebound spikes/bursts, are still considered unsuitable for lumping. Since these types of spiking are, in certain phenomena, considered to be relevant for the synchrony, the last chapter studies **spatially extended neurons as extension to neural fields**. In other words, an extension to the general framework is proposed which facilitates the inclusion of more complex spiking patterns. Effectively simplifying the fast spiking dynamics of a single neuron yields a firing rate model which is easily extended across space. Results are consistent with traditional reductions based on integrate-and-fire neurons, both with and without spike frequency adaptation, but the main outcome is the formulation of a neural field based on Izhikevich neurons [68]. Although a clear correspondence is shown between the original spiking neuron network and the neural field, the reduction still needs refinements, both on the level of modeling as well as the mathematical analysis.

In spite of the fact that the role of epileptic seizures appears diminished in some of the chapters, the focus will nonetheless be on emergent behavior of networks and dynamical transitions between different states. Hence, a clear application of these results with respect to epilepsy is within reach.

Chapter 2
A qualitative reduction of a detailed model

Abstract Two models of the neocortex are developed to study normal and pathological neuronal activity. One model contains a detailed description of a neocortical microcolumn represented by 656 neurons, including superficial and deep pyramidal cells, four types of inhibitory neurons and realistic synaptic contacts. Simulations show that neurons of a given type exhibit similar behavior in this detailed model. This observation is captured by a population model which describes the activity of large neuronal populations with two differential equations with two delays. Both models appear to have similar sensitivity to variations of total network excitation. Analysis of the population model reveals the presence of multistability, which was also observed in various simulations of the detailed model[1].

2.1 Introduction

Epilepsy is a neurological disease, characterized by an increased risk of recurring seizures, that affects nearly 1% of the world population. This disease can be controlled pharmacologically in about 75% of the cases, although a multidrug regimen, with all the side effects resulting from drug-drug interactions, is often required to adequately control these patients. The remaining 25% of patients has a intractable epilepsy which cannot be controlled adequately with drug treatment [87]. Despite the introduction of many novel drugs throughout the last decades the prevalence of intractable epilepsy has not decreased. One possible explanation for this observation is that the existing anti-epileptic drugs (AED) target only a few specific mechanisms of epileptogenesis, whereas other etymologies, yet unidentified, may require different treatment.

[1] Adapted from S Visser, HGE Meijer, HC Lee, W van Drongelen, MJAM van Putten and SA van Gils, *Comparing epileptiform behavior of mesoscale detailed models and population models of neocortex*, Journal of Clinical Neurophysiology **27** (2010), no. 6.

As most patients with epilepsy remain seizure free most of the time, it can be time consuming to collect enough pathological data for analysis. This is partially due to the limitations in spatial and temporal resolution of recording equipment. For instance, scalp EEG mainly displays collective phenomena of cortical dynamics with a very limited sensitivity for subcortical circuits that are presumably relevant in certain types of epilepsies (e.g. absence epilepsy).

Modeling may improve our understanding of epileptogenesis and provide clues for novel treatments. Such models exist at many levels of abstraction, ranging from describing the brain as a black box with a certain input/output relation to a detailed description of the individual neurons in the brain. In order to reveal new mechanisms behind seizures any useful model should have a sufficient connection with physiology to relate observed (neurological) behavior to the pathological condition of the patient.

A straightforward approach to model neuronal activity in the brain is to model individual neurons in the brain and their mutual interactions. We refer to models of this type as detailed models. As individual cells and connections can be modeled with various levels of complexity, different types of detailed models exist. Several detailed model have been proposed of the complete brain [86, 69], but these do not focus on pathological behavior. Detailed models of the brain primarily intended to study epileptiform activity have been developed as well, but these consider only a limited number of neurons [115, 113, 112, 110]. This limitation, however, does not preclude the possibility of formulating important, testable hypotheses. For instance, predictions regarding epileptiform activity have been made with a detailed model that were subsequently confirmed *in vitro* [113].

Because these detailed models are substantial in both size and complexity, analyzing their behavior is a hazardous task. For that reason we are interested in studying a more abstract class of models which gives a more concise description of neuronal activity than detailed models, so-called population models. Rather than describing properties of individual neurons, these models describe the dynamics of population-averaged quantities, such as the mean membrane potential of all neurons in the populations, the mean firing rate or the fraction of active neurons within the population.

Most population models are based on the original work done by Wilson and Cowan [132] who derived a model for two generic interconnected populations; one population containing only excitatory and the other only inhibitory neurons. Potential mechanisms for transitions between normal and epileptic activity have been studied with population models in absence epilepsy [81, 13, 100] and mesial temporal lobe epilepsy [130].

A fundamental problem of population models, however, is that they are based on averaging procedures that cannot be justified rigorously. For that reason it is difficult to relate parameters of population models to physiological properties of the neurons within the pop-

ulations. One should therefore be cautious during analysis of the model and continuously investigate the physiological relevance of the parameters considered.

We do not favor one modeling approach over the other, since we believe that both types of models should be analyzed simultaneously in order to study new mechanisms for seizure onsets. In our opinion, hypotheses should be formulated through bifurcation analysis of simpler population models and then subsequently tested in a detailed model. This step, which to our knowledge is rarely performed, is crucial because it gives the lumped parameters of the population model a relevance and clinical significance by mapping them onto a set of physiological parameters in a detailed model. Similarity between both models should ideally be determined by quantitative measures.

We present two models of the neocortex, one detailed model and the other based on the population approach. We consider changes of parameters and show that both models have similar sensitivity to these parameters.

2.2 Methods

Areas of the neocortex make numerous connections with each other and with deeper subcortical brain regions such as the thalamus. These regions of neocortex are organized into a collection of macrocolumns that each perform an elementary task [23]. These macrocolumns can then be split into mesocolumns, that are in turn split into microcolumns within which the activity of neurons is strongly correlated. Such a microcolumn contains roughly 1,000 neurons and covers an area of about 10,000 μm^2 of the neocortex. The local structure of a microcolumn consists of several layers that are tightly connected with each other. Since these local connections are better characterized than long-range connections to either the thalamus or other neocortical columns, we only focus on modeling a small area of the neocortex without long-range interactions.

Two modelling approaches are used; the first being a detailed neuron model analyzed at a meso-scale of 656 neurons and the other a simpler two-population model.

2.2.1 Detailed model

2.2.1.1 Description

A small patch of the neocortex is modeled by connecting detailed models of individual neurons with artificial synapses, similar to [115, 113, 112]. We summarize this model and its underlying assumptions below, together with an overview of the modifications made.

The model describes the activity of pyramidal neurons in layers 2/3 and 5 of the neocortex, referred to as superficial cells and deep cells respectively, and four types of inhibitory interneurons: three types of basket cells (each of a different size) and chandelier cells. All neurons are discretized into several compartments that describe the physiological structure of a cell with a soma and a dendritic tree. The interneurons consist, due to their limited size, of two compartments, whereas the superficial and deep pyramidal cells are described by 5 and 7 compartments respectively. Cells are placed randomly in a three dimensional space, complying with the following depth ranges for each cell type. The depth of the superficial pyramidal cells varies between 250µm and 750µm whereas the deep pyramidal cells' depths vary between 1000µm and 1500µm and the depth of the interneurons is between 250µm and 1500µm. The minimal separation between two cells is 2µm.

Voltage-gated sodium and potassium channels are taken from [12] and maximal conductances for ion channels are copied from [112]. Superficial pyramidal cells contain persistent sodium channels which cause the cells to burst intrinsically.

Action potentials are assumed to have a constant conduction velocity of 0.08m/s through axons, inducing a time lag for synaptic transmission proportional to the distance between cells. After arrival of an action potential an exponentially decaying postsynaptic current is generated that has two time constants [12, chap. 6].

Connections of neurons are randomly determined in a way such that the connection probability depends on the cell types (both sending and receiving neurons) as well as the distance between the cells. Both types of pyramidal neurons can connect to all neurons within a certain range. Basket cells will only inhibit pyramidal cells and other basket cells. Chandelier cells make inhibitory connections to somas of pyramidal cells exclusively, close to the location where the axon sprouts from the soma. The model contains neither gap junctions nor long-range connections to other columns.

2.2.1.2 Meso-scale implementation

A realization of this model with 656 neurons (2x 256 pyramidal cells and 4x 36 interneurons) is implemented in C++, making it a meso-scale simulation. We randomly generate one network, consisting of 43124 connections, and we only consider simulations with this specific network topology.

Next, an interface is developed that converts the neuronal activity of the network to a local field potential (LFP), representing a small electrode placed on or nearby the network, e.g. an electrocorticogram (ECoG) electrode. The algorithm is based on the method of "sinks and sources" as described in [95], except that only the superficial pyramidal neurons are considered rather than all neurons, because these large cells are closest to the electrode. Therefore they will have the largest contribution to the EEG compared to the

smaller interneurons and the deep cells that lie farther away. The obtained signal is unfiltered and should be interpreted as a DC recording.

2.2.2 Population model

2.2.2.1 Description

The activity of a neuron in a microcolumn is strongly correlated with the activity of nearby neurons due to tight connectivity and synchronization. It is therefore a natural step to consider the average activity of a large group of neurons rather than the behavior of individual neurons.

Here, a microcolumn of the neocortex is modeled using two populations, representing the average activity of the superficial and the deep pyramidal cells, respectively. First, it is assumed that neither of the populations can exhibit self-sustained activity in the absence of activity of the other population, hence the activity of the populations is modeled to decay exponentially over time. Next, when the activity of a layer increases, more action potentials are sent to neurons in the other layer where excitatory synapses are activated after some time lag. This increases the activity in that layer. Rather than modeling a population of inhibitory interneurons, we model the inhibition caused by pyramidal cells that excite interneurons that, in turn inhibit the pyramidal cells (see also figure 2.1).

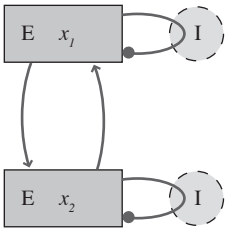

Fig. 2.1 Schematic overview of the population model: two connected excitatory (E) populations are considered as well as the feedback of the inhibitory (I) populations that is modeled as an intrinsic property.

The above described model leads to the following set of delayed differential equations (DDEs):

$$\begin{aligned} \frac{dx_1}{dt} &= -\mu_1 x_1(t) - \mathscr{F}_1(x_1(t-\tau_i)) + \mathscr{G}_1(x_2(t-\tau_e)), \\ \frac{dx_2}{dt} &= -\mu_2 x_2(t) - \mathscr{F}_2(x_2(t-\tau_i)) + \mathscr{G}_2(x_1(t-\tau_e)), \end{aligned} \tag{2.1}$$

with x_1 and x_2 the activity of the neuronal populations of superficial and deep pyramidal cells respectively. The constants μ_1 and μ_2 represent the intrinsic rate of exponential decay of neuronal activity within a population. The functions $\mathscr{F}_i(x)$ and $\mathscr{G}_i(x)$ are both sigmoidal functions that determine the activation of the inhibitory and excitatory synapses respectively. The delay τ_e is the time needed for action potentials to travel from one layer to another, whereas τ_i is the time lag for the inhibitory feedback loop. Both delays include the extra time lag caused by activation of the synapses.

The two-population network given in equation (2.1) is an example of a graded Hopfield network with delays. Several of these networks have been analyzed in [9, 103], but their analysis focused mainly on studying steady states rather than (periodic) oscillations.

To simplify the model and decrease the number of parameters, we analyze the symmetric system:

$$\mu_1 = \mu_2 := \mu, \qquad \mathscr{F}_1(x) = \mathscr{F}_2(x) := \mathscr{F}(x), \qquad \mathscr{G}_1(x) = \mathscr{G}_2(x) := \mathscr{G}(x). \tag{2.2}$$

The following expressions are chosen for the synaptic activation functions:

$$\begin{aligned} \mathscr{F}(x) &= \alpha_i \left(\tanh(\sigma_i x - 1) + \tanh(1)\right) \cosh^2(1), \\ \mathscr{G}(x) &= \alpha_e \left(\tanh(\sigma_e x - 1) + \tanh(1)\right) \cosh^2(1), \end{aligned} \tag{2.3}$$

with α_i and α_e the strengths of the inhibitory and excitatory connections and σ_i and σ_e the rates at which their synapses saturate. For negative values of x both $\mathscr{F}(x)$ and $\mathscr{G}(x)$ are negative; representing a suppression of the synaptic background activity.

We choose the following values for the parameters: $\mu = 3$, $\tau_i = 4$, $\tau_e = 7$, $\alpha_i = 0.2$, $\alpha_e = 1.5$, $\sigma_i = 2$ and $\sigma_e = 1.2$. The delays are chosen similar to the delays in the detailed model. Because the number of excitatory synapses in the detailed model outnumbers the inhibitory, α_e is chosen larger than α_i. For the same reason, we choose $\sigma_i > \sigma_e$ because the inhibitory synapses will saturate faster due to their low number.

2.2.3 Simulating epilepsy

2.2.3.1 Decreased excitation

As shown in [113], the neocortex can exhibit epileptiform activity when excitatory synapses in the network are weakened. Because this opposes most expectations, we try to reproduce the results of this experiment with both models. In the detailed meso-scale model, the global levels of excitation can be modified by adding or removing excitatory synapses.

Modifying the levels of excitation in the population model can be achieved in several ways. The parameter α_e represents the excitation between layers and is therefore a proper

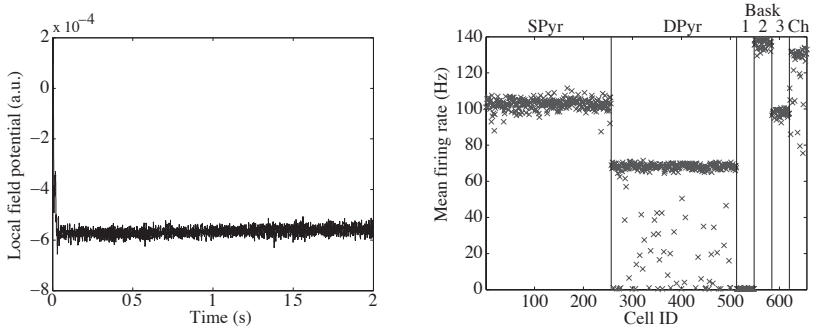

Fig. 2.2 Simulation of meso-scale detailed model for **high excitation**. The LFP in the left panel shows desynchronized activity. The right panel depicts mean firing rate of individual neurons (see text).

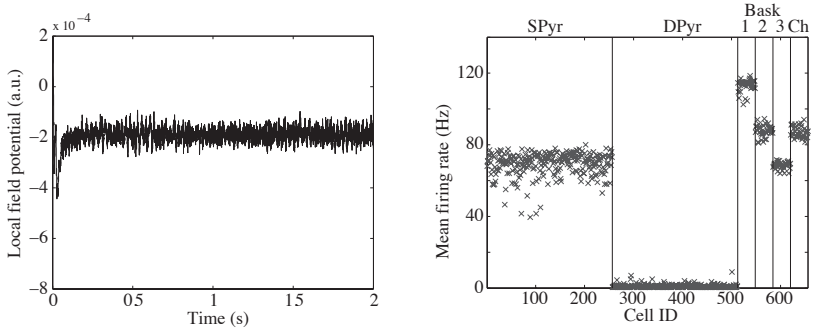

Fig. 2.3 Simulation of meso-scale detailed model for **moderate excitation**. The LFP shows irregular bursting, especially at 0.5s.

candidate parameter. On the other hand, the parameter μ determines the rate at which the activity within a layer decreases. If the network contains more excitatory synapses, more connections are made within the population and the activity will therefore decrease at a lower rate. We have chosen to vary the parameter μ to modify the levels of excitation because we assume that more intralayer connections exist than interlayer connections.

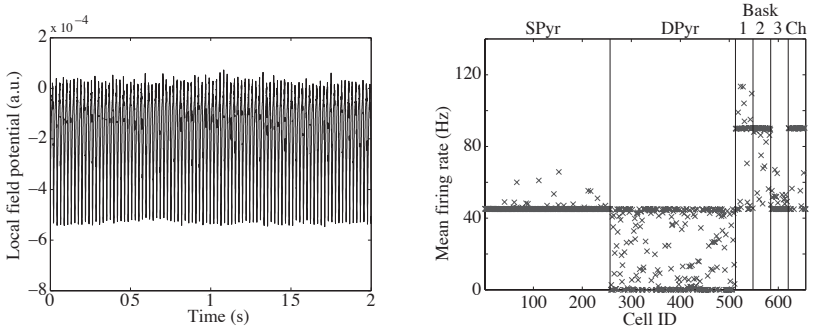

Fig. 2.4 Simulation of meso-scale detailed model for **low excitation**. The LFP shows oscillatory activity.

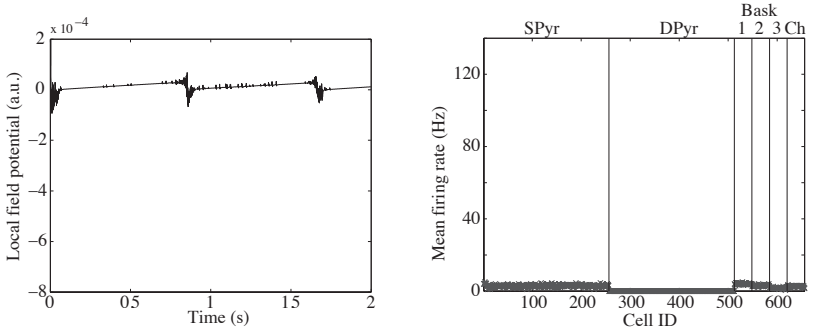

Fig. 2.5 Simulation of meso-scale detailed model for **very low excitation**. The LFP shows regular bursting.

2.3 Results

2.3.1 Meso-scale detailed model

2.3.1.1 Validation

The meso-scale detailed model is evaluated for different levels of excitation, beginning at a high value of excitation and then decreasing excitation below the normal level.

For high levels of excitation the network exhibits saturated, desynchronized activity in which all neurons fire action potentials at a high frequency with a very low correlation (figure 2.2). When the network excitation is set to normal physiological values, the microcolumn's behavior shows irregular bursts (figure 2.3). For low values of excitation, we observe fast oscillations in the EEG of 50Hz (figure 2.4). A closer analysis of these oscillations reveals that the populations of superficial and deep pyramidal cells are alternately

active. After reducing the excitation to exceptionally low levels, one fifth of the normal level, the oscillations cease and the network reaches a state of burst-suppression behavior. These network bursts are initiated by the intrinsically bursting superficial pyramidal neurons, which synchronize easily but fail to initiate activity in other layers due to the low level of excitation. Hence the network remains silent apart from these short bursts of activity.

Oscillating and regular bursting behavior, typical epileptiform activity, are only observed in networks with weak excitatory synapses. Contrarily, desynchronized activity and irregular bursting on the other hand, are exclusively seen in simulations with high levels of excitation. These results are in correspondence with the findings of [113].

2.3.1.2 Activity of populations

Next we study the activity of individual neurons during simulations of the different types of network behavior. For each neuron in the network the mean firing rate of action potentials is determined by dividing of the total number of action potentials of a neuron by the total simulation time. The results are shown in the right panels of the figures 2.2 to 2.5, in which the mean firing rate is depicted for all neurons. The first group of 256 neurons represents the activity of the superficial pyramidal neurons, whereas the second group depicts the activity of the deep cells. The four other groups contain interneurons of different types: the first three columns contain basket cells of increasing size and the latter column holds the chandelier cells.

As a first observation we note that the variation of the mean firing rate of individual neurons is small for neurons within a population. For example, note the result for low excitation (figure 2.4) in which the firing rate of many neurons is identical to that of others. Furthermore, both the type 2 basket cells and the chandelier cells have similar firing rates as well as the superficial pyramidal cells and type 3 basket cells.

Generally we observe that the activity of most neurons decreases gradually as the levels of excitation are reduced, except for the deep pyramidal cells whose activity drops suddenly for normal levels of excitation and recovers again for lower levels. As the levels of excitation are high, the small basket cells (type 1) experience an excitation block, indicating that the excitatory synapses remain continuously activated due to the absence of a rhythm. Hence, the neuronal activity is desynchronized.

By counting the number of action potentials $n_{AP,i,j}$ of population i in time bin j, we define the instant firing rate $f_{i,j}$ of neurons within population i as follows:

$$f_{i,j} = \frac{n_{AP,i,j}}{N_i T_j}, \tag{2.4}$$

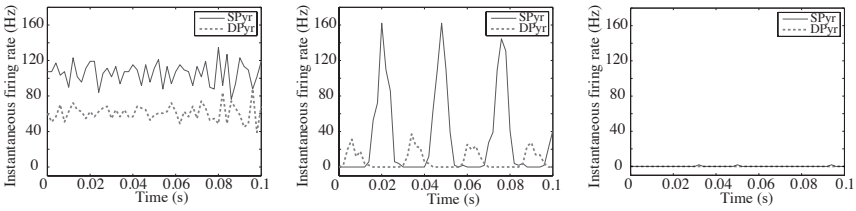

Fig. 2.6 Instant firing rate of both excitatory populations is plotted during simulations with (left) high, (center) low and (right) very low excitation. Note the desynchronized activity in the left and the alternating activity in the center panel.

with N_i the number of neurons in population i and T_j the size of time bin j. Figure 2.6 shows the instantaneous firing rate of the pyramidal neurons for several levels of excitation in the network. The desynchronized activity is now clearly visible as is the alternating activity during the oscillations.

2.3.2 Population model

These results, indicating that neurons of a given type in the detailed model have very similar behavior in the detailed model, encourage us to study a population model that describes the activity of these clusters rather than the individual neurons.

2.3.2.1 Analysis of bifurcations

To understand the dynamics available to the population model, we perform a bifurcation analysis. Figure 2.7 shows a caricature of the bifurcation diagram of the population model for varying decay rate μ of the population's activity. Every curve in the diagram represents a specific type of limiting behavior of the model: either a fixed point or a limit cycle. Fixed points are depicted with a thin line of which the vertical component is the population's activity at that fixed point. Limit cycles are indicated with a thick line that corresponds with the maximal activity reached by a population during a period. Solid lines are used to mark stable limiting behavior, meaning that it will force nearby orbits to exhibit similar behavior as the limiting behavior itself, whereas dashed lines designate unstable types of behavior that will repel nearby orbits.

Because the origin is always a fixed point of the system (2.1), we choose this point as initial point for our analysis. For high values of μ the origin is a stable fixed point of the system. When decreasing the parameter μ, the origin retains its stability until the critical

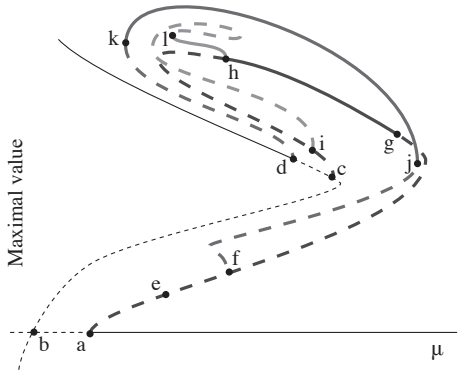

Fig. 2.7 Bifurcation diagram of the population model, representing possible solutions of the system. Curves represent steady states (thin lines) and periodic orbits (thick lines). Solid lines indicate stable solutions and dashed lines correspond to unstable solutions. See text for a description of the curves and bifurcation points a-l.

point (a) is crossed at which it undergoes a subcritical Andronov-Hopf bifurcation and a family of (unstable) limit cycles arises. Continuation of the unstable equilibrium yields a branch point at (b) where it coincides with a another unstable equilibrium. Analyzing the evolution of this new equilibrium reveals a fold bifurcation and two successive subcritical Hopf bifurcations at (c) and (d) after which it becomes stable.

Closer inspection of the limit cycles that appeared at (a) yields a family of symmetric oscillations representing synchronous neuronal activity. This branch passes a Neimark-Sacker bifurcation at (e) and a supercritical period-doubling bifurcation at (f) where it spawns a branch of asymmetric periodic solutions with its period initially doubled. The symmetric branch folds over and undergoes another period-doubling bifurcation at (g) where it becomes stable until it undergoes another period-doubling at (h). Beyond (h) the branch folds over, experiences another period-doubling bifurcation at (i) until it terminates in the Hopf bifurcation (c).

Following the branch of asymmetric solutions that emerges at (f), we find that it folds twice to gain stability at (j). At the left end of the diagram, stability is lost in another fold bifurcation (k) and the branch eventually terminates at the Hopf bifurcation (d).

Next we continue the branch of limit cycles spawned at the period-doubling bifurcation (h), at which the populations exhibit synchronous activity at half the original frequency. The branch is stable at first but loses stability in (l) due to three successive fold bifurcations after which it ends in the period-doubling at (i).

We summarize the results of this bifurcation analysis. The population model can, in principle, display all the basic types of behavior previously seen from the detailed model (c.f. 3.1.1). For large values of μ larger than (j), the origin is the only stable solution of the system, indicating that all activity eventually dies out. If μ is smaller than (a), only one

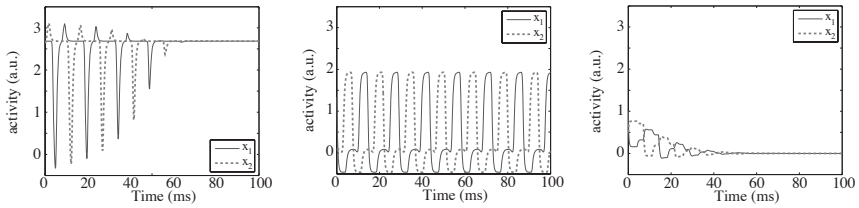

Fig. 2.8 Simulation results for the population model for different levels of excitation. The excitation is changed in each of the panels (left) $\mu = 2$, (center) $\mu = 3$ and (right) $\mu = 4$.

stable equilibrium is present at a high level of activity at which both populations remain continuously activate. Either of these steady states is symmetric in the sense that both populations exhibit identical behavior. Asymmetric steady states, in which one population is continuously active and the other quiescent, are not present.

If the value of μ lies between (j) and (k), the network can generate periodic behavior where both neuronal populations are alternately activated. Whenever μ takes values between (l) and (d), the system has four stable solutions: two equilibria and two types of oscillations.

2.3.2.2 Behavior

Simulations are performed for the population model given in (2.1) for different values of μ to study the effects of altering excitation. For high levels of excitation ($\mu = 2$), the simplified model reaches a steady state at with high level constant activity (left panel of 2.8). At moderate levels of excitation ($\mu = 3$), the model manifests oscillations in which both populations are antiphasically active (middle panel). For very low levels of excitation ($\mu = 4$), all activity dies out and both populations become quiescent (right panel).

2.3.3 Comparison

2.3.3.1 Behavior

After analyzing both the detailed model and the population model individually, we compare their results in this section.

We note that the desynchronized behavior observed in the detailed model is similar to the high steady state in the population model, because the detailed model reveals that

individual neurons in the excitatory populations are continuously active without a distinct rhythm. Both models exhibit this type of behavior for high levels of excitation.

For normal levels of excitation, the detailed model displays irregular bursts of activity, in which the superficial pyramidal cells are clearly more active than the deep cells (figure 2.3). This type of behavior, in which one population clearly dominates the other, can never be observed in the population model as no asymmetric steady states are found in the bifurcation analysis. In future work, we will break the symmetry of the population model and include specific properties of the excitatory neurons, such that asymmetric steady states, corresponding with the observed behavior, are likely to exist. Even though the population model is unable to exhibit this type of behavior, we question the relevance of this result of the detailed model because of the unnatural dominance of the superficial population.

When the excitation in the network is low, the network shows oscillatory behavior in which neurons in the pyramidal populations are alternately active (figure 2.6). This corresponds extremely well with the family of asymmetric limit cycles observed in the population model (figure 2.8 center).

For very low values of excitation in the population model, we find that activity of both populations dies out eventually (figure 2.8 right). This behavior matches closely with the burst-suppression of the detailed model, that is observed at very low levels of excitation, because it is quiescent for most of the time. We recall that the regular bursts occur on a long time scale (close to 1 second) and that the population does not contain such long time scales. Furthermore, the bursts of activity are initiated by the superficial pyramidal cells that burst intrinsically. Since spontaneous activity is not included in the population model, we do consider these behaviors similar.

2.3.3.2 Multistability and bifurcations

Bifurcation analysis of the population model reveals the presence of multistability of at most four attractors. These attractors and their stability are well-defined in the population model, but undetermined in the detailed model. For instance, if the detailed model is close to a bifurcation point, it can repeatedly switch from one type of behavior to another (see figure 2.9). This type of behavior, in which both states appear intermittently, is caused by the chaotic nature of the detailed model. The population model does not capture this intermittent behavior, but it describes the attractors to which switches can be made.

Moreover in the detailed model, we have found evidence for the occurrence of period-doubling bifurcations and the existence of multistability for synchronous and asynchronous neuronal activity.

Finally, two simulations were also performed in which the conduction velocity of action potentials through axons varied slowly over time (figure 2.10). As the conduction velocity slowly increases (fig 2.10, left) the frequency of the oscillations seems to double at $t \approx$

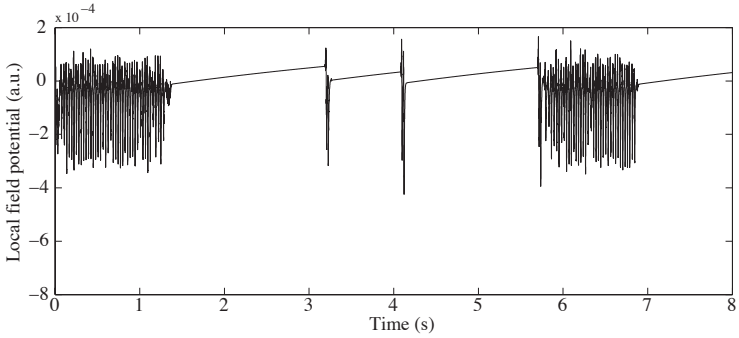

Fig. 2.9 Compare with figures 2.4 and 2.5. For values of excitation between low and very low, the model's behavior switches between oscillations and regular bursts.

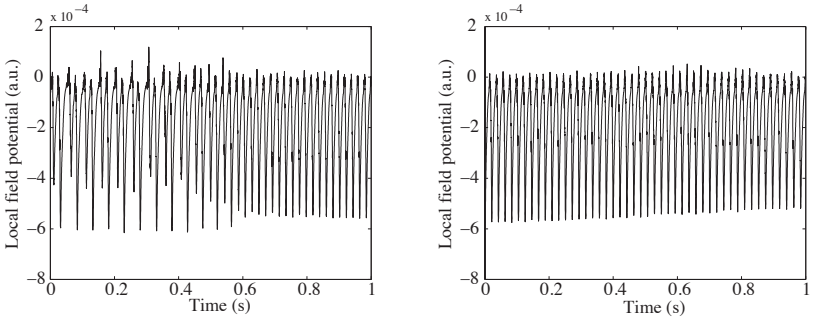

Fig. 2.10 A period doubling bifurcation under the effect of hysteresis. (left) the conduction velocity of action potentials increases slowly from 0.08m/s to 0.088m/s due to which the system undergoes a period doubling bifurcation. (right) the conduction velocity in decreased continuously from 0.088m/s to 0.08m/s and the fast oscillations persist.

0.6s. If the conduction velocity is slowly returned to its original value (fig 2.10, right) then these fast oscillations persist. This confirms the multistability predicted by the bifurcation analysis of the population model, in which we found both symmetric and asymmetric stable limit cycles for a wide range of values for μ.

2.4 Discussion

In this work we studied two models of the neocortex to examine neuronal activity during epileptiform network behavior. The first model is based on a detailed description of 656 neurons, consisting of two types of pyramidal cells and four types of interneurons. For

validation we compared this model to [113], because the network shows similar types of behavior (i.e. desynchronized, irregular bursting, oscillatory and regular bursting) when the network excitation is changed. The second model is a population model, consisting of two delay differential equations, that represents the activity of pyramidal neurons in both superficial and deep layers of the neocortex. Analysis of this model reveals comparable behavior as the detailed model for corresponding changes of excitation levels in the network. Determination of the bifurcation diagram of the population model yields an understanding of the more exotic types of behavior observed in the detailed model, like multistability, intermittency and period doublings (figures 2.9 and 2.10).

The fact that these two models exhibit similar behavior reveals, in our opinion, a new way to analyze transitions of neuronal activity in the brain. First, bifurcations of an associated population model with lumped parameters can be studied, from which new hypotheses can be formulated regarding emergent epileptiform network behavior. Next, values of the lumped parameters of the population model should be translated into physiological parameters in the detailed model to gain physiological insight intro the role these parameters play in inducing epileptiform behavior in the detailed model. This would allow for hypotheses generated from the population model to be verified in a model, which incorporates details of single neurons, which is important since drug therapies have their targets at subcellular level ultimately.

Whereas several hypotheses have been formed using population models [81, 100], none of these have been further confirmed in a detailed model. This impedes any attempt to put these results into a physiological and clinical relevant perspective

We are aware of the limitations of both of our models (for instance omitting the thalamocortical feedback loop by only considering neocortical structures) and we present this work merely as an starting point for future work. Both models can be expanded by including thalamocortical connections enabling us to study other types of epilepsy can be studied as well, instead of only neocortical epilepsy. The proposed population model is not fully examined for the presence of bifurcations with respect to parameters other than the level of excitation μ and we expect further study to reveal new predictions for mechanisms behind the generation of epileptiform activity.

Chapter 3
On stability and bifurcations in a lumped model of neocortex

Abstract A lumped model of neural activity in neocortex is studied to identify regions of multi-stability of both steady states and periodic solutions. Presence of both steady states and periodic solutions is considered to correspond with epileptogenesis. The model, which consists of two delay differential equations with two fixed time lags, is mainly studied for its dependency on varying connection strength between populations. Equilibria are identified, and using linear stability analysis, all transitions are determined under which both trivial and non-trivial fixed points lose stability. Periodic solutions arising at some of these bifurcations are numerically studied with a two-parameter bifurcation analysis[1].

3.1 Introduction

Epilepsy is a neurological disease characterized by an increased risk of recurring seizures that affects about 1% of the world population. Such seizures typically manifest themselves as brief periods in which neural activity is more synchronized than a certain baseline level. In lumped models of neural activity in the brain, these seizures are, for that reason, often characterized as large-amplitude oscillations [84]. Many causes might exist for the neural network to start oscillating, e.g., a slow parameter or an external factor might cause a bifurcation [130], or a perturbation might force the system to a different attractor [81].

In this paper, we study the attractors and their bifurcations in a lumped model of superficial and deep pyramidal cells in neocortex that has been shown to correspond well with a large detailed model whose results conformed to experiments [113, 125]. The structure of this model is shown in Figure 3.1. Our main goal is to identify the dominating stable attractors in the system as well as their bifurcations for varying connection strength of the

[1] Adapted from S Visser, HGE Meijer, MJAM van Putten and SA van Gils, *Analysis of stability and bifurcations of fixed points and periodic solutions of a lumped model of neocortex with two delays*, Journal of Mathematical Neuroscience **2** (2012), no. 8.

neural populations. The model proposed in [125] is essentially a continuous time two-node Hopfield network with discrete time delays and feedback that is governed by the following equations:

$$\begin{aligned}\frac{dx_1}{dt}(t) &= -\mu_1 x_1(t) - \mathscr{F}_1(x_1(t-\tau_i)) + \mathscr{G}_1(x_2(t-\tau_e)) \\ \frac{dx_2}{dt}(t) &= -\mu_2 x_2(t) - \mathscr{F}_2(x_2(t-\tau_i)) + \mathscr{G}_2(x_1(t-\tau_e))\end{aligned} \tag{3.1}$$

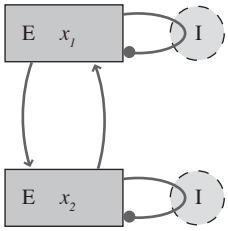

Fig. 3.1 Overview of the model. Two cortical layers (red and blue) with excitatory pyramidal cells are connected mutually. The inhibition of the interneurons (green) is modeled intrinsically.

where x_i is the node's activity, μ_i the natural decay rate of activity, τ_i the time lag of feedback inhibition, τ_e the delay of feedforward excitation and both $\mathscr{F}_i(x)$ and $\mathscr{G}_i(x)$ are bounded monotonically increasing functions that represent inhibitory and excitatory synaptic activation, respectively.

Small Hopfield networks of this and similar forms have been studied in detail by various researches [7, 9, 19, 21, 20, 22, 49, 59, 58, 63, 96, 103, 127, 128, 134, 137, 136] . For example, Olien and Bélair [96] studied a two-node network with both delayed feedforward and delayed feedback connections between the nodes. Later, the same model was analyzed further by Wuan and Rei [127]. The delays in this model, however, are node-specific (the delays for all outgoing connections of a node are unique for that node) instead of connection-specific (the delays are unique for each type of connection: excitatory and inhibitory). The latter case applies to our network.

We particularly notice the work by Shayer and Campbell [103] that studies a model very similar to the system (3.1) except for the fact that they choose the activation functions as odd functions. Although they numerically identify multi-stability of steady states and a periodic solution, their study mainly focuses on analytical determination of the stability and bifurcations of the trivial equilibrium in terms of the time lag parameters. In 2005, Campbell *et al.* studied the numerical continuation of periodic solutions in a ring of neurons [21]. We will extend a similar approach to a two-parameter bifurcation study in this work.

Because Hopfield networks originate from computer science to solve mathematical programming problems [129], it is more common to study models of the Wilson-Cowan type for physiological modeling [132]. On that note, we like to point to a study by Coombes and Laing of a Wilson-Cowan type model, which is very similar to our model, in which they observe a variety of steady states, periodic solutions and chaos [30]. While Hopfield models are uncommon in mathematical neuroscience, we are not the first to study these models with a physiological relevance. For instance, Song *et al.* studied two clusters, each consisting of an excitatory and an inhibitory node that projected onto each other with delayed connections [105]. They assumed that the connections between the nodes could be faster in one direction than in the other, and they studied the model's dependency on this difference in time lags. Furthermore, they are, to our knowledge, the only group that has performed a numerical bifurcation study of periodic orbits in two parameters for this type of model.

Due to the physiological background of our model, the delays are known and we consider fixed values of τ_i and τ_e. Because of that, we are primarily interested in the parameters related to connection strength as these may be amended with anti-epileptic drugs. Although these results will depend on the chosen values of the delays, we elaborate on their robustness under variations of these delays in the discussion.

Another difference with the pioneering works [9, 103] is related to symmetry in the model. They have chosen their functions $\mathscr{F}_i$ and $\mathscr{G}_i$ as odd functions, which introduces a reflectional symmetry. For physiological reasons, the model considered in this paper uses non-symmetric activation functions for the synapses because the activation of synapses is thought to be stronger than the deactivation. In order to reduce the number of parameters, we choose the following:

$$\mu_1 = \mu_2 := \mu, \qquad \mathscr{F}_1(x) = \mathscr{F}_2(x) := \mathscr{F}(x), \qquad \mathscr{G}_1(x) = \mathscr{G}_2(x) := \mathscr{G}(x).$$

This choice of parameters and activation functions makes the model $\mathbb{Z}_2$-symmetric. The following expressions are chosen for the synaptic activation functions

$$\mathscr{F}(x) = a_i S(\sigma_i x), \quad \mathscr{G}(x) = a_e S(\sigma_e x) \tag{3.2}$$

for certain S that is smooth, strictly increasing and satisfies $S(0) = 0$ and $S'(0) = 1$. Typically, $S(x)$ is bounded and sigmoidal, i.e., S has exactly one inflection point. The results in section 2 are independent of the specific shape of S, but we will specify S for the numerical bifurcation analysis.

In the remaining part of this article, we study the non-dimensionalized version of (3.1) by taking $\tilde{x}_i(\tilde{t}) := x_i(\mu\tilde{t})$:

$$\begin{aligned}\frac{d\tilde{x}_1}{d\tilde{t}}(\tilde{t}) &= -\tilde{x}_1(\tilde{t}) - \alpha_1 S(\beta_1 \tilde{x}_1(\tilde{t}-\tau_1)) + \alpha_2 S(\beta_2 \tilde{x}_2(\tilde{t}-\tau_2)),\\ \frac{d\tilde{x}_2}{d\tilde{t}}(\tilde{t}) &= -\tilde{x}_2(\tilde{t}) - \alpha_1 S(\beta_1 \tilde{x}_2(\tilde{t}-\tau_1)) + \alpha_2 S(\beta_2 \tilde{x}_1(\tilde{t}-\tau_2)),\end{aligned} \tag{3.3}$$

with $\alpha_1 := \frac{a_i}{\mu}$, $\beta_1 := \sigma_i$, $\alpha_2 := \frac{a_e}{\mu}$, $\beta_2 := \sigma_e$, $\tau_1 := \mu\tau_i$ and $\tau_2 := \mu\tau_e$. For convenience, we drop the tildes from now on and switch to vector notation:

$$\dot{\mathbf{x}}(t) = \mathbf{f}(\mathbf{x}_t), \text{ with } \mathbf{x}_t \in C([-h,0],\mathbb{R}^2) \text{ and } h = \max(\tau_1,\tau_2). \tag{3.4}$$

In the following section, we will study this system analytically by determining its fixed points and the linear stability of these points. We will identify a stability region in parameter space and classify the bifurcations on the edge of this region. For Hopf bifurcations of the trivial steady state, we compute the first Lyapunov coefficient to study the criticality of these bifurcations. In the 'Numerical bifurcation analysis' section, we use software packages to determine (numerically) how the presence and stability of the bifurcating periodic solutions depend on the parameters α_1 and α_2.

3.2 Equilibria: linear stability and bifurcations

In this section, we study the equilibria as well as their linear stability. Necessary conditions for saddle-node, trans-critical and Hopf bifurcations are derived. Thereafter, the first Lyapunov coefficient is evaluated for the Hopf bifurcations to determine their criticality.

3.2.1 Equilibria and stability region

First we note, since $S(0) = 0$, that the origin $(x_1,x_2) = (0,0)$ is always a fixed point of the system (3.4). For the non-trivial fixed points, the following holds:

Theorem 3.1. *The system* (3.4) *admits exclusively symmetric fixed points:*

$$\mathbf{f}(\mathbf{x}^*) = 0 \implies \mathbf{x}^* = (x^*,x^*) \text{ for some } x^* \in \mathbb{R}.$$

Proof. First we note that, since $S(x)$ is a continuous strictly increasing function, its inverse function $S^{-1}(x)$ exists, and it is also continuous and strictly increasing. Next define:

$$H(x) := \frac{1}{\beta_2} S^{-1}\left(\frac{1}{\alpha_2}(x + \alpha_1 S(\beta_1 x))\right).$$

Because of monotonicity of both S and S^{-1} and positiveness of all parameters, H is continuous and strictly increasing as well.

Fixed points of (3.4) satisfy $\mathbf{f}(\mathbf{x}^*) = 0$ which is equivalent to:

$$\begin{cases} x_2^* = H(x_1^*), \\ x_1^* = H(x_2^*). \end{cases} \tag{3.5}$$

Assume that the equilibrium is asymmetric and that $x_1^* < x_2^*$ without loss of generality. Application of H on both sides of this inequality and use of the conditions in (3.5) yield:

$$x_2^* = H(x_1^*) < H(x_2^*) = x_1^*.$$

This contradicts our assumption; hence, we conclude that $x_1^* = x_2^* = x^*$.

Due to the symmetric positions of these fixed points, the linearization $\mathbf{u}(t)$ at these equilibria takes the following form:

$$\begin{aligned} \dot{u}_1(t) &= -u_1(t) - k_1 u_1(t-\tau_1) + k_2 u_2(t-\tau_2), \\ \dot{u}_2(t) &= -u_2(t) - k_1 u_2(t-\tau_1) + k_2 u_1(t-\tau_2), \end{aligned} \tag{3.6}$$

with

$$k_1 := \alpha_1 \beta_1 S'(\beta_1 x^*) \qquad k_2 := \alpha_2 \beta_2 S'(\beta_2 x^*). \tag{3.7}$$

Both k_1 and k_2 take positive values only because S' is positive as well as the parameters α_i and β_i for $i = 1, 2$.

Next, we look for exponential solutions of the form $\mathbf{u}(t) = e^{\lambda t}\mathbf{c}$ with $\mathbf{c} \in \mathbb{C}^2$. For a non-trivial solution of (3.6), it is required that $\Delta(\lambda)\mathbf{c} = 0$, where $\Delta(\lambda)$ is the characteristic matrix:

$$\Delta(\lambda) = \begin{bmatrix} \lambda + 1 + k_1 e^{-\lambda\tau_1} & -k_2 e^{-\lambda\tau_2} \\ -k_2 e^{-\lambda\tau_2} & \lambda + 1 + k_1 e^{-\lambda\tau_1} \end{bmatrix}, \tag{3.8}$$

Non-trivial solutions $\mathbf{c}$ exist if the characteristic equation is satisfied:

$$\begin{aligned} 0 &= \det \Delta(\lambda) \\ &= \underbrace{(\lambda + 1 + k_1 e^{-\lambda\tau_1} + k_2 e^{-\lambda\tau_2})}_{:=\Delta_+(\lambda)} \underbrace{(\lambda + 1 + k_1 e^{-\lambda\tau_1} - k_2 e^{-\lambda\tau_2})}_{:=\Delta_-(\lambda)}. \end{aligned} \tag{3.9}$$

From this decomposition, it follows that the spectrum of (3.6) is the union of the spectra of the decoupled equations:

$$\dot{v}_-(t) = -v_-(t) - k_1 v_-(t-\tau_1) + k_2 v_-(t-\tau_2), \tag{3.10a}$$

$$\dot{v}_+(t) = -v_+(t) - k_1 v_+(t-\tau_1) - k_2 v_+(t-\tau_2). \tag{3.10b}$$

The spectra of linear DDEs with two delays, like (3.10), have been studied extensively since the 1960s (for instance, Bellman, Cooke and Hale [10, 60]). The main consensus of these works is that the stability region often has a complex shape in terms of the parameters of the differential equation. The majority of the results in the remainder of this section and the next one (i.e. 'Bifurcations' section) could be considered as 'common knowledge'. For the purpose of clarity, however, we have chosen to present a short derivation of these results.

We start by denoting the following theorem regarding symmetry of solutions:

Theorem 3.2. *Roots of Δ_- correspond to symmetric solutions, whereas roots of Δ_+ relate to asymmetric solutions.*

Proof. Let $\mathbb{Z}_2$ act on $\mathbb{R}^2$ so that $-1 \in \mathbb{Z}_2$ acts as $\xi(x,y) : (x,y) \mapsto (y,x)$, then:

$$\Delta_-(\lambda) = 0 \Leftrightarrow \begin{cases} \Delta(\lambda)v = 0 \\ \xi v = v \end{cases} \quad \text{and} \quad \Delta_+(\lambda) = 0 \Leftrightarrow \begin{cases} \Delta(\lambda)v = 0 \\ \xi v = -v \end{cases} . \tag{3.11}$$

Using the characteristic equation, we can find a relation between the parameters (k_1, k_2) and the eigenvalues:

Theorem 3.3. *Let $\lambda = \rho + i\omega$ for $\rho, \omega \in \mathbb{R}$ satisfy the characteristic equation* (3.9) *and let $\tau_2 > \tau_1 > 0$, then the following inequality holds:*

$$|k_1| + |k_2| \geq e^{\rho\tau}\sqrt{(1+\rho)^2 + \omega^2}, \quad \tau = \begin{cases} \tau_2 & \rho < 0 \\ \tau_1 & \rho \geq 0 \end{cases}. \tag{3.12}$$

Proof. Solutions of the characteristic equation (3.9) satisfy either $\Delta_+(\lambda) = 0$ or $\Delta_-(\lambda) = 0$. Upon assuming $\Delta_+(\lambda) = 0$, it follows that:

$$e^{\max(-\rho\tau_1, -\rho\tau_2)}(|k_1| + |k_2|) \geq |k_1|e^{-\rho\tau_1} + |k_2|e^{-\rho\tau_2} \geq |1 + \rho + i\omega|,$$

which yields the inequality (3.12). A similar argument for $\Delta_-(\lambda)$ yields the same inequality.

Corollary 3.4. *An equilibrium of the system* (3.4) *is asymptotically stable if $|k_1| + |k_2| < 1$.*

Proof. The inequality (3.12) yields in this case:

$$e^{\rho\tau}\sqrt{(1+\rho)^2 + \omega^2} < 1, \tag{3.13}$$

which can only hold for $\rho < 0$. Therefore, all roots of the characteristic matrix have a negative real part and the equilibrium is asymptotically stable.

Having obtained a minimal stability region in the Corollary 3.4, we study conditions for bifurcations of equilibria to expand the minimal stability region determined by Corollary 3.4.

3.2.2 Bifurcations

The stability of an equilibrium of a DDE is lost when one or more eigenvalues pass through the origin or the imaginary axis. The first case, in which a real eigenvalue crosses through the origin, is characterized in the following theorem:

Theorem 3.5. *The linearized system* (3.6) *has at least one zero eigenvalue if and only if* $1+k_1+k_2=0$ *or* $1+k_1-k_2=0$.

Proof. Substitution of $\lambda = 0$ into the characteristic equation (3.9) yields that either $\Delta_+(0)=0$ or $\Delta_-(0)=0$ and hence:

$$\Delta_+(0)=0 \implies 1+k_1+k_2=0, \tag{3.14a}$$

$$\Delta_-(0)=0 \implies 1+k_1-k_2=0. \tag{3.14b}$$

Since the origin is always a fixed point of the system, the conditions in Theorem 3.5 correspond to transcritical bifurcations. For non-trivial fixed points, these conditions imply either a fold bifurcation or a trans-critical bifurcation. Because k_1 and k_2 are both positive, saddle-node bifurcations from Δ_+ cannot occur. This, in combination with Theorem 3.2, leads to the conclusion that no symmetry-breaking steady-state bifurcations exist, a result which we also obtained in Theorem 3.1.

The case in which a pair of complex eigenvalues passes the imaginary axis is summarized in the following theorem:

Theorem 3.6. *Two piecewise continuous functions* $\mathbf{h}_+(\omega)$ *and* $\mathbf{h}_-(\omega)$ *exist in parameter space* (k_1,k_2) *for which the characteristic equation* (3.9) *has a pair of purely imaginary roots* $\lambda=\pm i\omega$. *Furthermore, when* $\omega=-\tan\omega\tau_1=-\tan\omega\tau_2$, *a line* $k_1+\sigma k_2=c$ *exists for some* c *and* $\sigma=\pm1$ *for which* (3.9) *has roots* $\pm i\omega$.

Proof. Substituting $\lambda = i\omega$ with $\omega > 0$ into (3.9) yields that either $\Delta_+(i\omega)=0$ or $\Delta_-(i\omega)=0$. The roots of $\Delta_+(i\omega)$ are considered first:

$$i\omega+1+k_1e^{-i\omega\tau_1}+k_2e^{-i\omega\tau_2}=0.$$

Splitting this equation in its real and imaginary part gives:

$$\begin{bmatrix}\cos(\omega\tau_1) & \cos(\omega\tau_2)\\ \sin(\omega\tau_1) & \sin(\omega\tau_2)\end{bmatrix}\begin{bmatrix}k_1\\k_2\end{bmatrix}=\begin{bmatrix}-1\\\omega\end{bmatrix}. \tag{3.15}$$

In the case that this matrix is invertible, we find the unique solution (k_1, k_2) in terms of ω by matrix inversion:

$$\begin{bmatrix} k_1 \\ k_2 \end{bmatrix} = \mathbf{h}_+(\omega) := \frac{-1}{\sin(\omega(\tau_2 - \tau_1))} \begin{bmatrix} \sin(\omega\tau_2) & \cos(\omega\tau_2) \\ -\sin(\omega\tau_1) & -\cos(\omega\tau_1) \end{bmatrix} \begin{bmatrix} 1 \\ \omega \end{bmatrix}. \tag{3.16}$$

In the other case, the matrix is not invertible and, hence, its determinant is zero, yielding:

$$\tan\omega\tau_1 = \tan\omega\tau_2. \tag{3.17}$$

Combined with the condition that $\begin{bmatrix} -1, \omega \end{bmatrix}^T \in \mathscr{R}(A)$, A being the matrix in (3.15), follows that:

$$\omega = -\tan(\omega\tau_1) = -\tan(\omega\tau_2). \tag{3.18a}$$

This yields the line of solutions:

$$k_1 + \sigma k_2 = -\frac{1}{\cos(\omega\tau_1)} \tag{3.18b}$$

for $\sigma = \pm 1$ such that $\cos\omega\tau_1 = \sigma\cos\omega\tau_2$.

The roots of $\Delta_-(i\omega)$ are identified in a similar manner, yielding:

$$\begin{bmatrix} k_1 \\ k_2 \end{bmatrix} = \mathbf{h}_-(\omega) := \frac{-1}{\sin(\omega(\tau_2 - \tau_1))} \begin{bmatrix} \sin(\omega\tau_2) & \cos(\omega\tau_2) \\ \sin(\omega\tau_1) & \cos(\omega\tau_1) \end{bmatrix} \begin{bmatrix} 1 \\ \omega \end{bmatrix}. \tag{3.19}$$

Furthermore, the same line of solutions and corresponding condition as in (3.18) hold for $\Delta_-(i\omega)$. For a Hopf bifurcation to occur, any of the equations (3.16–3.19) must be satisfied.

In Theorem 2, we have already shown that Hopf bifurcations caused by Δ_- correspond to symmetric periodic solutions. For Hopf bifurcations induced by Δ_+, the following holds:

Theorem 3.7. *Hopf bifurcations corresponding with Δ_+ yield asymmetric periodic solutions, i.e., $x_1(t) = x_2(t + \frac{1}{2}T)$ with T the period of the solution.*

Proof. Let $\lambda = i\omega_0$ for $\omega_0 > 0$ be a simple root of Δ_+ (i.e., of algebraic multiplicity one) and p a corresponding eigenvector of $\Delta(i\omega_0)$. Then, from Hopf bifurcation theory, we know that, for ε, sufficiently small C^1 functions $\mathbf{k}^*(\varepsilon)$, $\omega^*(\varepsilon)$ and $\mathbf{x}^*(\varepsilon)$ exist, taking values in $\mathbb{R}^2$, $\mathbb{R}$ and $C([-h,0],\mathbb{R}^2)$, respectively. Furthermore, $\mathbf{k}^*(\varepsilon) \to \mathbf{h}_+(\omega_0)$, $\omega^*(\varepsilon) \to \omega_0$ and $\mathbf{x}(\varepsilon)(t) = \varepsilon\Re(e^{i\omega^*(\varepsilon)t}p) + o(\varepsilon)$ for $\varepsilon \downarrow 0$. For $\mathbf{k} = \mathbf{k}^*(\varepsilon)$ and ε, sufficiently small $\frac{2\pi}{\omega^*(\varepsilon)}$-periodic solutions $\mathbf{x}(t) = \mathbf{x}^*(\varepsilon)(t+\theta)$ exist with $\theta \in [0, 2\pi/\omega^*(\varepsilon))$.

Since $\Delta_+(i\omega_0) = 0$, it follows from (3.11) that $\xi p = -p$. As the full non-linear equation commutes with ξ, it follows that the bifurcating periodic solution inherits this symmetric property:

$$\mathbf{x}(t + \frac{\pi}{\omega^*(\varepsilon)}) = \varepsilon\Re(e^{i\omega^*(\varepsilon)t + i\pi}p) = \xi\mathbf{x}(t) \tag{3.20}$$

So, the condition for asymmetric periodic solutions is satisfied.

The different conditions for eigenvalues to have zero real part, as determined in Theorems 3.5 and 3.6, are displayed in the (k_1,k_2)-plane in Figure 3.2. Due to the sine terms in the denominators of $\mathbf{h}_+$ and $\mathbf{h}_-$, these functions consist of numerous branches separated by asymptotes. Intersections of these curves correspond to parameters at which the system satisfies conditions for two co-dimension one bifurcations and so we expect (at least) the following co-dimension two bifurcations: Bogdanov-Takens, fold-Hopf and Hopf-Hopf.

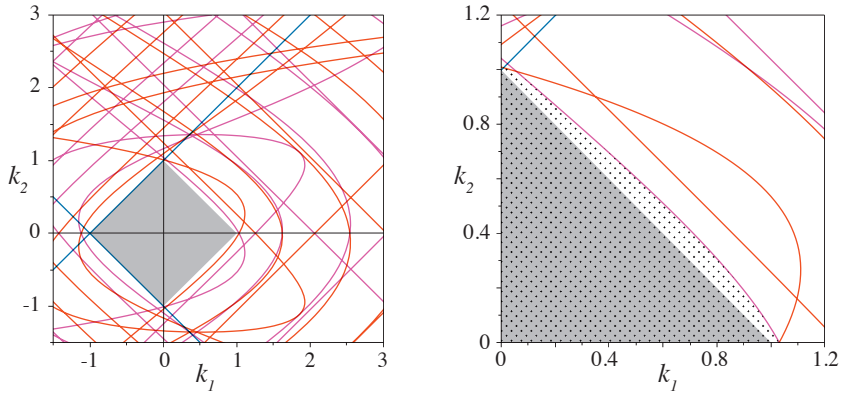

Fig. 3.2 Bifurcation curves in the (k_1,k_2)-plane. $\tau_1 = 11.6$ and $\tau_2 = 20.3$. The right plot shows a detail of the first quadrant only. Blue shows the conditions for fold or transcritical bifurcations (3.14a) and (3.14b) and red and magenta depict Hopf bifurcations; equations $\mathbf{h}_+$ and $\mathbf{h}_-$, respectively. The gray area represents the stability region as in Corollary 3.4. The full stability region is hatched in the right diagram.

Studying the right diagram of Figure 3.2, we observe that the bifurcation curves do not coincide with the bounds of the stability region from Corollory 3.4. Hence, it appears that parameters exist outside this square stability region for which it still holds that all eigenvalues have negative real part. We now determine the full stability region around the origin of the (k_1,k_2)-plane by showing that instabilities are exclusively induced by low frequencies. More precisely:

Theorem 3.8. *The square* $|k_1| + |k_2| < \sqrt{1+\omega_0^2}$ *contains no eigenvalues* $\lambda = \pm i\omega$ *for* $\omega \geq \omega_0 > 0$.

Proof. This follows from substitution of $\lambda = i\omega_0$ into Theorem 3.3 and the fact that $\sqrt{1+\omega_0^2}$ is a monotically increasing function.

So, if we choose ω_0 sufficiently large as dictated by Theorem 3.8, no other bifurcations are located inside the bifurcation diagrams of Figure 3.2 for $\omega > \omega_0$. Hence, we can extend the stability region from the square region to the nearest bifurcation. This new stability region is hatched in the right diagram of Figure 3.2.

Since we are mainly interested in stable solutions, we consider only bifurcation curves that bound the stability region. Even though we identified a bounded stability region in parameter space, we cannot assure that this is the only region in which fixed points are stable. As shown in [85], the roots of either Δ_- or Δ_+ can contain multiple, disjoint regions in parameter space in which all roots have negative real parts. Since in our case, however, the eigenvalues of (3.6) are the union of the eigenvalues of the (3.10), we conjecture that no other stable regions exist in parameter space than the one shown in Figure 3.2.

For the fixed parameters $\tau_1 = 11.6$ and $\tau_2 = 20.3$, we find that the stability region in the first quadrant is bounded by a line of fold bifurcations (3.14b) as well as both curves $\mathbf{h}_+$ and $\mathbf{h}_-$ of Hopf bifurcations; see also Figure 3.3. For clarity, we denote the domains of ω for which these curves bound the stability region by $\Omega_S(\mathbf{h}_+)$ and $\Omega_S(\mathbf{h}_-)$, respectively. We compute approximations of these ranges:

$$\Omega_S(\mathbf{h}_+) \approx (0.148, 0.150), \qquad \Omega_S(\mathbf{h}_-) \approx (0.250, 0.294). \tag{3.21}$$

Similarly, we identify the codim-2 bifurcations that bound the stability region. The fold-Hopf bifurcation is located at:

$$\mathbf{k}_{ZH} := \mathbf{h}_+(0.148) = \begin{bmatrix} 0.008 \\ 1.008 \end{bmatrix}. \tag{3.22}$$

For the Hopf-Hopf bifurcation, we find:

$$\mathbf{k}_{HH} := \mathbf{h}_+(0.150) = \mathbf{h}_-(0.294) = \begin{bmatrix} 0.056 \\ 0.995 \end{bmatrix}. \tag{3.23}$$

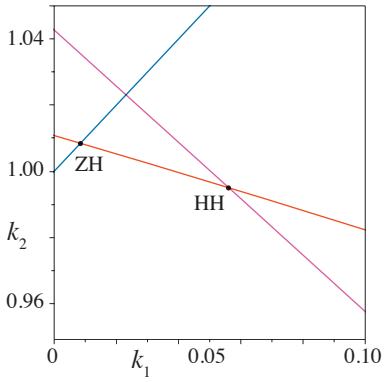

Fig. 3.3 Detail of bifurcations. Similar to Figure 3.2 but now showing the fine structure of branches bounding the stability region. The points ZH and HH correspond with the fold-Hopf and Hopf-Hopf bifurcations from (3.22) and (3.23). For clarity, we do not show the stability region. Blue, fold/transcritical; red, asymmetric Hopf; magenta, symmetric Hopf.

It follows from (3.7) that, for the trivial equilibrium, the bifurcation diagram in the (k_1,k_2)-plane determines the bifurcation diagram in the (α_1,α_2)-plane up to linear rescaling.

3.2.3 The first Lyapunov coefficient

Hopf bifurcations give rise to either stable or unstable periodic solutions depending on the criticality. Therefore, we determine the first Lyapunov coefficient. Since it is easier to relate k_1 and k_2 to α_1 and α_2 in the origin than at non-trivial fixed points, we only consider Hopf bifurcations at the origin.

We follow the method described in [41]. Let p and q be eigenvectors of the characteristic matrix $\Delta(i\omega)$ and $\Delta^*(i\omega)$, respectively. We normalize these vectors such that $q^T\Delta'(i\omega)p = 1$. By choosing $p = [1,1]^T$ as an eigenvector of $\Delta(i\omega)$, q takes the form:

$$q = q_0\begin{bmatrix}1\\1\end{bmatrix} := \frac{1}{2(1-k_1\tau_1e^{-i\omega\tau_1}+k_2\tau_2e^{-i\omega\tau_2})}\begin{bmatrix}1\\1\end{bmatrix}. \tag{3.24}$$

For $\phi(t) = pe^{i\omega t}$, the first Lyapunov coefficient of a (candidate) Hopf bifurcation is defined as the real part of c_1:

$$\begin{aligned}c_1 =& \frac{1}{2}q^TD^3\mathbf{f}(0)(\phi,\phi,\bar{\phi})\\ &+ q^TD^2\mathbf{f}(0)(e^{0\cdot}\Delta(0)^{-1}D^2\mathbf{f}(0)(\phi,\bar{\phi}),\phi)\\ &+ \frac{1}{2}q^TD^2\mathbf{f}(0)(e^{2i\omega\cdot}\Delta(2i\omega)^{-1}D^2\mathbf{f}(0)(\phi,\phi),\bar{\phi}).\end{aligned} \tag{3.25}$$

We note that $\mathbf{f}$ is symmetric, i.e., $\mathbf{f}_j([x,x]) = f(x)$ for $j = 1,2$, and that it does not contain any cross terms, that is $\frac{\partial^2}{\partial x_1\partial x_2}\mathbf{f}([x_1,x_2]) = 0$. Therefore, both components of the differential operators $D^2\mathbf{f}([x,x])$ and $D^3\mathbf{f}([x,x])$ will be identical when evaluated for symmetric arguments and we denote these components by $f''(x)$ and $f'''(x)$, respectively. By using the multi-linear properties of the operators, we expand c_1:

$$\begin{aligned}c_1 =& \frac{1}{2}q_0\begin{bmatrix}1&1\end{bmatrix}f'''(0)(e^{i\omega t},e^{i\omega t},e^{-i\omega t})\begin{bmatrix}1\\1\end{bmatrix}\\ &+ q_0\begin{bmatrix}1&1\end{bmatrix}f''(0)(e^{i\omega t},e^{-i\omega t})f''(0)(e^{0t},e^{i\omega t})\Delta(0)^{-1}\begin{bmatrix}1\\1\end{bmatrix}\\ &+ \frac{1}{2}q_0\begin{bmatrix}1&1\end{bmatrix}f''(0)(e^{i\omega t},e^{i\omega t})f''(0)(e^{2i\omega t},e^{-i\omega t})\Delta(2i\omega)^{-1}\begin{bmatrix}1\\1\end{bmatrix}.\end{aligned} \tag{3.26}$$

Evaluation of the differential operators and the matrix inversions yields:

$$c_1 = q_0\Bigg(-S'''(0)(\alpha_1\beta_1^3 e^{-i\omega\tau_1} - \alpha_2\beta_2^3 e^{-i\omega\tau_2}) + \frac{2S''(0)^2(\alpha_1\beta_1^2 - \alpha_2\beta_2^2)(\alpha_1\beta_1^2 e^{-i\omega\tau_1} - \alpha_2\beta_2^2 e^{-i\omega\tau_2})}{1+\alpha_1\beta_1 - \alpha_2\beta_2} + \frac{S''(0)^2(\alpha_1\beta_1^2 e^{-2i\omega\tau_1} - \alpha_2\beta_2^2 e^{-2i\omega\tau_2})(\alpha_1\beta_1^2 e^{-i\omega\tau_1} - \alpha_2\beta_2^2 e^{-i\omega\tau_2})}{1+2i\omega+\alpha_1\beta_1 e^{-2i\omega\tau_1} - \alpha_2\beta_2 e^{-2i\omega\tau_2}}\Bigg). \quad (3.27)$$

As the real part of this expression is too intricate to study analytically, we study the first Lyapunov coefficient only numerically.

In Figure 3.2, we observe that, for chosen parameter $\tau_1 = 11.6$ and $\tau_2 = 20.3$, the stability region is primarily bounded by the curve $\mathbf{h}_-(\omega)$ and so we study the Lyapunov coefficient along this boundary. Similarly as in [125], we choose $\beta_1 = 2$, $\beta_2 = 1.2$ and

$$S(x;a) = (\tanh(x-a) + \tanh(a))\cosh^2(a), \quad (3.28)$$

with $a = 1$. Values of α_1 and α_2 are parameterized along the boundary using (3.7) and (k_1,k_2) given by $\mathbf{h}_-(\omega)$ with $\omega \in \Omega_S(\mathbf{h}_-)$. In this case, we find that the first Lyapunov coefficient has a root at:

$$\mathbf{k}_{GH} := \mathbf{h}_-(0.281) = \begin{bmatrix} 0.491 \\ 0.614 \end{bmatrix}. \quad (3.29)$$

Such a root corresponds with a generalized Hopf bifurcation at which the criticality of the Hopf bifurcation changes. Hence, for $\omega < 0.281$, the Hopf bifurcations are supercritical and for $\omega > 0.281$ the bifurcations are subcritical.

So far, we have studied the fixed points and their bifurcations extensively, and we have shown that the system can exhibit stable periodic solutions. Since the further development of these periodic solutions cannot be studied with a local analysis of points, we must use a different approach to continue this study. Therefore, we explore the behavior of the periodic solutions numerically in the next section.

3.3 Numerical bifurcation analysis

Here, we investigate the outcome of the periodic solutions that emanate from the Hopf bifurcations in the above text. We turn to a numerical analysis since the orbits cannot be determined analytically. More specifically, we use DDE-BIFTOOL [46] to study non-trivial fixed points, and for continuation of periodic solutions, we use Knut [101]. In the following analysis, we only describe branches of solutions that are by some means associated with stable solutions. Branches not resulting in stable solutions are not discussed further.

3.3.1 One parameter bifurcations in α_2

First, a bifurcation analysis is done in a single parameter. Here, we have chosen to vary the parameter α_2 that represents the total amount of excitation in the system. The inhibition α_1 is fixed at 0.069, and the function S is chosen as (3.28) with $a = 1$.

The bifurcation diagram is shown in Figure 3.4, and corresponding parameter values for the bifurcations are shown in Table 3.1. Each curve represents, for different solutions, the maximum value reached during one period of the solution at different parameter values. The color corresponds with the type of solution, while thick/thin lines correspond to stable/unstable branches.

Table 3.1 Overview of approximate parameter values for codim-1 bifurcations in α_2. Parameter α_1 is fixed at 0.069.

Point	α_2
H_1	0.771
B_1	0.948
F_1	0.5211
H_2	0.5212
H_3	0.5212
H_4	1.052
PD_1	0.650
LPC_1	0.462
PD_2	0.465
PD_3	0.596
LPC_2	0.615
PD_4	0.522
LPC_3	0.464
LPC_4	0.619

3.3.1.1 Fixed points

The origin is a natural starting point of our discussion of the bifurcation analysis because it is always a fixed point of (3.4). The origin is stable until it undergoes a subcritical Hopf bifurcation H_1. Thereafter, it goes through two other Hopf bifurcations and a branch point B_1. For this value of α_1, these Hopf bifurcations involve only unstable periodic solutions.

Next, we follow the fixed point that emerges from the branch point B_1. This fixed point encounters numerous Hopf bifurcations until it reaches a fold bifurcation F_1. Thereafter, it rapidly undergoes two distinct subcritical Hopf bifurcations: H_2 and H_3, becoming stable at H_3. Continuing the intersecting fixed point at B_1 in the other direction, the steady state goes

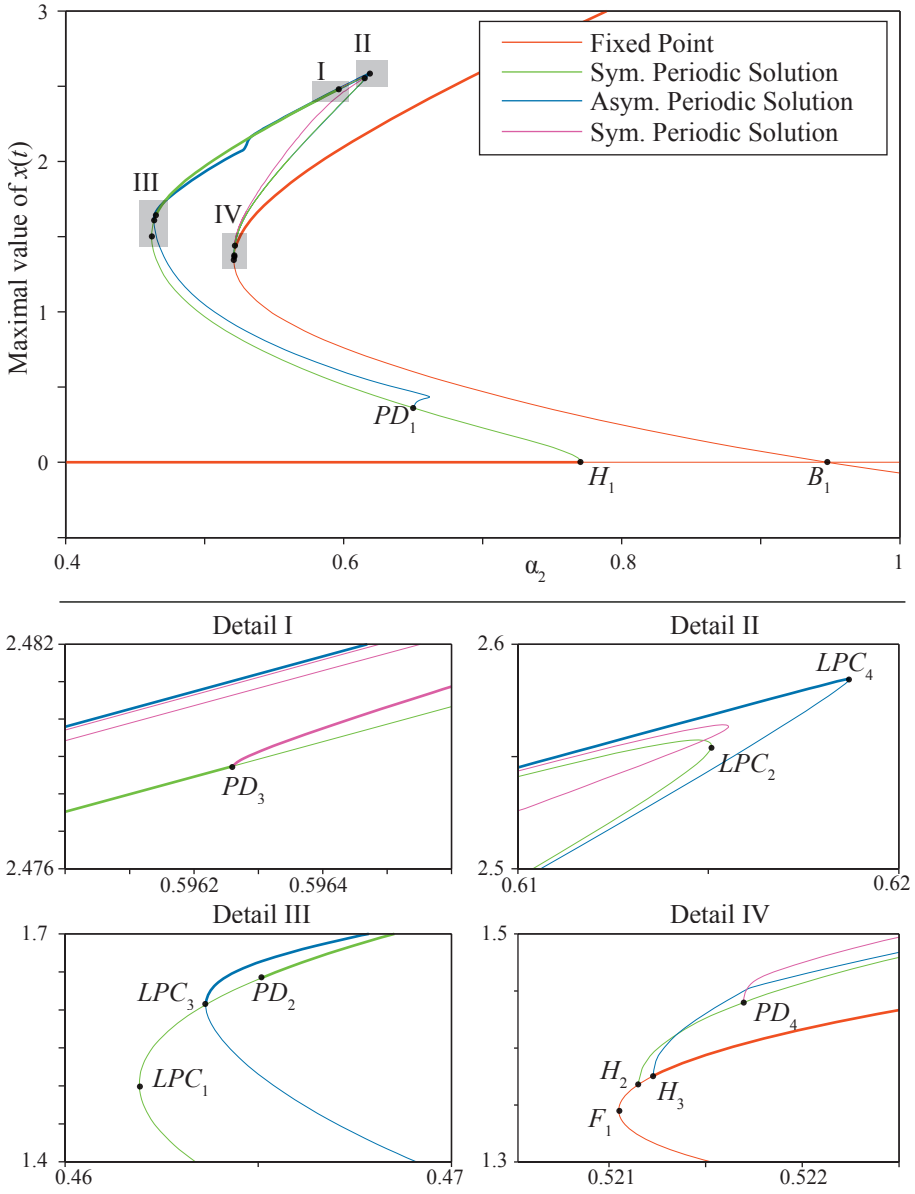

Fig. 3.4 Bifurcations in one parameter. The top shows the bifurcation diagram in α_2. Different colors represent different solutions, and a thick/thin line indicates that such a solution is stable/unstable. The four diagrams at the bottom show details of the four marked regions in the top diagram. $\tau_1 = 11.6, \tau_2 = 20.3, \alpha_1 = 0.069, \beta_1 = 2, \beta_2 = 1.2$.

through two Hopf bifurcations until it gains stability at the subcritical Hopf bifurcation H_4 (not shown).

The appearance of Hopf bifurcations for fixed points is detailed in the 'Bifucations'section and Figure 3.2. If the trivial fixed point is considered, the variation of a single parameter maps the coefficients k_1 and k_2 into a straight line (3.7). This line, labeled E_T, is shown in the k_1, k_2-plane in Figure 3.5. The coefficients k_1 and k_2 belonging to non-trivial equilibria, however, vary in a more complex manner when a single parameter is adjusted. Once plotted, it becomes clear that this branch encounters 18 Hopf bifurcations between departure from and return to the stability region for this specific value of α_1 (see the curve E_N in Figure 3.5).

Whether a Hopf bifurcation is caused by a crossing of Δ_- or Δ_+ determines whether this Hopf bifurcation results in symmetric or asymmetric periodic solutions. Hence, we conclude that Hopf bifurcations H_1, H_2 and H_4 yield symmetric periodic solutions, and that H_3 yields asymmetric ones.

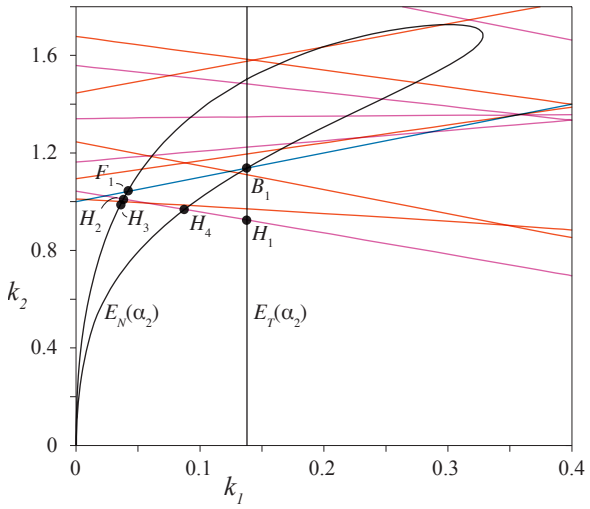

Fig. 3.5 Mapping to (k_1, k_2)-plane. The curves $E_T(\alpha_2)$ and $E_N(\alpha_2)$ show the parametrization of the origin (trivial fixed point) and non-trivial fixed points, respectively, for fixed α_1. This figure illustrates how some solution branches can regain stability after encountering numerous bifurcations. Blue, fold/transcritical; red, asymmetric Hopf; magenta, symmetric periodic solution; black, parametrization of fixed points.

3.3.1.2 Periodic solutions

Next, we investigate the periodic solutions emanating from the Hopf bifurcations H_1, H_2 and H_3. The branch of unstable periodic solutions that emerges from H_1 consists of symmetric solutions. This matches with the analytical results since H_1 lies on $\mathbf{h}_-$ and it,

therefore, corresponds with symmetric solutions. The branch subsequently goes through a subcritical Neimark-Sacker bifurcation (not shown), a supercritical period-doubling bifurcation PD_1, a limit point of cycles LPC_1 and a subcritical period-doubling bifurcation PD_2 at which it finally becomes stable. Then, the solution remains stable until it undergoes a supercritical period doubling bifurcation PD_3, folds over in LPC_2, goes through a subcritical period doubling bifurcation PD_4 and terminates in the Hopf bifurcation H_2.

Solutions branching from PD_1 are asymmetric. This branch folds over near PD_1 and a second time at LPC_3 where it gains stability. Following this branch, stability is lost at LPC_4 and it ends in Hopf bifurcation H_3. We mention a branch sprouting from PD_3 of symmetric solutions that is initially stable but then folds over three times before it terminates in PD_4. Even though these solutions are initially stable, we have been unable to find these solutions in simulations because their domain of attraction is relatively small.

3.3.1.3 Summary

For fixed α_1, we find that system can have one or two stable steady states. More specifically, for values of α_2 between H_3 and H_1, two stable equilibria coexist. Stable symmetric periodic solutions exist for α_2 between PD_2 and PD_3, and stable asymmetric periodic solutions between LPC_3 and LPC_4. Multi-stability of two equilibria and two periodic solutions exists for α_2 between H_3 and PD_3. This is illustrated in Figure 3.6 where we calculated time series of the model with fixed parameters ($\alpha_2 = 0.55$) but varying initial conditions:

$$[x_1, x_2](t) = [0, 0.1], \tag{3.30a}$$

$$[x_1, x_2](t) = [1.5, 1.7], \tag{3.30b}$$

$$[x_1, x_2](t) = \left[1 + 1.2\sin\left(\frac{2\pi}{15}t\right), 0.8 + 1.3\sin\left(\frac{2\pi}{15}t\right)\right], \tag{3.30c}$$

$$[x_1, x_2](t) = \left[0.7 + 0.7\sin\left(\frac{\pi}{30}t\right), 0.6 - 0.9\sin\left(\frac{\pi}{30}t\right)\right], \tag{3.30d}$$

with $-20.3 \leq t \leq 0$. All four types of limiting behavior, as determined by the preceding bifurcation analysis, are observed.

3.3.2 Two parameter bifurcations in α_1 and α_2

As stated before, we are mainly interested in the bifurcations at which stable solutions become unstable. These bifurcations (found with a one parameter analysis) are, therefore, continued in two parameters (α_1 and α_2). Figure 3.7 shows the relevant part of the bifurcation diagram of the system and Table 3.2 presents parameter values of the indicated bifurcation points. A small detail is magnified, but it shows a caricature of the complex

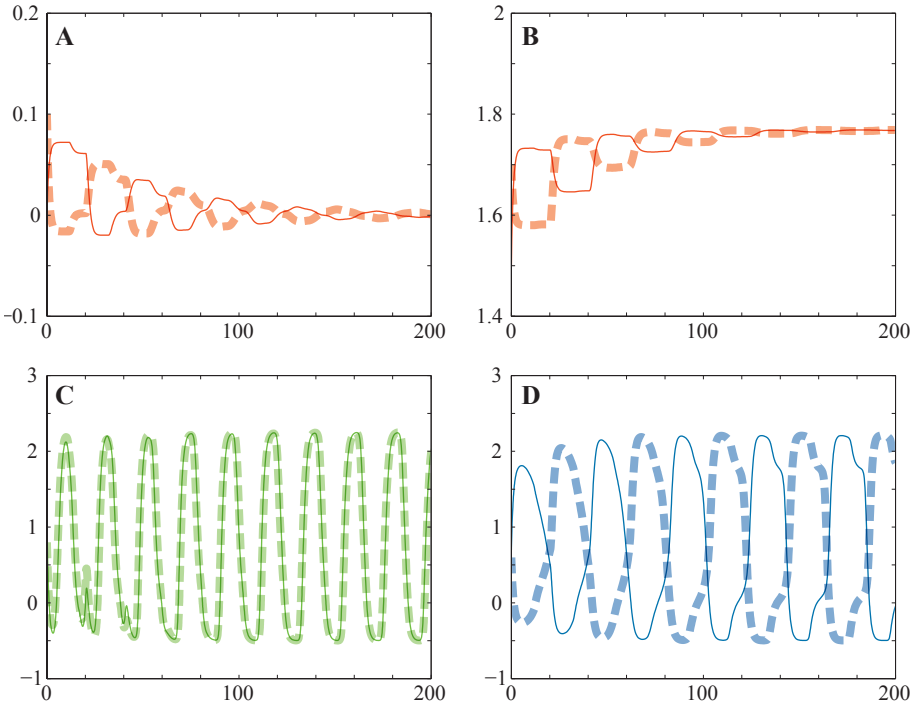

Fig. 3.6 Time series in multi-stable regime. Time series of the system for $\alpha_2 = 0.55$, other parameters as in Figure 3.4 and initial conditions given by (3.30). Solid and dashed lines correspond with x_1 and x_2. Solutions of all four stable branches are obtained: (**A**) trivial steady state, (**B**) non-trivial steady state, (**C**) symmetric periodic solutions and (**D**) asymmetric periodic solutions. Colors of these time series correspond with the branches in Figure 3.4.

structure. Mixed colors are used to indicate the co-existence of multiple stable solutions, but for clarity, we also show the stability regions for each type of solution separately in Figure 3.8.

3.3.2.1 Steady states

In the one-parameter analysis, we have found that the origin and the non-trivial steady state turn unstable at Hopf bifurcations H_1 and H_3, respectively. Continuing H_1 in two parameters yields a Hopf bifurcation curve, and on this curve, we find a Hopf-Hopf bifurcation HH_1. Following the second Hopf branch (H_5) involved, we find a transcritical-Hopf point ZH_1 as it collides with B_1. This corresponds with the analysis of 'Bifurcations' section where we showed the existence of zero-Hopf and Hopf-Hopf points; see (3.22) and (3.23)). The arrangement of these curves is the same as in Figure 3.3 except for scaling. Since all involved Hopf curves at the points HH_1 and ZH_1 are subcritical, it follows then

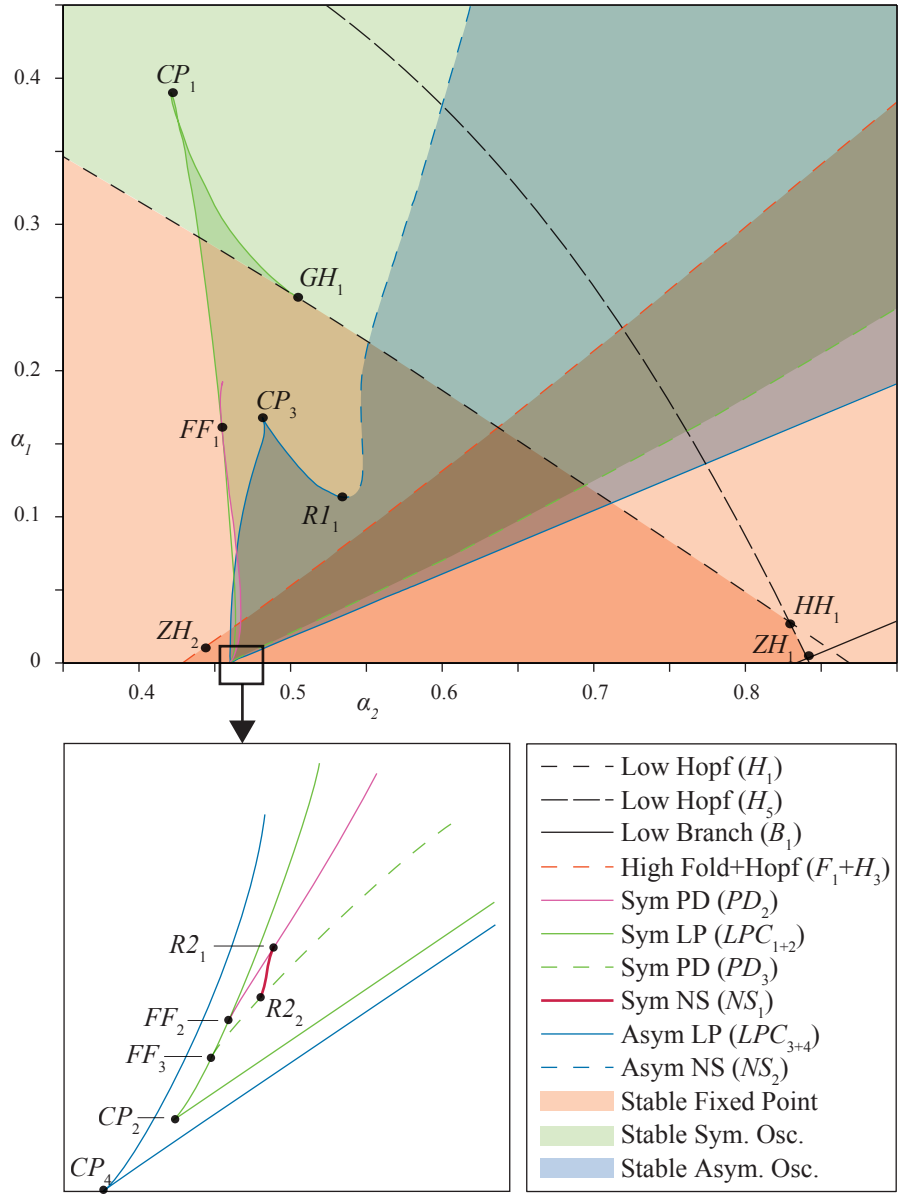

Fig. 3.7 Bifurcations in two parameters. Bifurcation diagram in α_1 and α_2. Colored regions mark stability regions of indicated solutions. Overlapping areas, depicted with mixed colors, correspond with multistability. See text for a description of the points. Stability regions for individual solutions are shown in Figure 3.8 for clarity.

from the normal form analysis [74] that, for these parameters, no extra stable solutions exist near these points. Our analysis of the first Lyapunov coefficient also revealed the ex-

Table 3.2 Overview of approximate parameter values for codim-2 bifurcations in α_1 and α_2.

Point	α_2	α_1
HH_1	0.829	0.028
ZH_1	0.840	0.004
GH_1	0.512	0.246
ZH_2	0.440	0.008
FF_1	0.455	0.158
$R2_1$	0.460	2.9e-4
FF_2	0.460	2.8e-4
$R2_2$	0.460	2.9e-4
FF_3	0.460	2.8e-4
CP_1	0.421	0.390
CP_2	0.460	2.8e-4
CP_3	0.481	0.168
$R1_1$	0.531	0.114
CP_4	0.460	0

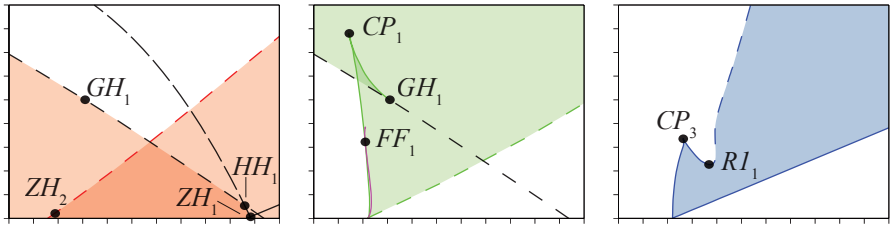

Fig. 3.8 Regions of multi-stability. Identical to Figure 3.7, but showing the stability regions of each type of solution separately. Two partially overlapping 'triangles' corresponding with stability of fixed points (left), stability region for symmetric periodic solutions with a small area of bistability caused by cusp point CP_1 (middle), and region in parameter space where stable asymmetric periodic solutions exist (right).

istence of a generalized Hopf bifurcation; see (3.29). We numerically identify this point GH_1 along the branch of H_1 by finding an emanating branch of limit point of cycles LPC_1 with Knut. When the Hopf bifurcation H_3 of the non-trivial equilibrium is followed, a zero-Hopf bifurcation ZH_2 is found as H_3 collides with fold bifurcation F_1. We remark that the curves H_3 and F_1 are undistinguishable in the diagram since they are close to each other for all (α_1, α_2) considered. The bifurcation ZH_2 is a simple case ([74], $s = 1, \theta > 0$), yielding no additional stable solutions. These curves and the corresponding stability regions are shown in Figures 3.7 and 3.8. Bi-stability is indicated by the overlapping, darker region.

3.3.2.2 Symmetric periodic solutions

The stability region of the symmetric periodic solutions is bounded by PD_2 and PD_3. Continuation of PD_2 for stronger inhibition reveals a fold-flip bifurcation FF_1 where the period doubling bifurcation hits LPC_1 branch. Thereafter, it bends away and terminates. Continuing the LPC_1 curve in the same direction, we first find a cusp point CP_1 after which the curve ends in the generalized Hopf bifurcation GH_1. When PD_2 is continued in the other direction (less inhibition), it undergoes a 1:2-resonance bifurcation $R2_1$ (i.e., the period doubling branch encounters a period-doubling), and thereafter, it is subjected to a fold-flip bifurcation FF_2 with LPC_1. Following the LPC_1 curve at FF_2, we encounter another fold-flip bifurcation FF_3 and a cusp bifurcation CP_2. At this cusp point, the branch merges with LPC_2. The branch PD_3 does not undergo any bifurcation when continued for stronger inhibition. Continuation in the other direction reveals a 1:2-resonance bifurcation $R2_2$ and the previously identified fold-flip bifurcation FF_3. Unfolding the 1:2-resonance bifurcations $R2_1$ and $R2_2$ reveals that both points are connected by the curve NS_1 of Neimark-Sacker bifurcations. Therefore, this curve is also part of the boundary of the stability region of symmetric periodic solutions. From the unfolding of these 1:2-resonance bifurcations, we know that branches of stable homoclinic orbits should exist. However, we have been unable to continue these branches.

3.3.2.3 Asymmetric periodic solutions

From single parameter continuation, it follows that stable asymmetric oscillations are bounded by LPC_3 and LPC_4. Continuation of LPC_3 yields a cusp point CP_3 and a 1:1-resonance bifurcation $R1_1$ at which the branch becomes unstable. Hereafter, the stability region is bounded by a branch of Neimark-Sacker bifurcations NS_2 that sprouts from $R1_1$. When LPC_3 is continued in the other direction, it undergoes a cusp bifurcation (CP_4) at $\alpha_1 = 0$ where LPC_3 merges with LPC_4.

3.3.2.4 Summary

With the two-parameter bifurcation analysis, we find that a large part of parameter space corresponds with multi-stability. In the center, we find a region with four different stable solutions: two steady states and two periodic solutions. Furthermore, it can be seen that steady states destabilize for strong values of inhibitory feedback (α_1 large) since only periodic solutions exist in the upper part of the bifurcation diagram.

3.3.3 Comparison with a realistic model

As this two-parameter bifurcation study might seem contrived for a fairly simple model, we like to make a comparison with a study of a more biologically realistic model. Van Drongelen *et al.* analyzed a small model of neocortex consisting of 656 neurons to study emergent epileptiform activity [113]. For similar reasons as in this study, they varied only parameters related to excitatory and inhibitory synaptic strength, and they then obtained Figure 3.9. In this figure, the behavior of their realistic model for different choices of parameters is categorized in one of five categories: desynchronized, irregular bursting, oscillatory, regular bursting and saturated activity. The small exemplary time series show for each class the characteristic behavior of the model except for saturated activity. This latter state is best described as a state in which all neurons are non-stop activated in an incoherent manner.

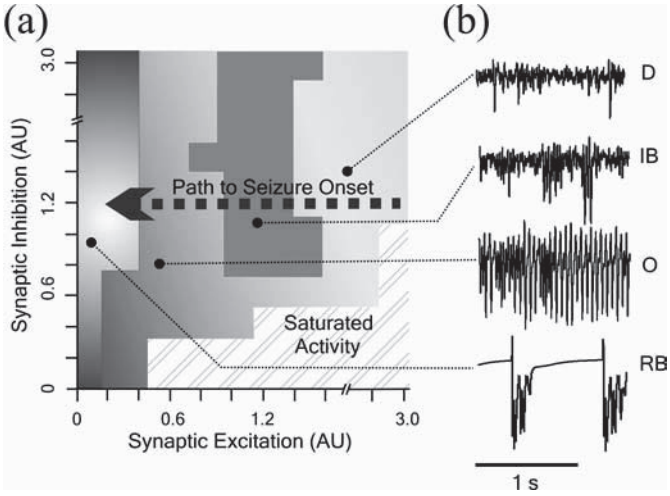

Fig. 3.9 Behavior of a detailed network. This figure, copied with permission from [113], shows the behavioral changes of a large physiologically detailed model of neocortex. For varying strengths of excitatory and inhibitory connections, the model's behavior is classified in one of five categories. See text for a description of the network states and their correspondence to the population model.

In the regular bursting state, the model is rather quiet apart from a burst of activity that occurs regularly about every second. These bursts are primarily generated by slow dynamical processes in the underlying neurons. In the absence of slow processes, the network would exhibit no activity in this state [113]. Hence, this type of behavior should be compared with the trivial steady state of our model. Furthermore, the non-trivial steady state in our simplified model corresponds with saturated activity in the detailed model because the network is very active, but no clear oscillations or rhythms are observed. Finally, the

oscillatory state can be compatible with both the symmetric and asymmetric periodic solutions in our model. With these analogues for the observed types of network behavior in our mind, the bifurcation diagram in Figure 3.7 displays several strong similarities with the detailed network model in Figure 3.9. For low excitation, both models exhibit regular bursting/trivial steady-state solutions. Furthermore, we see in both cases a triangular region at the bottom in which both models exhibit saturated/non-trivial steady-state solutions. Finally, we observe that the above-mentioned regions are separated by a regime of oscillatory solutions. We also note that not all types of behavior in the detailed model have a counterpart in the simplified model, but we will elaborate on this in the discussion.

3.4 Discussion

In this paper, we have studied a continuous time two-node Hopfield network with two discrete time delays. The model has been derived in [125], and it describes the activity of two excitatory neural populations located in different layers of the mammalian neocortex. Inhibitory connections are assumed to exist only between neurons within the same population, whereas excitatory connections are exclusively made between both populations. Furthermore, a bifurcation study in the same article has shown that the model is able to produce different types of behavior that correspond to a realistic 656-neuron model of neocortex as proposed in [112]. This detailed model is able to reproduce phenomena observed in *in vitro* experiments in mouse [113]. By studying the population model more thoroughly, we hope to gain a better understanding of the complex dynamics seen in the realistic 656-neuron model. In this way, new experiments for both *in silico* and *in vitro* environments can be proposed.

Even though Hopfield networks of this and similar forms have been studied thoroughly in other works, these works mainly consider changes of the dynamics under variation of the time delays. As the time lags in our model are fixed because of the physiological background, we are mainly interested in the dynamics' dependency on connectivity parameters. As a new contribution to this field, we have focused our study of the model on varying connection strengths of excitatory and inhibitory connections.

All the bifurcations that we have identified in the model, both analytically and numerically, satisfied the non-degeneracy condition. Combined with the fact that the model depends smoothly on all parameters, all these bifurcations are structural. Hence, local variations of parameters will result in local variations of the bifurcations and the stability region. Some of the delicate bifurcation structures that we identified will be more sensitive to parameter variations, but only because of their limited separation in parameter space.

For the steady states in the model, we have analytically determined conditions in terms of the coupling parameters for which these states become unstable due to bifurcations.

We have found that both the trivial and the non-trivial equilibria undergo fold as well as Hopf bifurcations. The non-trivial equilibria, however, are the solution of a transcendental equation, and therefore, we have studied these bifurcations numerically. In this manner, we have identified a region in parameter space of bi-stability in which both the trivial and a non-trivial fixed point are stable.

By studying the first Lyapunov coefficient at the Hopf bifurcations in the system, we have found both supercritical and subcritical bifurcations. Furthermore, we have analytically determined the type of bifurcating periodic solution, either symmetric (in-phase) or asymmetric (anti-phase) oscillations. The evolution of the periodic solutions arising at the Hopf bifurcations is studied numerically with continuation software. A large region in parameter space is determined in which both types of periodic solutions co-exist. Furthermore, we have identified numerous codim-2 bifurcations: cusp, generalized Hopf, zero-Hopf, Hopf-Hopf, fold-flip and both 1:1 and 1:2 resonance bifurcations. In the area where bistability exists between these different solutions, simulations have shown that the solutions often tend to the asymmetric solutions.

Combining the stability regions of the steady states and the periodic solutions, we have found a region in parameter space in which four types of stable solutions co-exist: the trivial fixed point, a non-trivial fixed point and both symmetric and asymmetric periodic solutions. Although it has been shown in [83] that small Hopfield networks can exhibit chaotic behavior, we have not found such behavior in this study.

The biological relevance of these results is, in our opinion, significant as well. We have shown that the complex bifurcation structure of the model matches with the dynamical changes seen in a biologically relevant model for variations of both excitatory and inhibitory strengths [113]. This relation is most clear for the regular bursting, oscillatory and saturated states of the detailed model because these have a clear equivalent attractor in the population model studied in this article. The other states of the detailed network, however, might be produced by the population model as part of a transient behavior.

Although the considered model has very little resemblance with the structures of a real brain, we still believe that studying models like these provide new insights. Complex bifurcation structures and multi-stability observed in these models reveal possible transitions of network behavior that might not have been considered before. For that reason, we plan to seek and analyze such critical transitions more accurately with a detailed model of neuronal activity.

Furthermore, we plan to investigate networks of similar systems in order to study emergent patterns. It is promising that the combined analytical/numerical study of a single column already shows interesting dynamics, in particular, multi-stability. We expect to find patterns in such networks that will be relevant to understand observed patterns in slice experiments.

Chapter 4
On neural fields with transmission delay

Abstract Neural field models with transmission delay may be cast as abstract delay differential equations (DDE). The theory of dual semigroups (also called sun-star calculus) provides a natural framework for the analysis of a broad class of delay equations, among which DDE. In particular, it may be used advantageously for the investigation of stability and bifurcation of steady states. After introducing the neural field model in its basic functional analytic setting and discussing its spectral properties, we elaborate extensively an example and derive a characteristic equation. Under certain conditions the associated equilibrium may destabilise in a Hopf bifurcation. Furthermore, two Hopf curves may intersect in a double Hopf point in a two-dimensional parameter space. We provide general formulas for the corresponding critical normal form coefficients, evaluate these numerically and interpret the results[1].

4.1 Introduction

Spatial coarse graining of neural networks leads to so-called neural field models in which the average firing rates of underlying populations of neurons, as opposed to individual neuronal spikes, are considered. Such models have not changed substantially since the seminal work of Wilson and Cowan [132, 133], Amari [2] and Nunez [94]. Due to intrinsic delays of axons, synapses, and dendrites in the natural system, the role of delays in spatiotemporal dynamics of neural activity has received considerable attention [80, 67, 65, 102, 123, 66, 64, 32, 30, 29]. Faugeras and coworkers investigated stability properties of stationary solutions using methods from functional analysis [120, 50, 121]. A first step towards Hopf bifurcation is made in [119], where Hopf bifurcation curves are

[1] Adapted from SA van Gils, SG Janssens, YuA Kuznetsov and S Visser, *On local bifurcations in neural field models with transmission delays*, Journal of Mathematical Biology, to appear.

computed. In [47] the principle of linearised stability and the Hopf bifurcation to periodic orbits were studied in the absence of delays.

To set the stage, we have in mind $p \geq 1$ populations consisting of neurons that occupy fixed positions in a non-empty, bounded, connected, open region $\Omega \subset \mathbb{R}^n$. For each $i = 1,\dots,p$ let $V_i(t,\mathbf{r})$ be the membrane potential at time t, averaged over those neurons in the ith population positioned at $\mathbf{r} \in \Omega$. These potentials are assumed to evolve in the absence of time dependent external stimuli according to the system of integro-differential equations

$$\frac{\partial V_i}{\partial t}(t,\mathbf{r}) = -\alpha_i V_i(t,\mathbf{r}) + \sum_{j=1}^{p} \int_\Omega J_{ij}(\mathbf{r},\mathbf{r}') S_j(V_j(t-\tau_{ij}(\mathbf{r},\mathbf{r}'),\mathbf{r}'))\, d\mathbf{r}' \tag{4.1}$$

for $i = 1,\dots,p$. The intrinsic dynamics exhibit exponential decay with $\alpha_i > 0$ for $i = 1,\dots,p$. The propagation delays $\tau_{ij}(\mathbf{r},\mathbf{r}')$ measure the time it takes for a signal sent by a type-j neuron located at position $\mathbf{r}'$ to reach a type-i neuron located at position $\mathbf{r}$. For the definitions and interpretation of the real valued connectivities J_{ij} and the positive, real valued synaptic activation functions S_j appearing in (4.1) we refer to §2 of [121].

The aim of this paper is to demonstrate how general theory from the field of delay equations can be used successfully to analyse stability and bifurcation of equilibrium solutions of (4.1). For this we consider a specific class of delay equations of the form

$$\begin{cases} \dot{x}(t) = F(x_t) & t \geq 0 \\ x(t) = \phi(t) & t \in [-h,0] \end{cases} \tag{DDE}$$

where Y is a Banach space, $F : C([-h,0];Y) \to Y$ is a smooth Y-valued function on the Banach space of continuous Y-valued functions equipped with the supremum norm,

$$x_t(\theta) := x(t+\theta) \quad \forall t \geq 0,\, \theta \in [-h,0]$$

is the *history* at time $t \geq 0$ and $\phi \in C([-h,0];Y)$ is an initial condition. The parameter $h \in (0,\infty)$ is a *finite* delay. As the reader may have expected, the acronym DDE stands for *delay differential equation*.

Systems of this type naturally extend the case of *classical* DDE with $Y = \mathbb{R}^n$ for which a rather complete dynamical theory based on perturbative calculus of dual semigroups [24], [25], [26], [27], [40] is available in [41]. Recently it was understood that, from an abstract viewpoint, various apparently different classes of delay equations can be cast and analysed within the same functional analytic framework of dual perturbation theory, largely independently of the particulars of a certain class. It is only in the choice of the underlying function spaces and the spectral analysis that these details matter. In [37] purely functional equations (also called renewal equations) as well as systems of renewal equations coupled to delay differential equations are investigated for the $\mathbb{R}^n$-valued case and finite delay. In [39] the analysis is extended to the case of infinite delay. In [38] abstract (Banach space

valued) renewal equations with infinite delay are considered. The forthcoming paper [117] treats general aspects of abstract equations of the type (DDE).

The outline of this paper is as follows: in §4.2 we introduce the functional analytic setting and state the equivalence between the abstract delay equation and an abstract integral equation using sun-star calculus. We also state a linearization theorem. In §4.3 we start with some general results on the resolvent and spectra, primarily based on [45]. For a specific class of connectivity functions, i.e. finite sums of exponentials, and in one spatial dimension, we explicitly calculate the spectrum and the resolvent. It turns out that the point spectrum is determined by a determinant condition. In §4.4 we give the normal form coefficients for the critical center manifold in case of Hopf and double Hopf bifurcation. This is applied in §4.5 to a scalar neural field equation with a bi-exponential connectivity function modelling an inverted Wizard hat. The system is discretised as in [50] and the spectrum of the discretised system is compared with the true spectrum, showing convergence. We identify in the true spectrum a Hopf point and a double Hopf point. For both cases the normal form coefficients are computed, which allows us to identify the sub-type of the bifurcation at hand. The theoretical results are confirmed by numerical experiments. We end this paper in §4.6 with conclusions and an outlook on future work.

Upon finishing this paper we encountered the online preprint [122], addressing similar questions. We feel that there are enough substantial differences between the two papers to render both of them interesting. Moreover, we have reasons to believe that the choice $Y = L_2(\Omega)$ for the spatial state space made in [122] leads to non-trivial technical complications, see §4.2.4 below. In this paper, we employ sun-star calculus, from which a number of general results is immediately available. The center manifold, for instance, was obtained in [41] for the abstract integral equation, covering what we need here.

4.2 Functional analytic setting

4.2.1 Basic definitions and assumptions

It is rather straightforward to associate with (4.1) a problem of the type (DDE), but see §4.2.4. To keep the setting as simple as possible, we focus on the single population case $p = 1$ when (4.1) takes the form

$$\frac{\partial V}{\partial t}(t,\mathbf{r}) = -\alpha V(t,\mathbf{r}) + \int_\Omega J(\mathbf{r},\mathbf{r}')S(V(t-\tau(\mathbf{r},\mathbf{r}'),\mathbf{r}'))\,d\mathbf{r}' \tag{4.2}$$

For mathematical convenience we extend the spatial domain Ω by its boundary $\partial\Omega$ and work on $\overline{\Omega} \equiv \Omega \cup \partial\Omega$ with Lebesgue measure $|\overline{\Omega}| < \infty$. We formulate a number of basic hypotheses on the modelling functions appearing in (4.2). These will be tacitly assumed to

hold throughout the remainder of this paper. More specific functional forms will be chosen in subsequent sections.

(H_J) The **connectivity kernel** $J \in C(\overline{\Omega} \times \overline{\Omega})$.

(H_S) The **synaptic activation function** $S \in C^\infty(\mathbb{R})$ and its kth derivative is bounded for every $k \in \mathbb{N}_0$.

(H_τ) The **delay function** $\tau \in C(\overline{\Omega} \times \overline{\Omega})$ is non-negative and not identically zero.

From (H_τ) we see that τ is bounded on the compact set $\overline{\Omega}$. Hence we may set

$$0 < h := \sup\{\tau(\mathbf{r}, \mathbf{r}') : \mathbf{r}, \mathbf{r}' \in \overline{\Omega}\} < \infty$$

Let $Y := C(\overline{\Omega})$ be the Banach space of continuous real-valued functions on $\overline{\Omega}$ with norm

$$\|y\| := \sup_{\mathbf{r} \in \Omega} |y(\mathbf{r})|,$$

We also set $X := C([-h, 0]; Y)$. When $\phi \in X$, $t \in [-h, 0]$ and $\mathbf{r} \in \Omega$ we will sometimes abuse notation and write $\phi(t, \mathbf{r})$ instead of $\phi(t)(\mathbf{r})$. On X we have the norm

$$\|\phi\| := \sup_{t \in [-h,0]} \|\phi(t, \cdot)\|$$

Define the nonlinear operator $G : X \to Y$ by

$$G(\phi)(\mathbf{r}) = \int_{\overline{\Omega}} J(\mathbf{r}, \mathbf{r}') S(\phi(-\tau(\mathbf{r}, \mathbf{r}'), \mathbf{r}'))\, d\mathbf{r}' \quad \forall \phi \in X, \forall \mathbf{r} \in \overline{\Omega} \tag{4.3}$$

The following lemma is standard, but in light of the difficulties pointed out in §4.2.4 we provide a detailed proof.

Lemma 4.1. *$G : X \to Y$ is well-defined by* (4.3).

Proof. Obviously, for any $\phi \in X$ the map

$$[-h, 0] \times \overline{\Omega} \ni (t, \mathbf{r}) \mapsto \phi(t, \mathbf{r}) \in \mathbb{R} \tag{4.4}$$

is continuous.

Now, given $\phi \in X$ we consider for points $\mathbf{r}, \bar{\mathbf{r}} \in \overline{\Omega}$,

$$\begin{aligned}
|G(\phi)(\mathbf{r}) - G(\phi)(\bar{\mathbf{r}})| \leq & \left| \int_{\overline{\Omega}} [J(\mathbf{r}, \mathbf{r}') - J(\bar{\mathbf{r}}, \mathbf{r}')] S(\phi(-\tau(\mathbf{r}, \mathbf{r}'), \mathbf{r}'))\, d\mathbf{r}' \right| \\
& + \left| \int_{\overline{\Omega}} J(\bar{\mathbf{r}}, \mathbf{r}') [S(\phi(-\tau(\mathbf{r}, \mathbf{r}'), \mathbf{r}')) - S(\phi(-\tau(\bar{\mathbf{r}}, \mathbf{r}'), \mathbf{r}'))]\, d\mathbf{r}' \right| \\
\leq & C_S \int_{\overline{\Omega}} |J(\mathbf{r}, \mathbf{r}') - J(\bar{\mathbf{r}}, \mathbf{r}')|\, d\mathbf{r}' \\
& + C_J \int_{\overline{\Omega}} |S(\phi(-\tau(\mathbf{r}, \mathbf{r}'), \mathbf{r}')) - S(\phi(-\tau(\bar{\mathbf{r}}, \mathbf{r}'), \mathbf{r}'))|\, d\mathbf{r}'
\end{aligned}$$

where $C_S > 0$ and $C_J > 0$ are constants bounding S and J. Let $\varepsilon > 0$ be given. By the uniform continuity of J on $\overline{\Omega} \times \overline{\Omega}$ there exists $\delta_J > 0$ such that the first integral does not exceed $|\overline{\Omega}|\varepsilon$ for all $\mathbf{r}, \bar{\mathbf{r}} \in \overline{\Omega}$ satisfying $|\mathbf{r} - \bar{\mathbf{r}}| \leq \delta_J$. Regarding the second integral, the continuity of (4.4) and (H_τ) implies the continuity of

$$\overline{\Omega} \times \overline{\Omega} \ni (\mathbf{r}, \mathbf{r}') \mapsto \phi(-\tau(\mathbf{r}, \mathbf{r}'), \mathbf{r}') \in \mathbb{R} \tag{4.5}$$

Let $I \subset \mathbb{R}$ be a compact interval containing the range of (4.5). Then S is uniformly continuous on I. Hence there exists $\delta_S > 0$ such that $|S(u) - S(v)| \leq \varepsilon$ for all $u, v \in I$ satisfying $|u - v| \leq \delta_S$. Since (4.5) is uniformly continuous, there exists $\delta' > 0$ such that $|\mathbf{r} - \bar{\mathbf{r}}| \leq \delta'$ implies $|\phi(-\tau(\mathbf{r}, \mathbf{r}'), \mathbf{r}') - \phi(-\tau(\bar{\mathbf{r}}, \mathbf{r}'), \mathbf{r}')| \leq \delta_S$ for all $\mathbf{r}' \in \overline{\Omega}$. Consequently, if $|\mathbf{r} - \bar{\mathbf{r}}| \leq \delta'$ then the second integral does not exceed $|\overline{\Omega}|\varepsilon$.

Using the definition (4.3) of the operator G, we see that studying (4.2) is equivalent to analyzing the following initial value problem

$$\begin{cases} \dot{V}(t) = -\alpha V(t) + G(V_t) & t \geq 0 \\ V(t) = \phi(t) & t \in [-h, 0] \end{cases} \tag{NF}$$

where $V : [-h, \infty) \to Y$ is the unknown and $\phi \in X$ is the initial condition. Then (NF) is of the form (DDE) when we define $F : X \to Y$ by

$$F(\phi) := -\alpha\phi(0) + G(\phi) \qquad \forall \phi \in X \tag{4.6}$$

with G given by (4.3). The notion of a solution of (DDE), and consequently (NF), is a direct generalisation of the solution concept for classical DDE.

Definition 4.2. A function $x \in C([-h, \infty); Y) \cap C^1([0, \infty); Y)$ that satisfies (DDE) is called a **global solution** of (DDE). ◊

Sometimes we will omit the qualifier *global* and simply speak of a *solution* of (DDE). We conclude with a simple observation, which follows directly from the fact that (H_S) implies that S satisfies a global Lipschitz condition.

Lemma 4.3. *The operator $F : X \to Y$ defined by* (4.6) *is globally Lipschitz continuous.*

Proof. It suffices to show that G satisfies a global Lipschitz condition. If $\phi, \overline{\phi} \in X$ and $\mathbf{r}, \mathbf{r}' \in \overline{\Omega}$, then

$$\begin{aligned} |\phi(-\tau(\mathbf{r}, \mathbf{r}'), \mathbf{r}') - \overline{\phi}(-\tau(\mathbf{r}, \mathbf{r}'), \mathbf{r}')| &\leq \sup_{\mathbf{r}'' \in \overline{\Omega}} |\phi(-\tau(\mathbf{r}, \mathbf{r}'), \mathbf{r}'') - \overline{\phi}(-\tau(\mathbf{r}, \mathbf{r}'), \mathbf{r}'')| \\ &\leq \sup_{t \in [-h, 0]} \sup_{\mathbf{r}'' \in \overline{\Omega}} |\phi(t, \mathbf{r}'') - \overline{\phi}(t, \mathbf{r}'')| = \|\phi - \overline{\phi}\| \end{aligned}$$

Hence we obtain

$$\|G(\phi)(\mathbf{r}) - G(\overline{\phi})(\mathbf{r})\| \leq |\overline{\Omega}| \sup_{\overline{\Omega}\times\overline{\Omega}} J \sup_{\mathbb{R}} S' \, \|\phi - \overline{\phi}\| \qquad \forall \mathbf{r} \in \overline{\Omega}$$

where the suprema are finite due to (H_J) and (H_S).

4.2.2 Dual semigroups and DDE

In this subsection we provide a very brief introduction to sun-star duality and its consequences for the analysis of (NF). For a more complete treatment we refer to [41] and, regarding the analysis of abstract DDE, the forthcoming paper [117].

In this subsection Y will be a Banach space and $X := C([-h,0];Y)$. In conjunction with (NF) we will assume that $Y = C(\overline{\Omega})$. From an abstract point of view, solving a delay equation amounts to obtaining the future state of the system, say at time $t > 0$, from knowledge of the present state. This is done in two steps. First, the present state (a continuous function on the time segment $[-h,0]$) is extended to the interval $[-h,t]$. Next the part of this extension living on $[t-h,t]$ is shifted back to $[-h,0]$. Dual perturbation theory provides a systematic method to embed X into a bigger Banach space, the so-called sun-star dual $X^{\odot\star}$, in which the extension and shifting operations are neatly separated. In broad lines, this works as follows.

If the extension problem is trivial, i.e. if $F \equiv 0$ in (DDE), then the solution semigroup corresponding to (DDE) is the shift semigroup T_0, defined as

$$(T_0(t)\phi)(\theta) = \begin{cases} \phi(t+\theta) & -h \leq t+\theta \leq 0 \\ \phi(0) & 0 \leq t+\theta \end{cases} \qquad \forall \phi \in X, t \geq 0, \theta \in [-h,0] \tag{4.7}$$

Let A_0 be its infinitesimal generator. We represent X^* by the space $\mathrm{NBV}([0,h];Y^*)$ of functions $\eta : [0,h] \to Y^*$ of bounded variation, normalised such that $\eta(0) = 0$ and $\eta(t+) = \eta(t)$ for all $t \in (0,h)$. Elements of X and X^* are in duality via an abstract bilinear Riemann-Stieltjes integral. Since X is not reflexive, the adjoint semigroup T_0^* may not be strongly continuous on X^*. Let $X^\odot \subset X^*$ be the maximal subspace of strong continuity of T_0^*. It is easy to see that $X^\odot$ is positively T_0^*-invariant and, moreover,

$$X^\odot = \overline{D(A_0^*)} \tag{4.8}$$

where A_0^* is the adjoint of A_0. Let $T_0^\odot$ be the strongly continuous semigroup on $X^\odot$ obtained by restriction of T_0^* to $X^\odot$. Its infinitesimal generator $A_0^\odot$ is precisely the part of A_0^* in $X^\odot$,

$$D(A_0^\odot) = \{\phi^\odot \in D(A_0^*) : A_0^*\phi^\odot \in X^\odot\}, \qquad A_0^\odot \phi^\odot = A_0^*\phi^\odot$$

In [56, Thm. 2.2] it is shown that $X^\odot$ may be identified with $Y^* \times L^1([0,h];Y^*)$ where the second factor is the space of Bochner integrable Y^*-valued functions on $[0,h]$.

Performing this construction once more, but now starting from the strongly continuous semigroup $T_0^\odot(t)$ on the Banach space $X^\odot$, we obtain the adjoint semigroup $T_0^{\odot\star}$ on the dual space $X^{\odot\star}$ and its strongly continuous restriction $T_0^{\odot\odot}$ to the positively invariant subspace $X^{\odot\odot} = \overline{D(A_0^{\odot\star})}$. The infinitesimal generator of $T_0^{\odot\odot}$ is again given by the part of $A_0^{\odot\star}$ in $X^{\odot\odot}$. Following [5, §1.2] we suppose that it is not possible to represent $X^{\odot\star} = Y^{**} \times [L^1([0,h];Y^*)]^*$ in terms of known functions or measures, since Y^{**} does not have the Radon-Nikodym property. However, the subspace $X^{\odot\odot}$ of strong continuity may be identified with $C([-h,0],Y^{**})$, see [56, Thm. 3.11]. Of course this representation is only semi-explicit, since a representation for Y^{**} itself is unknown. The original space X is canonically embedded into $X^{\odot\star}$ via $j : X \to X^{\odot\star}$ given by[2]

$$\langle \phi^\odot, j\phi \rangle := \langle \phi, \phi^\odot \rangle \quad \forall\, \phi \in X, \forall\, \phi^\odot \in X^\odot \tag{4.9}$$

Since Y is not reflexive, it follows that the range of j must be a proper subspace of $X^{\odot\odot}$. This fact is expressed by saying that X is *not* sun-reflexive with respect to the shift semigroup T_0, a situation that contrasts the classical case $Y = \mathbb{R}^n$.

We proceed to explain how (DDE), and consequently (NF), fits into the above abstract context. Define $\delta \in \mathscr{L}(X^\odot, Y^*)$ as

$$\delta\phi^\odot := y^* \qquad \forall\, \phi^\odot = (y^*, g) \in X^\odot \tag{4.10}$$

Then $\delta^* \in \mathscr{L}(Y^{**}, X^{\odot\star})$. Let $\ell \in \mathscr{L}(Y, X^{\odot\star})$ be the restriction of δ^* to Y, viewed as a subspace of Y^{**}. Explicitly,

$$\langle y, \delta\phi^\odot \rangle = \langle \phi^\odot, \ell y \rangle \qquad \forall\, y \in Y, \forall\, \phi^\odot \in X^\odot \tag{4.11}$$

Define $R : X \to X^{\odot\star}$ by $R := \ell \circ F$ with F as in (DDE). The following lemma will prove to be useful in §4.4.4. Observe that each $(y,f) \in Y \times L^\infty([-h,0];Y)$ defines an element of $X^{\odot\star}$. Hence we may identify $Y \times L^\infty([-h,0];Y)$ with a subspace of $X^{\odot\star}$.

Lemma 4.4. *$R(\phi) = (F(\phi), 0)$ for all $\phi \in X$. Hence R maps into $Y \times \{0\}$.*

Proof. Let $\phi \in X$ and write $R(\phi) = (y^{**}, w^*) \in X^{\odot\star}$ for certain $y^{**} \in Y^{**}$ and $w^* \in [L^1([0,h];Y^*)]^*$. Then, for any $\phi^\odot = (y^*, g) \in X^\odot$,

$$\langle \phi^\odot, R(\phi) \rangle = \langle y^*, y^{**} \rangle + \langle g, w^* \rangle \tag{4.12}$$

On the other hand, from the definition of R we obtain

[2] In this paper we adopt the 'postfix notation' for the action of a functional on a vector. That is, if W is a Banach space with dual space W^*, $w \in W$ and $w^* \in W^*$, then $\langle w, w^* \rangle := w^*(w)$.

$$\langle \phi^{\odot}, R(\phi)\rangle = \langle \phi^{\odot}, \ell F(\phi)\rangle = \langle F(\phi), \delta\phi^{\odot}\rangle = \langle F(\phi), y^*\rangle \tag{4.13}$$

where in the second equality we used (4.11) and the third equality is due to (4.10). By comparing (4.12) and (4.13) we see that y^{**} acts on y^* by point evaluation in $F(\phi) \in Y$ and $w^* = 0$. Hence $R(\phi) = (F(\phi), 0)$ and consequently R maps into $Y \times \{0\}$.

Remark 4.5. In the 'classical' case where $Y = \mathbb{R}^n$, the previous lemma shows that R is a (possibly non-linear) operator of finite rank that takes values in the 'point component' Y only, see [41, §§III.3 and VII.6]. In the present setting with $\dim Y = \infty$ we lose the former, but retain the latter property. ◊

We now consider the so-called *abstract integral equation* of the form

$$u(t) = T_0(t)\phi + j^{-1}\Big(\int_0^t T_0^{\odot\star}(t-s)R(u(s))\,ds\Big) \quad \forall t \geq 0 \tag{AIE}$$

where $\phi \in X$ is an initial condition, $u \in C([0,\infty);X)$ is the unknown and the convolution integral is of weak* Riemann type, see [41, §III.1] and also [41, Interlude 3.13 in Appendix II]. In [117] it is shown that this convolution integral takes values in the range of j. Consequently, the right-hand side of (AIE) is well-defined. The connection between (DDE) and (AIE) is revealed in the following theorem.

Theorem 4.6 (Equivalence of (DDE) **and** (AIE)**).** *Let $\phi \in X$ be given and let $R = \ell \circ F$ with $F \in C(X,Y)$. The following two statements hold.*

(i) *Suppose that $u \in C([0,\infty);X)$ satisfies* (AIE). *Define $x : [-h,\infty) \to Y$ by $x_0 := \phi$ and $x(t) = u(t)(0)$ for $t \geq 0$. Then x is a global solution of* (DDE) *in the sense of Definition 4.2.*

(ii) *Conversely, suppose that x is a global solution of* (DDE). *Define $u : [0,\infty) \to X$ by $u(t) := x_t$. Then $u \in C([0,\infty);X)$ and u satisfies* (AIE).

It is routine to show that (AIE) admits unique global solutions on $[0,\infty)$ if F is globally Lipschitz continuous. Thus, by Lemma 4.3 and Theorem 4.6 we find

Corollary 4.7. *For any $\phi \in X$ problem* (NF) *has a unique global solution.*

Of course, establishing well-posedness for (NF) does not require sun-star duality. Yet, it turns out that (AIE) is a very convenient tool in proving many standard results of dynamical systems for abstract DDE, such as the principle of linearised (in)stability, the existence of stable, unstable, and center manifolds, and theorems on local bifurcation. The following linearisation theorem is a direct generalisation of the corresponding result in the sun-reflexive case, see [41, §VII.5] or [26].

Theorem 4.8 (Linearisation at a steady state). *Let $F \in C^1(X,Y)$ and $R = \ell \circ F$ and let Σ be the strongly continuous non-linear semiflow on X associated with* (AIE). *Let $\hat{\phi} \in X$ be a steady state of Σ, i.e. $\Sigma(t)(\hat{\phi}) = \hat{\phi}$ for all $t \geq 0$. The following statements are true.*

(i) *For each $t \geq 0$ the operator $\Sigma(t) : X \to X$ is continuously Fréchet differentiable in $\hat{\phi}$ with derivative $D\Sigma(t)(\hat{\phi}) \in \mathscr{L}(X)$.*

(ii) *Upon defining $T(t) := D\Sigma(t)(\hat{\phi})$ for each $t \geq 0$ one obtains a strongly continuous semigroup in $\mathscr{L}(X)$. The domain of its generator A is given by*

$$D(A) = \{\phi \in X : \phi' \in X \text{ and } \phi'(0) = DF(\hat{\phi})\phi\}, \qquad A\phi = \phi' \tag{4.14}$$

(iii) *For every $\phi \in X$ the function $T(\cdot)\phi \in C([0,\infty), X)$ is the unique global solution of the linear abstract integral equation*

$$T(t)\phi = T_0(t)\phi + j^{-1}\Big(\int_0^t T_0^{\odot\star}(t-s)\ell DF(\hat{\phi})T(s)\phi\, ds\Big)$$

We observe that the above theorem produces a new strongly continuous semigroup T on X with generator A. For this semigroup we may likewise calculate the sun-star duality structure, just as we did for the shift semigroup T_0 defined by (4.7). It turns out that the spaces $X^{\odot}$ and, consequently, $X^{\odot\star}$ are the *same* for both semigroups. Indeed, if we put $B := \ell \circ DF(\hat{\phi}) \in \mathscr{L}(X, X^{\odot\star})$ and slightly abuse notation by writing $B^* \in \mathscr{L}(X^{\odot}, X^*)$ for the restriction of the adjoint of B to $X^{\odot}$, then just as in the sun-reflexive case [41, §III.2] one proves that the adjoint of the generator A of T is given by

$$D(A^*) = D(A_0^*), \qquad A^* = A_0^* + B^*$$

By (4.8) the sun-duals of X with respect to T_0 and T are identical and may both be denoted by $X^{\odot}$. Moreover,

$$D(A^{\odot}) = \{\phi^{\odot} \in D(A^*) : A^*\phi^{\odot} \in X^{\odot}\}, \qquad A^{\odot} = A^* \tag{4.15}$$

Let $A^{\odot\star} : D(A^{\odot\star}) \subseteq X^{\odot\star} \to X^{\odot\star}$ be its adjoint. For $A^{\odot\star}$ the situation is slightly more difficult than in the sun-reflexive case, because $D(A_0^{\odot\star}) \not\subseteq j(X)$. (Indeed, if it were true that $D(A_0^{\odot\star}) \subseteq j(X)$, then it would follow that $X^{\odot\odot} = \overline{D(A_0^{\odot\star})} \subseteq j(X)$ and X would be sun-reflexive with respect to T_0, also see [41, §III.8].) The next lemma is sufficient for our purposes in §4.4.4.

Lemma 4.9. *If $\phi \in C^1([-h,0];Y)$ then $j\phi \in D(A^{\odot\star})$ and $A^{\odot\star}j\phi = (0,\phi') + (DF(\hat{\phi})\phi, 0)$.*

4.2.3 Differentiability results

The following two results concern the smoothness of the operator G defined by (4.3) and appearing in the right-hand side of (NF). When $k = 1,2,\ldots$ we denote by $\mathscr{L}_k(X,Y)$ the space of bounded k-linear operators from X to Y. When $k = 1$ we write $\mathscr{L}(X,Y)$ instead of $\mathscr{L}_1(X,Y)$. For a review of differentiation in Banach spaces, we recommend [4, Ch. 9].

Lemma 4.10. *The operator $G : X \to Y$ defined by* (4.3) *is Fréchet differentiable with derivative $DG(\phi) \in \mathscr{L}(X,Y)$ in the point $\phi \in X$ given by*

$$(DG(\phi)\psi)(\mathbf{r}) = \int_{\overline{\Omega}} J(\mathbf{r},\mathbf{r}')S'(\phi(-\tau(\mathbf{r},\mathbf{r}'),\mathbf{r}'))\psi(-\tau(\mathbf{r},\mathbf{r}'),\mathbf{r}'))\,d\mathbf{r}' \tag{4.16}$$

for all $\psi \in X$ and all $\mathbf{r} \in \overline{\Omega}$.

Proof. First we consider the operator $DG(\phi)$ defined by the right-hand side of (4.16). Using standard methods as in the proof of Lemma 4.1 one shows that $DG(\phi)\psi \in Y$ for all $\psi \in X$. These steps are omitted. As in the proof of Lemma 4.3 we begin by noting that if $\mathbf{r},\mathbf{r}' \in \overline{\Omega}$ then

$$|\psi(-\tau(\mathbf{r},\mathbf{r}'),\mathbf{r}')| \le \sup_{\mathbf{r}''\in\overline{\Omega}} |\psi(-\tau(\mathbf{r},\mathbf{r}'),\mathbf{r}'')| \le \sup_{t\in[-h,0]}\sup_{\mathbf{r}''\in\overline{\Omega}} |\psi(t,\mathbf{r}'')| = \|\psi\| \tag{4.17}$$

This implies that $\|(DG(\phi)\psi)\| \le M\|\psi\|$ where $M > 0$ is a constant depending on Ω, J and S. Hence $DG(\phi) \in \mathscr{L}(X,Y)$.

Next we verify that $DG(\phi)$ is indeed the Fréchet derivative of G at ϕ. Introduce the shorthand notation $\phi^\tau(\mathbf{r},\mathbf{r}') := \phi(-\tau(\mathbf{r},\mathbf{r}'),\mathbf{r}')$. For $\eta \in X$ and $\mathbf{r} \in \overline{\Omega}$,

$$\begin{aligned} &G(\phi+\eta)(\mathbf{r}) - G(\phi)(\mathbf{r}) - [DG(\phi)\eta](\mathbf{r}) \\ &\quad = \int_{\overline{\Omega}} J(\mathbf{r},\mathbf{r}')\left[S(\phi^\tau(\mathbf{r},\mathbf{r}') + \eta^\tau(\mathbf{r},\mathbf{r}')) - S(\phi^\tau(\mathbf{r},\mathbf{r}')) - S'(\phi^\tau(\mathbf{r},\mathbf{r}'))\eta^\tau(\mathbf{r},\mathbf{r}')\right] d\mathbf{r}' \end{aligned}$$

Consider the integrand for fixed $\mathbf{r}'$. It follows from the Mean Value Theorem that there exists $c = c(\phi,\eta,\mathbf{r},\mathbf{r}') \in (0,1)$ such that

$$S(\phi^\tau(\mathbf{r},\mathbf{r}') + \eta^\tau(\mathbf{r},\mathbf{r}')) - S(\phi^\tau(\mathbf{r},\mathbf{r}')) = \eta^\tau(\mathbf{r},\mathbf{r}')S'(\phi^\tau(\mathbf{r},\mathbf{r}') + c\eta^\tau(\mathbf{r},\mathbf{r}'))$$

Consequently,

$$\begin{aligned} &S(\phi^\tau(\mathbf{r},\mathbf{r}') + \eta^\tau(\mathbf{r},\mathbf{r}')) - S(\phi^\tau(\mathbf{r},\mathbf{r}')) - S'(\phi^\tau(\mathbf{r},\mathbf{r}'))\eta^\tau(\mathbf{r},\mathbf{r}') \\ &\qquad = \left[S'(\phi^\tau(\mathbf{r},\mathbf{r}') + c\eta^\tau(\mathbf{r},\mathbf{r}')) - S'(\phi^\tau(\mathbf{r},\mathbf{r}'))\right]\eta^\tau(\mathbf{r},\mathbf{r}') \end{aligned}$$

Since S' is uniformly continuous on compact intervals and $|\phi^\tau(\mathbf{r},\mathbf{r}')| \le \|\phi\|$ and $|\eta^\tau(\mathbf{r},\mathbf{r}')| \le \|\eta\|$ for all $\mathbf{r},\mathbf{r}' \in \overline{\Omega}$, it follows that for every $\varepsilon > 0$ there exists $\delta > 0$ such that

$$|S'(\phi^\tau(\mathbf{r},\mathbf{r}') + c\eta^\tau(\mathbf{r},\mathbf{r}')) - S'(\phi^\tau(\mathbf{r},\mathbf{r}'))| \le \varepsilon \qquad \forall\,\mathbf{r},\mathbf{r}' \in \overline{\Omega}$$

provided $\|\eta\| \le \delta$. Therefore, if $\|\eta\| \le \delta$ then

$$\|G(\phi+\eta) - G(\phi) - DG(\phi)\eta\| \le M\varepsilon\|\eta\|$$

where $M > 0$ depends on Ω and J. This establishes differentiability.

Proposition 4.11. *The operator G defined by* (4.3) *is in $C^\infty(X,Y)$. For $k = 1,2,\ldots$ its kth Fréchet derivative $D^kG(\phi) \in \mathscr{L}_k(X,Y)$ in the point $\phi \in X$ is given by*

$$(D^kG(\phi)(\psi_1,\ldots,\psi_k))(\mathbf{r}) = \int_{\overline{\Omega}} J(\mathbf{r},\mathbf{r}')S^{(k)}(\phi(-\tau(\mathbf{r},\mathbf{r}'),\mathbf{r}'))\prod_{i=1}^{k}\psi_i(-\tau(\mathbf{r},\mathbf{r}'),\mathbf{r}')\,d\mathbf{r}'$$

for $\psi_1,\ldots,\psi_k \in X$ and $\mathbf{r} \in \overline{\Omega}$.

Proof. For $k = 1$ the statement reduces to Lemma 4.10. Fix $k \geq 2$. We need to check that $D^{k-1}G : X \to \mathscr{L}_{k-1}(X,Y)$ has Fréchet derivative $D^kG(\phi) \in \mathscr{L}_k(X,Y)$ in the point $\phi \in X$. Again we remark that $D^kG(\phi)(\psi_1,\ldots,\psi_k) \in Y$ but we omit the proof. We begin by observing that $D^kG(\phi) \in \mathscr{L}_k(X,Y)$. Indeed, by (4.17) we have

$$\|D^kG(\phi)(\psi_1,\ldots,\psi_k)\| \leq M\|\psi_1\|\cdot\ldots\cdot\|\psi_k\|$$

for all $\psi_1,\ldots,\psi_k \in X$, where $M > 0$ is a constant depending on Ω, J and S.

We conclude by verifying that $D^kG(\phi)$ is indeed the derivative of $D^{k-1}G$ at $\phi \in X$. Using the same shorthand notation as in the proof of Lemma 4.10, we consider, for $\eta \in X$, $\psi = (\psi_1,\ldots,\psi_{k-1}) \in X^{k-1}$ with $\|\psi_i\| \leq 1$ for all $i = 1,\ldots,k-1$ and $\mathbf{r} \in \Omega$,

$$\begin{aligned}(D^{k-1}G(\phi+\eta)\psi)(\mathbf{r}) - (D^{k-1}G(\phi)\psi)(\mathbf{r}) - (D^kG(\phi)(\eta,\psi))(\mathbf{r})& \\ = \int_{\overline{\Omega}} J(\mathbf{r},\mathbf{r}')R(\mathbf{r},\mathbf{r}')\prod_{i=1}^{k-1}\psi_i^\tau(\mathbf{r},\mathbf{r}')\,d\mathbf{r}'&\end{aligned}$$

where

$$R(\mathbf{r},\mathbf{r}') := S^{(k-1)}(\phi^\tau(\mathbf{r},\mathbf{r}') + \eta^\tau(\mathbf{r},\mathbf{r}')) - S^{(k-1)}(\phi^\tau(\mathbf{r},\mathbf{r}')) - S^{(k)}(\phi^\tau(\mathbf{r},\mathbf{r}'))\eta^\tau(\mathbf{r},\mathbf{r}')$$

Exactly as in the proof of Lemma 4.10 we may use the Mean Value Theorem and uniform continuity of $S^{(k)}$ on compact intervals to conclude that for each $\varepsilon > 0$ there exists $\delta > 0$ such that $\|\eta\| \leq \delta$ implies $|R(\mathbf{r},\mathbf{r}')| \leq \varepsilon\|\eta\|$ for all $\mathbf{r},\mathbf{r}' \in \overline{\Omega}$. Hence we have

$$\|D^{k-1}G(\phi+\eta)\psi - D^{k-1}G(\phi)\psi - D^kG(\phi)(\eta,\psi)\| \leq M\varepsilon\|\eta\|$$

provided $\|\eta\| \leq \delta$, where $M > 0$ depends on Ω and J.

4.2.4 Choosing the spatial state space

We believe that our choice for $Y = C(\overline{\Omega})$ made in §4.2.1 deserves some comments. In [50, 121] the authors instead elect to work with the Hilbert space $Y = L^2(\Omega)$. In our opinion this choice suffers from at least three mathematical complications.

The definition of G

It is no longer clear that G is well-defined by (4.3). Namely, apart from square integrability one also needs to verify the following. If $\phi, \overline{\phi} \in X$ and for all $t \in [-h, 0]$ one has

$$\phi(t, \mathbf{r}') = \overline{\phi}(t, \mathbf{r}') \qquad \text{a.e. } \mathbf{r}' \in \Omega \tag{4.18}$$

(where a.e. stand for *almost everywhere*, i.e. $\phi(t, \cdot)$ and $\overline{\phi}(t, \cdot)$ represent the same element in $L^2(\Omega)$) then this should imply that for almost all $\mathbf{r} \in \Omega$ one has

$$\phi(-\tau(\mathbf{r}, \mathbf{r}'), \mathbf{r}') = \overline{\phi}(-\tau(\mathbf{r}, \mathbf{r}'), \mathbf{r}') \qquad \text{a.e. } \mathbf{r}' \in \Omega \tag{4.19}$$

There are bounded $\tau \in C(\Omega \times \Omega)$ for which this implication fails. For example, let $\Omega = (0, 1)$, write $x = \mathbf{r}$ and $r = \mathbf{r}'$ and let ψ and $\overline{\psi}$ be representatives of the same element in $L^2(\mathbb{R})$ that differ in zero. If we define

$$\phi(t, r) := \psi(r + t), \qquad \overline{\phi}(t, r) := \overline{\psi}(r + t) \qquad \forall r \in \Omega$$

then $\phi, \overline{\phi} \in X$ and (4.18) holds for all $t \in [-1, 0]$. However, if $\tau(x, r) = r$, independent of $x \in \Omega$, then $\phi(-\tau(x, r), r) = \psi(0)$ and $\overline{\phi}(-\tau(x, r), r) = \overline{\psi}(0)$ which shows that for all $x = \mathbf{r} \in \Omega$ we have *in*equality in (4.19). Clearly, this choice of τ is very unrealistic, but it does indicate a problem that needs to be addressed when one works with spaces of equivalence classes of measurable functions. It is not obvious that a more realistic choice such as $\tau(x, r) := |x - r|$ does *not* exhibit the above phenomenon.

First order Fréchet differentiability

Even if we assume that the above problem can be solved satisfactorily by imposing additional (physiologically plausible) conditions on τ, there remains the question of whether the first order Fréchet derivative of G appearing in Lemma 4.10 maps X into Y when $Y = L^2(\Omega)$. For the sake of simplicity, let us assume that $J(\mathbf{r}, \mathbf{r}') \equiv 1$ and $\phi \equiv 0$. Then the mapping

$$\Omega \ni \mathbf{r} \mapsto \int_\Omega \psi(-\tau(\mathbf{r}, \mathbf{r}'), \mathbf{r}')\, d\mathbf{r}' \in \mathbb{R} \tag{4.20}$$

should be in $L^2(\Omega)$ for all $\psi \in X$. This is not obvious. An attempt to prove this statement is contained in the proof following [50, Lemma 3.1.1]. The authors write, for $\mathbf{r} \in \Omega$,

$$\left(\int_\Omega \psi(-\tau(\mathbf{r}, \mathbf{r}'), \mathbf{r}')\, d\mathbf{r}' \right)^2 \leq \int_\Omega \psi^2(-\tau(\mathbf{r}, \mathbf{r}'), \mathbf{r}')\, d\mathbf{r}' \leq \sup_{t \in [-h, 0]} \int_\Omega \psi^2(t, \mathbf{r}')\, d\mathbf{r}'$$

The first estimate is by the Cauchy-Schwarz inequality. As it stands, the second estimate only seems to be valid under certain extra conditions on ψ and / or τ, since τ depends on the integration variable.

Higher order Fréchet differentiability

In verifying second order differentiability we encounter problems similar to those pointed out above. Another complication appears in conjunction with derivatives of order three and higher. For instance, consider $k = 3$ in Proposition 4.11. Let $\Omega = (0,1)$ and write x and y for $\mathbf{r}$ and $\mathbf{r}'$. Define $\psi \in X$ by $\psi(t,r) := r^{-\frac{1}{3}}$ for all $t \in [-h,0]$ and $r \in \Omega$. Then clearly $\psi \in X$ but the integral

$$\int_\Omega \psi^3(-\tau(x,r),r)\,dr$$

diverges for all $x \in \Omega$ so $D^3G(0)$ does not map X into Y.

Which space to choose instead?

It appears that the choice $Y = L^p(\Omega)$ with $1 \leq p < 1$ is not very fortunate. Moreover, from a biological point of view it is rather unclear why the membrane potentials should be merely p-integrable on Ω and not necessarily bounded.

Thus we are led to consider alternatives. Within the class of Hilbert spaces the Sobolev space $H^k(\Omega)$ comes to mind. By standard Sobolev embedding theory each element of $H^k(\Omega)$ has a (unique) continuous representative, provided $k \in \mathbb{N}$ is sufficiently large (depending on the dimension of Ω). Moreover, $H^k(\Omega)$ is a Banach algebra under mild conditions on Ω [1, Thm. 5.23]. However, for arbitrary $\phi \in X$ the mapping (4.20) cannot be expected to possess k weak derivatives in $L^2(\Omega)$.

Other possibilities are $Y = L^\infty(\Omega)$, $Y = B(\overline{\Omega})$ and $Y = C(\overline{\Omega})$, where $B(\overline{\Omega})$ is the Banach space of everywhere bounded, measurable functions on $\overline{\Omega}$. Note that the first two spaces differ in the sense that $L^\infty(\Omega)$ consists of *equivalence classes* of *essentially* bounded, measurable functions on Ω. The first choice satisfies all our needs, but it may potentially suffer from the problem indicated in §4.2.4. The second choice takes care of all the above technical complications but also introduces new ones. Most notably, the Arzelá-Ascoli theorem, used in §4.3.1, does not hold in $B(\overline{\Omega})$. The choice $Y = C(\overline{\Omega})$ seems to be fitting both from a modelling as well as from a technical perspective.

4.3 Resolvents and spectra

Let $DG(\hat{\phi}) \in \mathscr{L}(X,Y)$ be the Fréchet derivative of G at the *steady state vector* $\hat{\phi} \in X$, i.e. $\hat{\phi}$ is independent of time (but possibly dependent on space) and

$$-\alpha\hat{\phi} + G(\hat{\phi}) = 0 \tag{4.21}$$

by (NF). Using Lemma 4.10 we obtain

$$(DG(\hat{\phi})\phi)(\mathbf{r}) = \int_{\overline{\Omega}} J_0(\mathbf{r},\mathbf{r}')\phi(-\tau(\mathbf{r},\mathbf{r}'),\mathbf{r}')\,d\mathbf{r}' \qquad \forall\,\phi \in X, \forall\,\mathbf{r} \in \overline{\Omega} \tag{4.22}$$

where

$$J_0(\mathbf{r},\mathbf{r}') := J(\mathbf{r},\mathbf{r}')S'(\hat{\phi}(-\tau(\mathbf{r},\mathbf{r}'),\mathbf{r}')) \tag{4.23}$$

In this section we are interested in the spectral properties of the linear problem

$$\begin{cases} \dot{V}(t) = -\alpha V(t) + DG(\hat{\phi})V_t & t \geq 0 \\ V(t) = \phi(t) & t \in [-h,0] \end{cases} \tag{4.24}$$

with $\alpha > 0$, which is a special case of the problem

$$\begin{cases} \dot{x}(t) = -\alpha x(t) + Lx_t & t \geq 0 \\ x(t) = \phi(t) & t \in [-h,0] \end{cases} \tag{4.25}$$

where Y is a complex Banach space, $X = C([-h,0];Y)$, $L \in \mathscr{L}(X,Y)$ and $\alpha \in \mathbb{C}$.

Remark 4.12. For the spectral analysis of this section it is necessary to work in Banach spaces over $\mathbb{C}$. So, whenever we discuss the spectral properties of (4.24), we implicitly assume that the spaces X and Y and the operators acting between them have been complexified. In fact, one should also complexify the sun-star duality structure introduced in §4.2.2. This task is not entirely trivial and rather tedious. Fortunately it has been carried out in [41, §III.7]. ♢

In §4.3.1 we make several standard observations on the structure of the spectrum of the generator of the strongly continuous semigroup solving (4.25). Familiarity with the basics of spectral theory and semigroup theory is presumed, for which we recommend [107, Ch.V] and [45]. We would also like to mention the nice application-inspired paper [6] for a detailed treatment of abstract linear DDE with bounded right-hand sides, partially in the context of Hale's [61] formal duality approach. Some of our statements are similar to those found in [121, §3.1], but our approach (as well as the choice of state space, see the remarks in §4.2.4) is sometimes different. For instance, following [41, Def. II.4.22] and [6, §4.1] we believe that the employment of Browder's (instead of Kato's) definition of the essential spectrum leads to somewhat simpler arguments.

In §4.3.2 we specialise to (4.24) and choose $Y = C(\overline{\Omega})$ and $L = DG(\hat{\phi})$. It is shown how to obtain explicit representations of resolvents and eigenvectors for a particular (but still rather general) choice of connectivity function J.

4.3.1 Spectral structure

We recall from Theorem 4.8 in §4.2.2 that the strongly continuous semigroup T on X corresponding to the global solution of (4.25) is generated by $A : D(A) \subset X \to X$ where

$$D(A) = \{\phi \in X : \phi' \in X \text{ and } \phi'(0) = -\alpha\phi(0) + L\phi\}, \qquad A\phi = \phi' \tag{4.26}$$

At this point we establish some standard notation. Let $S : D(S) \subset U \to U$ be a closed linear operator on a complex Banach space U. We denote by $\rho(S) \subset \mathbb{C}$, $\sigma(A)$ and $\sigma_{\mathrm{p}}(A)$ the resolvent set, the spectrum and the point spectrum of S, respectively. When $z \in \rho(S)$ we write[3] $R(z,S) := (z-S)^{-1}$ for the resolvent of S at z. For any $z \in \mathbb{C}$ we let $\mathscr{R}(z-S)$ and $\mathscr{N}(z-S)$ denote the range and the nullspace of $z-S$.

The results in this subsection are rather easy consequences of the following generalisation of [41, Thm. IV.3.1 and Cor. IV.3.3]. It will turn out to be very convenient to employ tensor product $\otimes$ notation as introduced in [45, p. 520]. We recall the definition from there for the reader's convenience.

Definition 4.13. Let U, V be complex Banach spaces and let $\mathscr{F}(I,V)$ be a complex Banach space of V-valued functions defined on an interval $I \subseteq \mathbb{R}$. Let $B \in \mathscr{L}(U,V)$ and $g : I \to \mathbb{C}$. If the map $g \otimes v : I \ni s \mapsto g(s)v \in V$ is in $\mathscr{F}(I,V)$ for all $v \in V$, then we define $g \otimes B : U \to \mathscr{F}(I,V)$ by

$$[(g \otimes B)u](s) := (g \otimes Bu)(s) = g(s)Bu$$

for all $u \in U$ and $s \in I$. ◊

We also introduce some auxiliary operators. For each $z \in \mathbb{C}$ and $\theta \in [-h, 0]$ we set $\varepsilon_z(\theta) := e^{z\theta}$. With L as in (4.25) we define

$$\begin{aligned} L_z &\in \mathscr{L}(Y), & L_z f &:= L(\varepsilon_z \otimes f) \\ H_z &\in \mathscr{L}(X), & (H_z\phi)(\theta) &:= \int_\theta^0 e^{z(\theta-s)}\phi(s)\,ds \\ S_z &\in \mathscr{L}(X,Y), & S_z\phi &:= \phi(0) + LH_z\phi \end{aligned} \tag{4.27}$$

for all $f \in Y$, $\phi \in X$ and $\theta \in [-h, 0]$.

Proposition 4.14 ([45, Prop. VI.6.7]). *For every $z \in \mathbb{C}$ define $\Delta(z) \in \mathscr{L}(Y)$ by*

[3] It is customary to suppress the identity operator and write $\lambda - S$ instead of $\lambda I - S$.

$$\Delta(z) := z + \alpha - L_z \tag{4.28}$$

Then $\phi \in \mathscr{R}(z-A)$ if and only if

$$\Delta(z) f = S_z \phi \tag{4.29}$$

has a solution $f \in Y$ and, moreover, $z \in \rho(A)$ if and only if f is also unique. If such is the case, then

$$R(z,A)\phi = (\varepsilon_z \otimes \Delta(z)^{-1}) S_z \phi + H_z \phi \tag{4.30}$$

Furthermore, S_z is surjective for every $z \in \mathbb{C}$, so $\lambda \in \sigma(A)$ if and only if $0 \in \sigma(\Delta(\lambda))$. Finally, $\psi \in D(A)$ is an eigenvector corresponding to λ if and only if $\psi = \varepsilon_\lambda \otimes q$ where $q \in Y$ satisfies $\Delta(\lambda) q = 0$.

Corollary 4.15. *Let $z \neq -\alpha$. If L_z is compact, then $\mathscr{R}(z-A)$ is closed.*

Proof. From the part of Proposition 4.14 regarding (4.29) we have $\phi \in \mathscr{R}(z-A)$ if and only if $S_z \phi \in \mathscr{R}(\Delta(z))$. From the theory of compact operators [107, §5.5] it follows that $\Delta(z) = z + \alpha - L_z$ has closed range, since $z + \alpha \neq 0$. Now let $(\phi_n)_{n\in\mathbb{N}}$ be a sequence in $\mathscr{R}(z-A)$ converging to some $\phi \in X$. Then the sequence $(S_z \phi_n)_{n\in\mathbb{N}}$ in $\mathscr{R}(\Delta(z))$ converges to $S_z \phi \in \mathscr{R}(\Delta(z))$, since $\mathscr{R}(\Delta(z))$ is closed. Hence $\phi \in \mathscr{R}(z-A)$.

Remark 4.16. For the particular case (4.24) with $Y = C(\overline{\Omega})$ and $L = DG(\hat{\phi})$, compactness of L_z for each $z \in \mathbb{C}$ follows easily from the Arzelà-Ascoli theorem since L_z is a Fredholm integral operator with continuous kernel $J_0 e^{-z\tau}$. ◊

As $\dim Y = \infty$ the shift semigroup T_0 on X is no longer eventually compact. Consequently we need to consider the possibility that $\sigma(A)$ contains points that are *not* isolated eigenvalues of finite type.

Definition 4.17 ([17, Def. 11]). The Browder essential spectrum $\sigma_{\mathrm{ess}}(S)$ of a closed and densely defined operator $S : D(S) \subset U \to U$ consists of all $\lambda \in \sigma(S)$ for which at least one of the following three conditions holds:

(i) λ is an accumulation point of $\sigma(S)$;

(ii) $\mathscr{R}(\lambda - S)$ is not closed;

(iii) $\bigcup_{k\geq 0} \mathscr{N}[(\lambda - S)^k]$ has infinite dimension. ◊

We also recall that if λ is in the point spectrum $\sigma_{\mathrm{p}}(S)$, then the closure of the subspace appearing in (iii) is the generalised eigenspace $M(\lambda, S)$ corresponding to λ. Its dimension m_λ (which may be ∞) is the algebraic multiplicity of λ. If $m_\lambda < \infty$ then λ is called an eigenvalue of finite type. If $m_\lambda = 1$ then λ is called a simple eigenvalue.

Corollary 4.18. *Suppose L_z is compact for all $z \neq -\alpha$. Then $\sigma_{\mathrm{ess}}(A) \subseteq \{-\alpha\}$. Moreover, $\sigma(A) \setminus \{-\alpha\}$ consists of poles of $R(\cdot, A)$. The order of λ as a pole of $R(\cdot, A)$ equals the order of zero as a pole of $R(\cdot, \Delta(\lambda))$.*

Proof. Let $\lambda \in \sigma(A)$ and $\lambda \neq -\alpha$. Corollary 4.15 implies that (ii) in Definition 4.17 (with $S = A$ and $U = X$) cannot be true. Since $\lambda + \alpha \neq 0$ is in $\sigma(L_\lambda)$ and L_λ is compact, it follows (again from general spectral theory, see e.g. [107, §5.8]) that $\lambda + \alpha$ is a pole of $R(\cdot, L_\lambda)$, say of order $k \geq 1$. If we can prove that λ is a pole of order k of $R(\cdot, A)$, then we are done. Indeed, it then follows that in particular λ is isolated in $\sigma(A)$, so (i) in Definition 4.17 cannot hold. By [107, Thm.5.8-A] the same is true for (iii).

Let us therefore prove that λ is a pole of order k of $R(\cdot, A)$. First we remark that the map

$$\mathbb{C} \ni z \mapsto L_z \in \mathscr{L}(Y) \tag{4.31}$$

is continuous at λ. The proof of this fact is standard and has been omitted. If z is in $\rho(A)$ then $z + \alpha \in \rho(L_z)$ and

$$\Delta(z)^{-1} = (z + \alpha - L_z)^{-1} = \left[z + \alpha - (L_\lambda + (L_z - L_\lambda))\right]^{-1}$$

A continuity property of the resolvent [72, Theorem IV.3.15] together with the continuity of (4.31) at λ implies that for z sufficiently close to λ we have $z + \alpha \in \rho(L_\lambda)$ and

$$\Delta(z)^{-1} = (z + \alpha - L_\lambda)^{-1} + o(|\lambda - z|) \qquad \text{as } z \to \lambda$$

where $o(|\lambda - z|)$ denotes a term that vanishes as $z \to \lambda$. By (4.30) we see that for z sufficiently close to λ,

$$R(z, A) = (\varepsilon_z \otimes (z + \alpha - L_\lambda)^{-1}) S_z + H_z + o(|\lambda - z|) \tag{4.32}$$

where it was used that $\|S_z\|$ remains bounded as $z \to \lambda$, which can easily been seen from (4.27) (with λ replaced by z). This already establishes that λ is an isolated singularity of $R(\cdot, A)$. To conclude the proof we recall that $\lambda + \alpha$ is a pole of $R(\cdot, L_\lambda)$ of order $k \geq 1$. Hence λ itself is a pole of order k of the mapping

$$\mathbb{C} \ni z \mapsto (z + \alpha - L_\lambda)^{-1} \in \mathscr{L}(Y)$$

The result now follows from (4.32) since $\mathbb{C} \ni z \mapsto H_z \in \mathscr{L}(X)$ is analytic in $z = \lambda$ and the zero-order term in the power series expansion of $\mathbb{C} \ni z \mapsto S_z \in \mathscr{L}(X, Y)$ at $z = \lambda$ does not vanish, as is easily checked.

Hence, although for the application to (4.24) that we have in mind essential spectrum exists in the form of the exceptional point $-\alpha < 0$, it is properly contained in the left half-plane and therefore rather harmless. This situation seems to be quite common in DDE arising in population dynamics, see the remark in [6, p. 321]. As a pleasant consequence, most of the results in [41, §IV.2] have immediate analogues in the present setting. We will limit ourselves to the statement of two such results that are also important for the application of center manifold theory in §4.4.

Lemma 4.19 ([45, Thm. VI.6.6 and Corollary IV.3.11]). *The semigroup T generated by A is norm continuous for $t > h$. Consequently $\omega_0 = s(A)$, where ω_0 is the growth bound of T and $s(A)$ is the spectral bound of A.*

The above lemma implies that, for the linear problem (4.24), the (in)stability of the zero solution may be inferred from the location of the poles of $R(\cdot, A)$ in the complex plane. More precisely, we have the following result, which is a direct analogue of [41, Thm. IV.2.9].

Proposition 4.20. *Suppose $\beta > -\alpha$. Let*

$$\Lambda = \Lambda(\beta) := \{\lambda \in \sigma(A) : Re\,\lambda > \beta\}$$

and let $P_\Lambda \in \mathscr{L}(X)$ be the spectral projection associated with Λ, see [107, §5.7]. Then

$$X = \mathscr{R}(P_\Lambda) \oplus \mathscr{R}(I - P_\Lambda)$$

where the first summand is finite dimensional, the second summand is closed and both summands are positively T-invariant. Moreover, there exist $K > 0$ and $\varepsilon > 0$ such that

$$\begin{aligned} \|T(t)P_\Lambda\| &\le Ke^{(\beta+\varepsilon)t}\|P_\Lambda\| \qquad \forall t \le 0 \\ \|T(t)(I-P_\Lambda)\| &\le Ke^{(\beta+\varepsilon)t}\|I-P_\Lambda\| \qquad \forall t \ge 0 \end{aligned} \tag{4.33}$$

We observe that $T(t)P_\Lambda$ is well-defined in (4.33) for all $t \le 0$, since $T(t)$ extends uniquely to a *group* on the finite-dimensional range of P_Λ.

The extension of the above decomposition and exponential estimates to $X^{\odot\star}$ proceeds exactly as in [41, p.100 - 101].

4.3.2 Explicit computations

In the remainder of this section we consider a homogeneous neural field with transmission delays due to a finite propagation speed of action potentials as well as a finite, fixed delay $\tau_0 \ge 0$ caused by synaptic processes. Space and time are each rescaled such that $\overline{\Omega} = [-1, 1]$ and the propagation speed is 1. This yields

$$\tau(x, r) = \tau_0 + |x - r| \qquad \forall x, r \in \overline{\Omega} \tag{4.34}$$

For the connectivity function we take a linear combination of $N \ge 1$ exponentials,

$$J(x, r) = \sum_{i=1}^{N} \hat{c}_i e^{-\mu_i |x-r|} \qquad \forall x, r \in \overline{\Omega} \tag{4.35}$$

where

$$\hat{c}_i \in \mathbb{C} \text{ with } \hat{c}_i \neq 0, \qquad \mu_i \in \mathbb{C} \text{ with } \mu_i \neq \mu_j \text{ for } i \neq j$$

(As the number N of exponentials remains fixed, we suppress it in our notation.) In addition to (H_S) we also require here that $S(0) = 0$. We study the stability of a spatially homogeneous steady state $\hat{\phi} \equiv 0$ by analysing the spectrum of the linearised system (4.24). Following (4.23) we incorporate $S'(0)$ into the connectivity function,

$$J_0(x,r) = \sum_{i=1}^{N} c_i e^{-\mu_i |x-r|}, \quad c_i = S'(0)\hat{c}_i$$

In order to avoid overly convoluted notation we henceforth write J instead of J_0. Assuming the form (4.35), in the next two subsections we explicitly compute the point spectrum $\sigma_p(A)$ with A as in (4.26) as well as the resolvent operator $R(\lambda, A)$ for $\lambda \in \rho(A)$.

4.3.3 Characteristic equation

In this example the operator $\Delta(\lambda)$ introduced in (4.28) is given by

$$(\Delta(\lambda)q)(x) = (\lambda + \alpha)q(x) - \int_{-1}^{1} J(x,r) e^{-\lambda \tau_0} e^{-\lambda |x-r|} q(r)\, dr \tag{4.36}$$

for all $\lambda \in \mathbb{C}$, $q \in Y$ and $x \in \overline{\Omega} = [-1,1]$. We let

$$k_i := \lambda + \mu_i \qquad \forall i = 1, \ldots, N \tag{4.37}$$

and define for each $i = 1, \ldots, N$ the integral operator $K_i \in \mathscr{L}(Y)$ by

$$(K_i q)(x) = \int_{-1}^{1} e^{-k_i |x-r|} q(r)\, dr$$

and set $(Kq)(x) := [(K_1 q)(x), \ldots, (K_N q)(x)] \in \mathbb{C}^N$. By introducing $c := [c_1, \ldots, c_N] \in \mathbb{C}^N$, $\Delta(\lambda)$ is written as

$$\Delta(\lambda)q = (\lambda + \alpha)e^{\lambda \tau_0} q - (c \cdot Kq), \qquad (c \cdot Kq)(x) := (c \cdot Kq(x)) \tag{4.38}$$

where $(a \cdot b) := \sum_{i=1}^{N} a_i b_i$ is a pairing of two complex vectors $a = [a_1, \ldots, a_n]$ and $b = [b_1, \ldots, b_n]$. We solve the equation $\Delta(\lambda)q = 0$ by formulating a linear ODE in terms of q by repetitive differentiation. For this purpose the next lemma is useful.

Proposition 4.21. *All solutions $q \in Y$ of the equation $\Delta(\lambda)q = 0$ are in fact in $C^\infty(\overline{\Omega})$.*

Proof. The range of K_i is contained in $C^1(\overline{\Omega})$ and therefore any solution of the equation $\Delta(\lambda)q = 0$ is an element of $C^\infty(\overline{\Omega})$.

Let $q \in C^2(\overline{\Omega})$. The first derivative of $\Delta(\lambda)q$ with respect to the spatial variable contains terms that involve integration over the intervals $[-1,x]$ and $[x,1]$. The second derivative has a nicer structure:

$$D_x^2\Delta(\lambda)q = (\lambda+\alpha)e^{\lambda\tau_0}q^{(2)} + 2(c\cdot k)q - (ck^2\cdot Kq) \tag{4.39}$$

in which $q^{(2)}$ denotes the second derivative of q and for each $m \in \mathbb{N}$ the vectors k^m and ck^m in $\mathbb{C}^N$ have elements k_i^m and $c_i k_i^m$, respectively, for $i = 1,\ldots,N$. This identity allows for straightforward calculation of higher derivatives. For the following lemma we recall the definition in (4.37).

Lemma 4.22. *The set* $\mathscr{S} := \{\lambda \in \mathbb{C} : \exists i,j \in \{1,\ldots,N\}, i \neq j,\ s.t.\ k_i^2 = k_j^2\}$ *contains at most* $\frac{1}{2}N(N-1)$ *elements.*

Proof. All k_i are distinct since (by definition) all μ_i are distinct. So for $i \neq j$, $k_i^2 = k_j^2 \Rightarrow \lambda = -\frac{1}{2}(\mu_i+\mu_j) \in \mathscr{S}$. The number of (unique) elements in this set is at most the number of unique pairs $(i,j), i,j \leq N, i \neq j$, which equals $\frac{1}{2}N(N-1)$.

Lemma 4.23. *Let* $\lambda \notin \mathscr{S}$. *Then there exist unique vectors* $\zeta = [\zeta_0,\ldots,\zeta_{N-1}] \in \mathbb{C}^N$ *and* $\beta = [\beta_0,\ldots,\beta_N] \in \mathbb{C}^{N+1}$, *depending on* λ *and such that for every* $q \in C^{2N}(\overline{\Omega})$ *one has*

$$(\zeta_0 + \zeta_1 D_x^2 + \ldots + \zeta_{N-1}D_x^{2N-2} + D_x^{2N})\Delta(\lambda)q = (\beta_0 + \beta_1 D_x^2 + \ldots + \beta_{N-1}D_x^{2N-2} + \beta_N D_x^{2N})q$$

Proof. Let $Q := [q, q^{(2)}, \ldots, q^{(2N)}]$. Repeated differentiation of (4.39) yields the following system of equations:

$$\begin{bmatrix} \Delta(\lambda)q \\ D_x^2\Delta(\lambda)q \\ \vdots \\ D_x^{2N}\Delta(\lambda)q \end{bmatrix} = MQ - V \tag{4.40}$$

where

$$M := e^{\lambda\tau_0}(\lambda+\alpha)I + 2\underbrace{\begin{bmatrix} 0 & 0 & 0 & \ldots & 0 \\ (c\cdot k) & 0 & 0 & \ldots & 0 \\ (c\cdot k^3) & (c\cdot k) & 0 & \ldots & 0 \\ \vdots & \ddots & \ddots & \ddots & \vdots \\ (c\cdot k^{2N-1}) & \ldots & (c\cdot k^3) & (c\cdot k) & 0 \end{bmatrix}}_{:=\Xi^T}, \qquad V := \begin{bmatrix} (c\cdot Kq) \\ (ck^2\cdot Kq) \\ (ck^4\cdot Kq) \\ \vdots \\ (ck^{2N}\cdot Kq) \end{bmatrix}$$

and I is the identity matrix of size $N+1$. (Note that (4.40) is an equality that holds on $\overline{\Omega}$. Also, the definition of Ξ^T is not used in the current proof, but will reoccur in Appendix A.) We take a linear combination of the rows in (4.40) with the components of the vector $Z := [\zeta, 1] \in \mathbb{C}^{N+1}$ such that this combination of the elements of V in (4.40) vanishes. This

eliminates all integral terms entering (4.40) via Kq. Thus we seek ζ such that $Z^T V = 0$, i.e.

$$\begin{bmatrix} \zeta & 1 \end{bmatrix} \underbrace{\begin{bmatrix} 1 & 1 & \dots & 1 \\ k_1^2 & k_2^2 & \dots & k_N^2 \\ k_1^4 & k_2^4 & \dots & k_N^4 \\ \vdots & \vdots & & \vdots \\ k_1^{2N} & k_2^{2N} & \dots & k_N^{2N} \end{bmatrix}}_{:=\hat{W}^T} \begin{bmatrix} c_1 K_1 q \\ c_2 K_2 q \\ \vdots \\ c_N K_N q \end{bmatrix} = 0 \tag{4.41}$$

on $\overline{\Omega}$. If this equation is to be satisfied for any q, then we must have $\hat{W}Z = 0$, which is equivalent to

$$\underbrace{\begin{bmatrix} 1 & k_1^2 & k_1^4 & \dots & k_1^{2N-2} \\ 1 & k_2^2 & k_2^4 & \dots & k_2^{2N-2} \\ \vdots & \vdots & \vdots & & \vdots \\ 1 & k_N^2 & k_N^4 & \dots & k_N^{2N-2} \end{bmatrix}}_{:=W} \zeta = - \begin{bmatrix} k_1^{2N} \\ k_2^{2N} \\ \vdots \\ k_N^{2N} \end{bmatrix} \tag{4.42}$$

The $N \times N$ Vandermonde matrix W is invertible since all k_i^2 are distinct by Proposition 4.22. Hence ζ can be found by applying W^{-1} to (4.42). To find β we apply the row vector $[\zeta, 1]^T$ from the left to (4.40) to infer that $\beta^T = [\zeta, 1]^T M$. Hence

$$\beta = M^T \begin{bmatrix} \zeta \\ 1 \end{bmatrix} = -M^T \begin{bmatrix} W^{-1} & \varnothing \\ \varnothing & 1 \end{bmatrix} \begin{bmatrix} k_1^{2N} \\ k_2^{2N} \\ \vdots \\ k_N^{2N} \\ -1 \end{bmatrix} \tag{4.43}$$

which concludes the proof.

Remark 4.24. For $\lambda \in \mathscr{S}$ the vectors ζ and β still exist, but they are not unique, as can be seen from (4.42). For simplicity we do not consider this case here. $\Diamond$

Theorem 4.25. *Suppose $\lambda \notin \mathscr{S}$ and let $\{\beta_i\}_{i=1}^N$ as in Lemma 4.23. Then $\Delta(\lambda)q = 0$ implies*

$$\beta_0 q + \beta_1 q^{(2)} + \ldots + \beta_{N-1} q^{(2N-2)} + \beta_N q^{(2N)} = 0 \tag{4.44}$$

Proof. Since $\Delta(\lambda)q = 0$ on $\overline{\Omega}$ it holds that $D^m \Delta(\lambda)q = 0$ for all $m \in \mathbb{N}$. The result now follows from Lemma 4.23.

Our next objective is to obtain what one could call a converse to the above theorem. Specifically, we ask when for a given $\lambda \in \mathbb{C}$ with $\lambda \notin \mathscr{S}$ a solution q of (4.44) also satisfies $\Delta(\lambda)q = 0$. For this we start by noting that eigenvalues of the ODE (4.44) are roots of the characteristic polynomial

$$\mathscr{P}(\rho) = \beta_N \rho^{2N} + \beta_{N-1}\rho^{2N-2} + \ldots + \beta_1 \rho^2 + \beta_0 \tag{4.45}$$

Evaluating the coefficients β_i of this polynomial by means of (4.43) yields the following result. Its proof may be found in Appendix A.

Proposition 4.26. *For $\lambda \notin \mathscr{S}$ the characteristic polynomial $\mathscr{P}$ is given by*

$$\mathscr{P}(\rho) = \frac{e^{\lambda\tau_0}(\lambda+\alpha)}{2}\prod_{j=1}^{N}(\rho^2 - k_j(\lambda)^2) + \sum_{i=1}^{N} c_i k_i(\lambda) \prod_{\substack{j=1 \\ j\neq i}}^{N}(\rho^2 - k_j(\lambda)^2) \tag{4.46}$$

Since $\mathscr{P}$ is an even function, it follows that if $\rho \in \mathbb{C}$ is an eigenvalue of (4.44) then the same is true for $-\rho$.

Proposition 4.27. *If* (4.46) *has $2N$ distinct roots $\pm\rho_1(\lambda), \ldots, \pm\rho_N(\lambda)$ then the general solution of* (4.44) *is of the form*

$$q_\lambda(x) = \sum_{i=1}^{N}\left[\gamma_i e^{\rho_i(\lambda)x} + \gamma_{-i}e^{-\rho_i(\lambda)x}\right] \qquad \forall x \in \overline{\Omega} \tag{4.47}$$

where the coefficients $\gamma_{\pm i} \in \mathbb{C}$ are arbitrary.

For (4.47) to satisfy $\Delta(\lambda)q_\lambda = 0$, from (4.38) we see that

$$\begin{aligned} 0 = (\Delta(\lambda)q)(x) = e^{\lambda\tau_0}(\lambda+\alpha)\sum_{i=1}^{N}\left[\gamma_i e^{\rho_i x} + \gamma_{-i}e^{-\rho_i x}\right] \\ - \sum_{j=1}^{N} c_j \sum_{i=1}^{N}\left[\gamma_i \int_{-1}^{1} e^{-k_j|x-r|+\rho_i r}\,dr + \gamma_{-i}\int_{-1}^{1} e^{-k_j|x-r|-\rho_i r}\,dr\right] \end{aligned} \tag{4.48}$$

must hold for all $x \in \overline{\Omega}$. For notational convenience we have suppressed the dependence on λ of q, ρ_i and k. Recalling that $\overline{\Omega} = [-1,x] \cup [x,1]$ for each fixed $x \in \overline{\Omega}$, we split the domains of integration accordingly. If

$$k_j(\lambda) \neq \pm\rho_i(\lambda) \qquad \forall i,j = 1,2,\ldots,N \tag{4.49}$$

then (4.48) becomes

$$\begin{aligned} 0 = e^{\lambda\tau_0}(\lambda+\alpha)\sum_{i=1}^{N}\left[\gamma_i e^{\rho_i x} + \gamma_{-i}e^{-\rho_i x}\right] \\ - \sum_{j=1}^{N} c_j \sum_{i=1}^{N}\gamma_i\Big[\frac{2k_j}{k_j^2-\rho_i^2}e^{\rho_i x} - \frac{e^{-(k_j-\rho_i)}}{k_j-\rho_i}e^{k_j x} - \frac{e^{-(k_j+\rho_i)}}{k_j+\rho_i}e^{-k_j x}\Big] \\ + \sum_{j=1}^{N} c_j \sum_{i=1}^{N}\gamma_{-i}\Big[\frac{2k_j}{k_j^2-\rho_i^2}e^{-\rho_i x} - \frac{e^{-(k_j+\rho_i)}}{k_j+\rho_i}e^{k_j x} - \frac{e^{-(k_j-\rho_i)}}{k_j-\rho_i}e^{-k_j x}\Big] \end{aligned}$$

Sorting the terms according to their exponents in x while again suppressing dependence on λ of ρ_i and k yields

$$0=\sum_{i=1}^{N}\Big\{\gamma_i e^{\rho_i x}\Big[e^{\lambda\tau_0}(\lambda+\alpha)-\sum_{j=1}^{N}\frac{2c_jk_j}{k_j^2-\rho_i^2}\Big]+\gamma_{-i}e^{-\rho_i x}\Big[e^{\lambda\tau_0}(\lambda+\alpha)-\sum_{j=1}^{N}\frac{2c_jk_j}{k_j^2-\rho_i^2}\Big]\Big\}$$
$$+\sum_{j=1}^{N}c_je^{-k_j}\Big\{e^{k_jx}\Big[\sum_{i=1}^{N}\gamma_i\frac{e^{\rho_i}}{k_j-\rho_i}+\sum_{i=1}^{n}\gamma_{-i}\frac{e^{-\rho_i}}{k_j+\rho_i}\Big]+e^{-k_jx}\Big[\sum_{i=1}^{N}\gamma_i\frac{e^{-\rho_i}}{k_j+\rho_i}+\sum_{i=1}^{n}\gamma_{-i}\frac{e^{\rho_i}}{k_j-\rho_i}\Big]\Big\}$$

Proposition 4.26 guarantees that all coefficients of $e^{\pm\rho_i(\lambda)x}$ vanish. As for the remaining terms, all coefficients of $e^{\pm k_j(\lambda)x}$ should vanish as well. Thus we must have

$$\sum_{j=1}^{N}c_je^{-k_j}e^{k_jx}\Big[\sum_{i=1}^{N}\gamma_i\frac{e^{\rho_i}}{k_j-\rho_i}+\sum_{i=1}^{n}\gamma_{-i}\frac{e^{-\rho_i}}{k_j+\rho_i}\Big]=0$$
$$\sum_{j=1}^{N}c_je^{-k_j}e^{-k_jx}\Big[\sum_{i=1}^{N}\gamma_i\frac{e^{-\rho_i}}{k_j+\rho_i}+\sum_{i=1}^{n}\gamma_{-i}\frac{e^{\rho_i}}{k_j-\rho_i}\Big]=0$$

where dependence on λ of ρ_i and k was suppressed. This yields a set of $2N$ linear equations: one for each $e^{\pm k_j(\lambda)x}$. With $\Gamma=[\gamma_1,\gamma_2,\dots,\gamma_N,\gamma_{-1},\gamma_{-2},\dots,\gamma_{-N}]$ and the matrix $S(\lambda)$ defined by

$$S(\lambda):=\begin{bmatrix}S_\lambda^- & S_\lambda^+\\ S_\lambda^+ & S_\lambda^-\end{bmatrix} \tag{4.50}$$

where

$$[S_\lambda^-]_{j,i}:=\frac{e^{\rho_i(\lambda)}}{\lambda+\mu_j-\rho_i(\lambda)},\qquad [S_\lambda^+]_{j,i}:=\frac{e^{-\rho_i(\lambda)}}{\lambda+\mu_j+\rho_i(\lambda)}$$

we seek Γ such that

$$S(\lambda)\Gamma=0 \tag{4.51}$$

In order for this system to have a non-trivial solution $\Gamma=\Gamma_\lambda$, it is necessary (and sufficient) for the determinant of $S(\lambda)$ to vanish,

$$\det S(\lambda)=0 \tag{4.52}$$

This result is summarised in the following theorem.

Theorem 4.28. *Suppose that $\lambda\notin\mathscr{S}$ and assume that the characteristic polynomial $\mathscr{P}$ in* (4.46) *has $2N$ distinct roots, denoted by $\pm\rho_i(\lambda)$ for $i=1,2,\dots,N$. If λ satisfies* (4.52) *and* (4.49) *then $\lambda\in\sigma_{\rm p}(A)$. The corresponding eigenfunction is $\varepsilon_\lambda\otimes q_\lambda$, with q_λ given by* (4.47) *with Γ_λ a solution of* (4.51).

Remark 4.29. Two comments on the above Theorem seem in order.

(i) The above procedure can easily be adapted to cover the degenerate cases excluded in Theorem 4.28. All we need is to adjust the form of q_λ in Proposition 4.27. We do not pursue this for reasons of clarity and readability. Rather, in specific instances we check that degeneracy is not an issue.

(ii) We expect that that the order of λ as a root of (4.52) equals the multiplicity of λ as a pole of $R(\cdot,A)$, see Corollary 4.18 in §4.3.1. This would give an explicit way to

verify simplicity of critical eigenvalues in §4.4. We intend to comment on this issue in future work. ◊

4.3.4 Resolvent

Now that we are able to reduce determining the point spectrum, in this specific example and modulo a technical restriction, to a finite dimensional matrix problem, the next step is to determine the solution of the resolvent problem,

$$(z-A)\psi = \phi \tag{4.53}$$

i.e. to find a representation of $\psi \in X$ in terms of the given function $\phi \in X$ when $z \in \rho(A)$. For this task we see from Proposition 4.14 in §4.3.1 that we first need to solve

$$\Delta(z)\psi(0) = S_z\phi \tag{4.54}$$

For our specific example the above is equivalent to an integral equation for $q := \psi(0)$,

$$(z+\alpha)q(x) - \int_{-1}^{1} J(x,r)e^{-z\tau_0-z|x-r|}q(r)\,dr = h_z(x) \qquad \forall x \in \overline{\Omega} \tag{4.55}$$

where

$$h_z(x) := \phi(0,x) + \int_{-1}^{1}\int_{-\tau_0-|x-r|}^{0} J(x,r)e^{-z(\tau_0+s)-z|x-r|}\phi(s,r)\,ds\,dr \tag{4.56}$$

for all $x \in \overline{\Omega}$. Inspired by (4.47) we propose the following variation-of-constants Ansatz for its solution

$$q(x) = g(x) + \sum_{i=1}^{N}\left[\gamma_i(x)e^{\rho_i x} + \gamma_{-i}(x)e^{-\rho_i x}\right] \qquad \forall x \in \overline{\Omega}$$

where $\rho_{\pm i}(z)$ are distinct roots of (4.45). We seek $g \in C(\overline{\Omega})$ and $\gamma_{\pm 1}, \ldots, \gamma_{\pm N} \in C^1(\overline{\Omega})$. Substitution into (4.55) and suppressing dependence on z of h, ρ_i and k yields

$$\begin{aligned} e^{z\tau_0}h(x) =& e^{z\tau_0}(z+\alpha)g(x) + e^{z\tau_0}(z+\alpha)\sum_{i=1}^{N}\left[\gamma_i(x)e^{\rho_i x} + \gamma_{-i}(x)e^{-\rho_i x}\right] \\ &- \sum_{j=1}^{N} c_j e^{k_j x}\Big\{\int_x^1 e^{-k_j r}g(r)\,dr + \sum_{i=1}^{N}\int_x^1 \left[\gamma_i(r)e^{(-k_j+\rho_i)r} + \gamma_{-i}(r)e^{(-k_j-\rho_i)r}\right]dr\Big\} \\ &- \sum_{j=1}^{N} c_j e^{-k_j x}\Big\{\int_{-1}^x e^{k_j r}g(r)\,dr + \sum_{i=1}^{N}\int_{-1}^x \left[\gamma_i(r)e^{(k_j+\rho_i)r} + \gamma_{-i}(r)e^{(k_j-\rho_i)r}\right]dr\Big\} \end{aligned}$$

If (4.49) holds, we may integrate by parts and rearrange the terms,

$$
\begin{aligned}
e^{z\tau_0}h(x) =& e^{z\tau_0}(z+\alpha)g(x) + e^{z\tau_0}(z+\alpha)\sum_{i=1}^{N}\left[\gamma_i(x)e^{\rho_i x} + \gamma_{-i}(x)e^{-\rho_i x}\right] \\
&- \sum_{i,j=1}^{N} c_j\Big[\frac{e^{\rho_i x}}{k_j+\rho_i}\gamma_i(x) + \frac{e^{-\rho_i x}}{k_j-\rho_i}\gamma_{-i}(x) + \frac{e^{\rho_i x}}{k_j-\rho_i}\gamma_i(x) + \frac{e^{-\rho_i x}}{k_j+\rho_i}\gamma_{-i}(x)\Big] \\
&+ \sum_{j=1}^{N} c_j e^{k_j x}\Big\{\sum_{i=1}^{N}\Big[\frac{e^{-k_j+\rho_i}\gamma_i(1)}{k_j-\rho_i} + \frac{e^{-k_j-\rho_i}\gamma_{-i}(1)}{k_j+\rho_i}\Big] \\
&\qquad - \int_x^1 e^{-k_j r}\Big[g(r) + \sum_{i=1}^{N}\frac{e^{\rho_i r}}{k_j-\rho_i}\gamma_i'(r) + \frac{e^{-\rho_i r}}{k_j+\rho_i}\gamma_{-i}'(r)\Big]dr\Big\} \\
&+ \sum_{j=1}^{N} c_j e^{-k_j x}\Big\{\sum_{i=1}^{N}\Big[\frac{e^{-k_j-\rho_i}\gamma_i(-1)}{k_j+\rho_i} + \frac{e^{-k_j+\rho_i}\gamma_{-i}(-1)}{k_j-\rho_i}\Big] \\
&\qquad + \int_{-1}^x e^{k_j r}\Big[-g(r) + \sum_{i=1}^{N}\frac{e^{\rho_i r}}{k_j+\rho_i}\gamma_i'(r) + \frac{e^{-\rho_i r}}{k_j-\rho_i}\gamma_{-i}'(r)\Big]dr\Big\}
\end{aligned}
\tag{4.57}
$$

where again dependency of h, ρ_i and k on z was suppressed. When $z \notin \mathscr{S}$, Proposition 4.26 is applied and all terms involving $e^{\pm\rho_i(z)x}$ drop out. We can choose $g = g_z$ as

$$
g_z(x) := \frac{h_z(x)}{z+\alpha} \qquad \forall x \in \overline{\Omega}
$$

provided we can achieve that the remaining terms (i.e. the last four lines) of (4.57) vanish. So for $j = 1,2,\ldots,N$ it should hold that for every $x \in \overline{\Omega}$,

$$
\begin{aligned}
\int_x^1 e^{-k_j r}\Big\{g(r) + \sum_{i=1}^{N}\Big[\frac{e^{\rho_i r}}{k_j-\rho_i}\gamma_i'(r) + \frac{e^{-\rho_i r}}{k_j+\rho_i}\gamma_{-i}'(r)\Big]\Big\}dr - e^{-k_j}\sum_{i=1}^{N}\Big[\frac{e^{\rho_i}\gamma_i(1)}{k_j-\rho_i} + \frac{e^{-\rho_i}\gamma_{-i}(1)}{k_j+\rho_i}\Big] = 0 \\
\int_{-1}^x e^{k_j r}\Big\{-g(r) + \sum_{i=1}^{N}\Big[\frac{e^{\rho_i r}}{k_j+\rho_i}\gamma_i'(r) + \frac{e^{-\rho_i r}}{k_j-\rho_i}\gamma_{-i}'(r)\Big]\Big\}dr + e^{-k_j}\sum_{i=1}^{N}\Big[\frac{e^{-\rho_i}\gamma_i(-1)}{k_j+\rho_i} + \frac{e^{\rho_i}\gamma_{-i}(-1)}{k_j-\rho_i}\Big] = 0
\end{aligned}
\tag{4.58}
$$

with the same notational convention as before. We seek functions $\gamma_{\pm i}$ such that the integrands and the remaining terms in (4.58) vanish. This yields the system

$$
\underbrace{\begin{bmatrix} T_z^- & T_z^+ \\ T_z^+ & T_z^- \end{bmatrix}}_{:=T(z)}
\begin{bmatrix} P_z^+(x) & \varnothing \\ \varnothing & P_z^-(x) \end{bmatrix}
\Gamma'(x) = \frac{h_z(x)}{z+\alpha}\begin{bmatrix} -\mathbf{1} \\ \mathbf{1} \end{bmatrix}
\qquad \forall x \in \overline{\Omega}
$$

where $\mathbf{1} \in \mathbb{R}^N$ is the vector with one on each entry,

$$
[T_z^\pm]_{j,i} := \frac{1}{k_j(z) \pm \rho_i(z)}, \qquad P_z^\pm(x) := \operatorname{diag}_N\left[e^{\pm\rho_1(z)x}, \ldots, e^{\pm\rho_N(z)x}\right] \tag{4.59}
$$

and

$$
\Gamma = [\gamma_1, \ldots, \gamma_N, \gamma_{-1}, \ldots, \gamma_{-N}]
$$

If the matrix $T(z)$ is invertible, we find $\Gamma = \Gamma_z$ by matrix inversion and integration,

$$\Gamma_z(x) = \Gamma_{0,z} + \underbrace{\int_{x_0}^{x} \frac{h_z(r)}{z+\alpha} \begin{bmatrix} P_z^-(r) & \varnothing \\ \varnothing & P_z^+(r) \end{bmatrix} T(z)^{-1} \begin{bmatrix} -\mathbf{1} \\ \mathbf{1} \end{bmatrix} dr}_{:=\hat{\Gamma}_z(x)} \tag{4.60}$$

for some initial reference point x_0 in $\overline{\Omega}$ and integration constants $\Gamma_{0,z} \in \mathbb{C}^{2N}$. Any choice of integration constants results in a choince for Γ_z for which the integral terms in (4.58) vanish. In order to satisfy the remaining terms in (4.58), $\Gamma_{0,z}$ is chosen as

$$\Gamma_{0,z} = -S(z)^{-1} \begin{bmatrix} S_z^- & S_z^+ & 0 & 0 \\ 0 & 0 & S_z^+ & S_z^- \end{bmatrix} \begin{bmatrix} \hat{\Gamma}_z(1) \\ \hat{\Gamma}_z(-1) \end{bmatrix} \tag{4.61}$$

for $S(z)$, S_z^+, and S_z^- as in (4.50). Clearly, $S(z)^{-1}$ exists if and only if $\det S(z) \neq 0$, which is consistent with the fact that the resolvent operator $R(z,A)$ is not defined when $z \in \sigma_{\mathrm{p}}(A)$. We are now ready to formulate the key result of this section.

Theorem 4.30. *Suppose that $z \in \rho(A)$ and*

- *$z \notin \mathscr{S}$;*
- *the characteristic polynomial $\mathscr{P}$ has $2N$ distinct roots;*
- *condition* (4.49) *holds and;*
- *the matrix $T(z)$ is invertible.*

Then the solution of (4.53) *is given by $\psi_z = \varepsilon_z \otimes q_z + H_z\phi$ with*

$$q_z(x) = \frac{h_z(x)}{z+\alpha} + \sum_{i=1}^{N} \left[\gamma_{i,z}(x)e^{\rho_i(z)x} + \gamma_{-i,z}(x)e^{-\rho_i(z)x}\right] \qquad \forall x \in \overline{\Omega} \tag{4.62}$$

with Γ_z given by (4.60) *and h_z is as in* (4.56)*.*

Remark 4.31. The fourth condition in the above Theorem seems peculiar and of a different nature than the first three, which already occured as simplifying conditions in §4.3.3. We refrain from investigating this issue here. Wherever we need the result of this theorem, we check the fourth condition explicitly. ◊

4.4 Normal forms for local bifurcations

Let $\hat{\phi} \in X$ be a stationary point of the semiflow generated by (DDE). By Theorem 4.8 in §4.2.2 the linearisation of this semiflow at $\hat{\phi}$ defines a strongly continuous semigroup T of bounded linear operators on X, generated by A as in (4.14) and (4.26). If F is as in (4.6) then T will be the solution semigroup of the linear problem (4.24), which is of the form (4.25). In the present section we prepare for the computation of a critical normal

form when $\hat{\phi}$ undergoes a Hopf or a double Hopf bifurcation. The actual computation is performed in §4.5.

In §4.2.2 we alluded to the fact that a reformulation of equations of type (DDE), such as (NF), as an abstract integral equation of type (AIE) allows for a relatively straightforward application of basic dynamical results such as the center manifold theorem. Indeed, by (AIE) and the exponential estimates of Proposition 4.20 in §4.3.1 the general center manifold theory for AIE presented in [41, Ch. IX] is directly applicable to (DDE) in the setting of §4.2.2. We shall relegate a more detailed technical presentation to the forthcoming paper [117].

There exists an efficient approach based on Fredholm's solvability condition towards the derivation of explicit formulas for critical normal form coefficients of local bifurcations of dynamical systems. Once such formulas have been derived for a certain class of dynamical systems, they may be evaluated for specific equations using spectral information from the linearisation at the critical equilibrium or fixed point, together with information on the higher order derivatives of the particular non-linearity. The technique goes back to [33] and has been successfully applied to ordinary differential equations [73], [74, §8.7]) and iterated maps [88], [76], [54]. The resulting formulas have been implemented in the software packages `CONTENT` [75], its successor `MATCONT` [36] and `CL_MATCONT` for maps.

In the forthcoming paper [70] the method is applied to AIE and DDE. Here we briefly summarise the results related to Hopf and double Hopf bifurcations, obtained using the Fredholm solvability technique, see Lemma 4.33 below. In the Hopf case the corresponding formulae have been first obtained in [116, 41] using a different method. As expected, the formulae given below look very similar to those given in [73] and [74, §8.7]. However, one should pay special attention to their proper interpretation in the current functional analytic context.

4.4.1 Preliminaries

In §§4.4.2 and 4.4.3 we will consider the situation that $\hat{\phi} \in X$ is a stationary point of the non-linear semiflow generated by (DDE) and the linearised problem takes the form (4.25) with A as in (4.26) and L_z compact for all $z \neq -\alpha$. There is no loss of generality in assuming that $\hat{\phi} \equiv 0$. Suppose that A has $n_c \geq 1$ simple eigenvalues on the imaginary axis, counting multiplicities.

Remark 4.32. One may show that $\sigma(A) = \sigma(A^*) = \sigma(A^{\odot}) = \sigma(A^{\odot\star})$, see [41, p. 100 - 101] and also [45, Proposition IV.2.18]. We will use this fact in the remainder of this section. For a detailed discussion of the 'lifting' of the spectral properties of A to corresponding properties of the various (adjoint) generators, we refer to [41, p. 100 - 101]. $\Diamond$

This implies the existence of a non-trivial center subspace X_0 of finite dimension n_c and spanned by some basis Φ consisting of (generalized) eigenvectors corresponding to the critical eigenvalues of A. There exists a locally invariant center manifold $\mathscr{W}^c_{loc}$ that is tangent to X_0 at the origin. One can show that on $\mathscr{W}^c_{loc}$ the solution satisfies the abstract ODE

$$\dot{u}(t) = j^{-1}\left(A^{\odot\star} ju(t) + R(u(t))\right) \qquad \forall t \in \mathbb{R}$$

where the non-linearity R is given by Lemma 4.4 and is as smooth as the mapping F appearing in (4.6). Let $\xi(t)$ be the projection of $u(t)$ onto X_0. Then $\xi(t)$ can be expressed uniquely relatively to Φ. The corresponding coordinate vector $z(t)$ of $\xi(t)$ satisfies some ODE that is smoothly equivalent to the normal form

$$\dot{z}(t) = \sum_{1\le|\nu|\le 3} g_\nu z^\nu(t) + O(|z(t)|^4) \qquad \forall t \in \mathbb{R} \tag{4.63}$$

with unknown critical normal form coefficients $g_\nu \in \mathbb{R}^{n_c}$. Here ν stands for a multi-index of length n_c. If F is sufficiently smooth, we may define

$$B \in \mathscr{L}_2(X, X^{\odot\star}), \qquad B(\phi_1,\phi_2)) := D^2R(0)(\phi_1,\phi_2) \tag{4.64a}$$

$$C \in \mathscr{L}_3(X, X^{\odot\star}), \qquad C(\phi_1,\phi_2,\phi_3) := D^3R(0)(\phi_1,\phi_2,\phi_3) \tag{4.64b}$$

for all $\phi_i \in X$. The nonlinearity $R : X \to X^{\odot\star}$ may then be expanded as

$$R(\phi) = \frac{1}{2}B(\phi,\phi) + \frac{1}{3!}C(\phi,\phi,\phi) + O(\|\phi\|^4) \tag{4.65}$$

Let $\mathscr{H} : V \subset \mathbb{R}^{n_c} \to X$ be a mapping that is as smooth as F and defined on a neighbourhood V of the origin in the coordinate space $\mathbb{R}^{n_c}$ with image $\mathscr{H}(V) = \mathscr{W}^c_{loc}$. Then $\mathscr{H}$ admits an expansion

$$\mathscr{H}(z) = \sum_{1\le|\nu|\le 3} \frac{1}{\nu!} h_\nu z^\nu + O(|z|^4) \tag{4.66}$$

where ν is a multi-index of length n_c and $h_\nu \in X$ is an unknown coefficient. By the invariance of $\mathscr{W}^c_{loc}$ we have

$$\mathscr{H}(z(t)) = u(t) \qquad \forall t \in \mathbb{R}$$

Differentiating both sides with respect to time leads to the *homological equation*

$$A^{\odot\star} j\mathscr{H}(z) + R(\mathscr{H}(z)) = j(D\mathscr{H}(z)\dot{z}) \tag{4.67}$$

Substituting the expansions (4.63), (4.65) and (4.66) into (4.67) and equating coefficients of the corresponding powers of z, one recursively obtains the unknown coefficients h_ν and g_ν by solving linear operator equations of the form

$$(\lambda - A^{\odot\star})\phi^{\odot\star} = \psi^{\odot\star} \tag{4.68}$$

where $\lambda \in \mathbb{C}$ and $\psi^{\odot\star} \in X^{\odot\star}$ is given. If $\lambda \notin \sigma(A)$ then (4.68) has a unique solution $\phi^{\odot\star} \in D(A^{\odot\star})$ for any given right-hand side. On the other hand, when $\lambda \in \sigma(A)$ a solution $\phi^{\odot\star}$ of (4.68) need not exist for all right-hand sides $\psi^{\odot\star}$. The following key lemma provides a condition for solvability that is useful in this situation.

Lemma 4.33 (Fredholm solvability). *Let $\lambda \in \mathbb{C}\setminus\{-\alpha\}$. Suppose that $L_\lambda \in \mathscr{L}(Y)$ defined in* (4.27) *is compact. Then $\lambda - A^\odot : D(A^\odot) \subset X^\odot \to X^\odot$ has closed range. In particular,* (4.68) *is solvable for $\phi^{\odot\star} \in D(A^{\odot\star})$ given $\psi^{\odot\star} \in X^{\odot\star}$ if and only if $\langle \phi^\odot, \psi^{\odot\star}\rangle = 0$ for all $\phi^\odot \in N(\lambda - A^*)$.*

Proof. From Corollary 4.15 in §4.3.1 we infer that $\mathscr{R}(\lambda - A^*)$ is closed. We first prove that this implies that $\mathscr{R}(\lambda - A^\odot)$ is closed as well. Indeed, let $(\psi_n^\odot)_{n\in\mathbb{N}}$ be a sequence in $\mathscr{R}(\lambda - A^\odot)$ such that $\psi_n^\odot \to \psi^\odot \in X^\odot$. Then there is a sequence $(\phi_n^\odot)_{n\in\mathbb{N}}$ in $D(A^\odot)$ such that

$$\psi_n^\odot = (\lambda - A^\odot)\phi_n^\odot = (\lambda - A^*)\phi_n^\odot \qquad \forall\, n \in \mathbb{N}$$

where (4.15) was used in the second equality. Hence $\psi_n^\odot \in \mathscr{R}(\lambda - A^*)$ for all $n \in \mathbb{N}$, so there exists $\phi^\odot \in D(A^*)$ such that $(\lambda - A^*)\phi^\odot = \psi^\odot$. Now

$$A^*\phi^\odot = -(\lambda - A^*)\phi^\odot + \lambda\phi^\odot = -\psi^\odot + \lambda\phi^\odot \in X^\odot$$

so $\phi^\odot \in D(A^\odot)$ and $(\lambda - A^\odot)\phi^\odot = \psi^\odot$ by (4.15). Hence $\psi^\odot \in \mathscr{R}(\lambda - A^\odot)$.

The second statement in the lemma is obtained from Banach's Closed Range Theorem [135, §VII.5] by which it follows that (4.68) has a solution if and only if $\psi^{\odot\star}$ annihilates $N(\lambda - A^\odot)$, i.e. if and only if

$$\langle \phi^\odot, \psi^{\odot\star}\rangle = 0 \qquad \forall\, \phi^\odot \in N(\lambda - A^\odot)$$

To conclude the proof we show that $N(\lambda - A^\odot) = N(\lambda - A^*)$. Indeed, $N(\lambda - A^\odot) \subseteq N(\lambda - A^*)$ by virtue of (4.15). Conversely, suppose that $\phi^\odot \in N(\lambda - A^*)$. Then $\phi^\odot \in D(A^*)$ and $A^*\phi^\odot = \lambda\phi^\odot \in X^\odot$. Hence $N(\lambda - A^\odot) \supseteq N(\lambda - A^*)$ again by (4.15).

4.4.2 The Andronov-Hopf critical normal form

In this case $\sigma(A)$ contains a simple purely imaginary pair $\lambda_{1,2} = \pm i\omega_0$ with $\omega_0 > 0$ and no other eigenvalues on the imaginary axis. Let ϕ and $\phi^\odot$ be complex eigenvectors of A and A^* corresponding to $\lambda_1 = i\omega_0$ and satisfying $\langle \phi, \phi^\odot\rangle = 1$. The restriction of (DDE) to the critical center manifold $\mathscr{W}^c_{loc}$ is smoothly equivalent to the *Poincaré normal form*

$$\dot z = i\omega_0 z + g_{21} z|z|^2 + O(|z|^4) \tag{4.69}$$

where z is complex and the critical normal form coefficient g_{21} is unknown. Any point ξ in the *real* two-dimensional center subspace X_0 corresponding to $\lambda_{1,2}$ may be uniquely expressed with respect to the set $\Phi = \{\phi, \overline{\phi}\}$ by means of the smooth complex coordinate mapping

$$\xi \mapsto (z, \bar{z}), \quad z := \langle \xi, \phi^{\odot} \rangle$$

The homological equation (4.67) presently becomes

$$A^{\odot\star} j\mathscr{H}(z,\bar{z}) + R(\mathscr{H}(z,\bar{z})) = j\left(D_z\mathscr{H}(z,\bar{z})\dot{z} + D_{\bar{z}}\mathscr{H}(z,\bar{z})\dot{\bar{z}}\right)$$

with center manifold expansion

$$\mathscr{H}(z,\bar{z}) = z\phi + \bar{z}\overline{\phi} + \sum_{2\le j+k\le 3} \frac{1}{j!k!} h_{jk} z^j \bar{z}^k + O(|z|^4)$$

Note that since the image of $\mathscr{H}$ lies in the real space X, it follows that its coefficients satisfy $h_{kj} = \overline{h}_{jk}$. The derivates $\dot{z}$ and $\dot{\bar{z}}$ are given by (4.69) and its complex conjugate.

Comparing coefficients of the quadratic terms z^2 and $z\bar{z}$ leads to two non-singular linear equations for jh_{20} and jh_{11} with solutions

$$\begin{aligned} jh_{20} &= -(A^{\odot\star})^{-1} B(\phi, \overline{\phi}) \\ jh_{11} &= (2i\omega_0 - A^{\odot\star})^{-1} B(\phi, \phi) \end{aligned} \tag{4.70}$$

There are two equations corresponding to the cubic terms z^3 and $z^2\bar{z}$, the first of which is non-singular. The second one reads

$$(i\omega_0 I - A^{\odot\star}) jh_{21} = C(\phi,\phi,\overline{\phi}) + B(\overline{\phi}, h_{20}) + 2B(\phi, h_{11}) - 2g_{21} j\phi \tag{4.71}$$

An application of Lemma 4.33 to (4.71) yields

$$g_{21} = \frac{1}{2}\langle \phi^{\odot}, C(\phi,\phi,\overline{\phi}) + B(\overline{\phi}, h_{20}) + 2B(\phi, h_{11}) \rangle \tag{4.72}$$

with h_{20} and h_{11} implicitly given by (4.70). The cubic coefficient g_{21} determines the *first Lyapunov coefficient* l_1 by the formula

$$l_1 = \frac{1}{\omega_0} \operatorname{Re} g_{21}$$

It is well known [74] that in generic unfoldings of (4.69) $l_1 < 0$ implies a supercritical bifurcation of a limit cycle on the corresponding parameter-dependent locally invariant manifold, while $l_1 > 0$ implies a subcritical bifurcation of a limit cycle there.

Remark 4.34. Notice that the vector $\phi^{\odot}$ satisfies $A^*\phi^{\odot} = i\omega_0\phi^{\odot}$ instead of $A^*\phi^{\odot} = -i\omega_0\phi^{\odot}$ which is used in the finite dimensional case. The reason for this is that the pairing $\langle \cdot, \cdot \rangle$ between $X^{\odot}$ and $X^{\odot\star}$ is complex-linear in *both* arguments. Also, observe that

the values of the multilinear form in (4.72) and (4.70) are elements of the dual space $X^{\odot\star}$ of $X^{\odot}$, i.e. they are (bounded) linear functionals. This has been taken into account in the numerical computations of §4.5. A similar remark is valid for the expressions in §4.4.3. $\Diamond$

4.4.3 The double Hopf critical normal form

In this case $\sigma(A)$ contains two simple purely imaginary pairs

$$\lambda_{1,4} = \pm i\omega_1, \;\; \lambda_{2,3} = \pm i\omega_2$$

with $\omega_{1,2} > 0$, and no other eigenvalues on the imaginary axis. Let $\phi_{1,2}$ and $\phi_{1,2}^{\odot}$ be eigenvectors of A and A^*,

$$A\phi_1 = i\omega_1\phi_1, \quad A\phi_2 = i\omega_2\phi_2, \quad A^*\phi_1^{\odot} = i\omega_1\phi_1^{\odot}, \quad A^*\phi_2^{\odot} = i\omega_2\phi_2^{\odot}$$

As in the finite-dimensional case, it is always possible to scale these vectors such that the 'bi-orthogonality' relation

$$\langle \phi_j, \phi_i^{\odot} \rangle = \delta_{ij} \qquad (1 \le i, j \le 2)$$

is satisfied. In addition, we assume the non-resonance conditions

$$k\omega_1 \neq l\omega_2 \quad \text{for all } k,l \in \mathbb{N} \text{ with } k+l \le 5 \tag{4.73}$$

Then the restriction of (DDE) to the critical center manifold $\mathscr{W}^c_{loc}$ is smoothly equivalent to the *Poincaré normal form*

$$\begin{cases} \dot{z}_1 = i\omega_1 z_1 + g_{2100} z_1|z_1|^2 + g_{1011} z_1|z_2|^2 + g_{3200} z_1|z_1|^4 + g_{2111} z_1|z_1|^2|z_2|^2 \\ \qquad + g_{1022} z_1|z_2|^4 + O(\|(z_1, \overline{z_1}, z_2, \overline{z_2})\|^6) \\ \dot{z}_2 = i\omega_2 z_2 + g_{1110} z_2|z_1|^2 + g_{0021} z_2|z_2|^2 + g_{2210} z_2|z_1|^4 + g_{1121} z_2|z_1|^2|z_2|^2 \\ \qquad + g_{0032} z_2|z_2|^4 + O(\|(z_1, \overline{z_1}, z_2, \overline{z_2})\|^6) \end{cases} \tag{4.74}$$

where the constants g_{jklm} are all complex [74, Ch. VIII]. Define

$$\begin{bmatrix} p_{11} & p_{12} \\ p_{21} & p_{22} \end{bmatrix} = \begin{bmatrix} g_{2100} & g_{1011} \\ g_{1110} & g_{0021} \end{bmatrix}$$

and assume that

$$\mathrm{Re}\, p_{11} \mathrm{Re}\, p_{12} \mathrm{Re}\, p_{21} \mathrm{Re}\, p_{22} \neq 0$$

As in shown in [74, Ch. VIII] the restriction of (4.74) to $\mathscr{W}^c_{loc}$ is locally *smoothly orbitally equivalent* to

$$\begin{cases} \dot{z}_1 = i\omega_1 z_1 + p_{11} z_1 |z_1|^2 + p_{12} z_1 |z_2|^2 + i r_1 z_1 |z_1|^4 + s_1 z_1 |z_2|^4 \\ \qquad + O(\|(z_1, \bar{z}_1, z_2, \bar{z}_2)\|^6) \\ \dot{z}_2 = i\omega_2 z_2 + p_{21} z_2 |z_1|^2 + p_{22} z_2 |z_2|^2 + s_2 z_2 |z_1|^4 + i r_2 z_2 |z_2|^4 \\ \qquad + O(\|(z_1, \bar{z}_1, z_2, \bar{z}_2)\|^6) \end{cases} \tag{4.75}$$

Here p_{ij} and s_i are complex while r_i are real, for $1 \leq i, j \leq 2$. The real parts of s_i are given by

$$\operatorname{Re} s_1 = \operatorname{Re} g_{1022} + \operatorname{Re} g_{1011} \times \left[\frac{\operatorname{Re} g_{1121}}{\operatorname{Re} g_{1110}} - 2\frac{\operatorname{Re} g_{0032}}{\operatorname{Re} g_{0021}} - \frac{\operatorname{Re} g_{3200} \operatorname{Re} g_{0021}}{\operatorname{Re} g_{2100} \operatorname{Re} g_{1110}} \right]$$

and

$$\operatorname{Re} s_2 = \operatorname{Re} g_{2210} + \operatorname{Re} g_{1110} \times \left[\frac{\operatorname{Re} g_{2111}}{\operatorname{Re} g_{1011}} - 2\frac{\operatorname{Re} g_{3200}}{\operatorname{Re} g_{2100}} - \frac{\operatorname{Re} g_{2100} \operatorname{Re} g_{0032}}{\operatorname{Re} g_{1011} \operatorname{Re} g_{0021}} \right]$$

The real constants r_i are of secondary importance in the bifurcation analysis of a generic two-parameter unfolding of (4.75) and so we omit expressions for these. They can be extracted from the proof of [74, Lemma 8.14].

The double Hopf bifurcation is a complicated bifurcation, both from a computational as well as a conceptual viewpoint. An unfolding of (4.75) is best analysed by rewriting it in polar coordinates. The sixth-order terms may not be truncated, since they may affect the qualitative dynamics. Depending on the sign of

$$\operatorname{Re} p_{11} \operatorname{Re} p_{22} = \operatorname{Re} g_{2100} \operatorname{Re} g_{0021}$$

this bifurcation exhibits either 'simple' or 'difficult' dynamics, see [74, §8.6.2]. Assuming generic dependence on parameters, one may encounter invariant tori, chaotic dynamics, Neimark-Sacker bifurcations of cycles and Shilnikov homoclinic orbits. Note that, although computations up to and including fifth order are required to determine *all* critical coefficients, computations up to and including third order suffice to distinguish between 'simple' and 'difficult' cases.

The critical normal form coefficients may be obtained using a procedure similar to the Hopf case discussed in §4.4.2. We omit the details and only present the results, noting that the center manifold now has the formal expansion

$$\mathscr{H}(z_1, \bar{z}_1, z_2, \bar{z}_2) = z_1 \phi_1 + \bar{z}_1 \overline{\phi}_1 + z_2 \phi_2 + \bar{z}_2 \overline{\phi}_2 + \sum_{j+k+l+m \geq 2} \frac{1}{j!k!l!m!} h_{jklm} z_1^j \bar{z}_1^k z_2^l \bar{z}_2^m$$

At the second order in the corresponding homological equation, we find

$$
\begin{aligned}
jh_{1100} &= -(A^{\odot\star})^{-1}B(\phi_1,\overline{\phi}_1)\\
jh_{2000} &= (2i\omega_1 - A^{\odot\star})^{-1}B(\phi_1,\phi_1)\\
jh_{1010} &= [i(\omega_1+\omega_2) - A^{\odot\star}]^{-1}B(\phi_1,\phi_2)\\
jh_{1001} &= [i(\omega_1-\omega_2) - A^{\odot\star}]^{-1}B(\phi_1,\overline{\phi}_2)\\
jh_{0020} &= (2i\omega_2 - A^{\odot\star})^{-1}B(\phi_2,\phi_2)\\
jh_{0011} &= -(A^{\odot\star})^{-1}B(\phi_2,\overline{\phi}_2)
\end{aligned}
$$

All operators in the right-hand side of the above equations are invertible due to the assumptions (4.73) on the critical eigenvalues.

Further, one obtains the following equations for h_{jklm} with $j+k+l+m=3$:

$$
\begin{aligned}
jh_{3000} &= (3i\omega_1 - A^{\odot\star})^{-1}[C(\phi_1,\phi_1,\phi_1) + 3B(h_{2000},\phi_1)]\\
jh_{2010} &= [i(2\omega_1+\omega_2) - A^{\odot\star}]^{-1}[C(\phi_1,\phi_1,\phi_2) + B(h_{2000},\phi_2) + 2B(h_{1010},\phi_1)]\\
jh_{2001} &= [i(2\omega_1-\omega_2) - A^{\odot\star}]^{-1}[C(\phi_1,\phi_1,\overline{\phi}_2) + B(h_{2000},\overline{\phi}_2) + 2B(h_{1001},\phi_1)]\\
jh_{1020} &= [i(\omega_1+2\omega_2) - A^{\odot\star}]^{-1}[C(\phi_1,\phi_2,\phi_2) + B(h_{0020},\phi_1) + 2B(h_{1010},\phi_2)]\\
jh_{1002} &= [i(\omega_1-2\omega_2) - A^{\odot\star}]^{-1}[C(\phi_1,\overline{\phi}_2,\overline{\phi}_2) + B(\overline{h}_{0020},\phi_1) + 2B(h_{1001},\overline{\phi}_2)]\\
jh_{0030} &= (3i\omega_2 - A^{\odot\star})^{-1}[C(\phi_2,\phi_2,\phi_2) + 3B(h_{0020},\phi_2)]
\end{aligned}
$$

The cubic coefficients in the normal form (4.74) come from the Fredholm solvability conditions and are given by

$$
\begin{aligned}
g_{2100} &= \frac{1}{2}\langle \phi_1^{\odot}, C(\phi_1,\phi_1,\overline{\phi}_1) + B(h_{2000},\overline{\phi}_1) + 2B(h_{1100},\phi_1)\rangle\\
g_{1011} &= \langle \phi_1^{\odot}, C(\phi_1,\phi_2,\overline{\phi}_2) + B(h_{1010},\overline{\phi}_2) + B(h_{1001},\phi_2) + B(h_{0011},\phi_1)\rangle\\
g_{1110} &= \langle \phi_2^{\odot}, C(\phi_1,\overline{\phi}_1,\phi_2) + B(h_{1100},\phi_2) + B(h_{1010},\overline{\phi}_1) + B(\overline{h}_{1001},\phi_1)\rangle\\
g_{0021} &= \frac{1}{2}\langle \phi_2^{\odot}, C(\phi_2,\phi_2,\overline{\phi}_2) + B(h_{0020},\overline{\phi}_2) + 2B(h_{0011},\phi_2)\rangle
\end{aligned}
$$

Similarly, one can compute all remaining coefficients in (4.74) by proceeding to orders four and five. The resulting (lengthy) formulas are omitted. For the finite-dimensional case these can be found in [73].

4.4.4 Evaluation of normal form coefficients

The computability of the normal form coefficients derived in the previous subsections depends on the possibility to evaluate the dual pairing $\langle \phi^{\odot}, \phi^{\odot\star}\rangle$, where $\phi^{\odot} \in X^{\odot}$ is some eigenvector of A^* corresponding to a simple eigenvalue $\lambda \in \sigma(A)$ and $\phi^{\odot\star} \in X^{\odot\star}$. Moreover, the coefficients h_ν, with ν a certain multi-index, can only be computed once a repre-

sentation for the resolvent $R(\lambda, A^{\odot\star})$ is known, where $\lambda \in \rho(A)$. At first sight this seems to be a difficult task, since $X^{\odot} = Y^* \times L^1([0,h];Y^*)$ and hence

$$X^{\odot\star} = Y^{**} \times [L^1([0,h];Y^*)]^*$$

see §4.2.2, and, as remarked there, $[L^1([0,h];Y^*)]^* \neq L^\infty([-h,0];Y^{**})$. Moreover, a representation of the second dual space Y^{**} is generally unknown, e.g. when $Y = C(\overline{\Omega})$ as for (NF).

Remark 4.35. In §4.5 it will turn out that the second derivative B in (4.64a) vanishes due to a symmetry in (NF) for the particular modelling functions chosen. In the present subsection we deliberately do not exploit this information in order to illustrate a general principle. $\Diamond$

In this subsection we offer a way around these complications that works for equations of the type (DDE). We first deal with the problem of determining $R(\lambda, A^{\odot\star})$. From Lemma 4.4 in §4.2.2 it follows that the second and third derivatives defined in (4.64a) and (4.64b), as well as all derivatives of higher order, map into the closed subspace $Y \times \{0\}$ of $X^{\odot\star}$. By inspection of the expressions for the coefficients h_ν in §§4.4.2 and 4.4.3 one sees that it is sufficient to obtain a representation of the action of $R(\lambda, A^{\odot\star})$ on this space.

Lemma 4.36. *Suppose that $\lambda \in \rho(A)$. For each $y \in Y$ the function $\psi = \varepsilon_\lambda \otimes \Delta(\lambda)^{-1} y$ is the unique solution in $C^1([-h,0];Y)$ of the system*

$$\begin{cases} \lambda\psi(0) - DF(0)\psi = y \\ \lambda\psi - \psi' = 0 \end{cases} \tag{4.76}$$

Moreover, $\psi^{\odot\star} = j\psi$ is the unique solution in $D(A^{\odot\star})$ of $(\lambda - A^{\odot\star})\psi^{\odot\star} = (y,0)$.

Proof. We return to the setting of Proposition 4.14 in §4.3.1 with $L = DG(0)$. Since $\lambda \in \rho(A)$ it follows that $\Delta(\lambda)^{-1}$ exists. We start by showing that $\psi = \varepsilon_\lambda \otimes \Delta(\lambda)^{-1} y$ solves (4.76). Explicitly,

$$\psi(\theta) = e^{\lambda\theta}\Delta(\lambda)^{-1} y \qquad \forall\, \theta \in [-h,0]$$

so clearly $\psi \in C^1([-h,0];Y)$ and ψ satisfies the second equation in (4.76). From (4.6) we recall that $DF(0)\psi = -\alpha\psi(0) + DG(0)\psi$. Therefore,

$$\begin{aligned} \lambda\psi(0) - DF(0)\psi &= (\lambda+\alpha)\psi(0) - DG(0)\psi \\ &= (\lambda+\alpha)\Delta(\lambda)^{-1} y - DG(0)(\varepsilon_\lambda \otimes \Delta(\lambda)^{-1} y) \\ &= (\lambda+\alpha)\Delta(\lambda)^{-1} y - L_\lambda(\Delta(\lambda)^{-1} y) \\ &= \Delta(\lambda)\Delta(\lambda)^{-1} y = y \end{aligned}$$

Lemma 4.9 in §4.2.2 implies that $j\psi \in D(A^{\odot\star})$, where j is the embedding defined in (4.9), and

$$(\lambda - A^{\odot\star})j\psi = \lambda \begin{bmatrix} \psi(0) \\ \psi \end{bmatrix} - \begin{bmatrix} DF(0)\psi \\ \psi' \end{bmatrix} = (y,0)$$

But $\sigma(A^{\odot\star}) = \sigma(A)$ so $\psi^{\odot\star} = j\psi$ is the *unique* solution of $(\lambda - A^{\odot\star})\psi^{\odot\star} = (y,0)$. Consequently, ψ itself is the unique solution in $C^1([-h,0];Y)$ of (4.76).

The above lemma takes care of one of the two problems sketched above. Now suppose that $\lambda \in \sigma(A) \setminus \{-\alpha\}$ is a simple eigenvalue with eigenvector $\phi \in D(A)$. (Note that λ is isolated in $\sigma(A)$ by Corollary 4.18 in §4.3.1.) Let $\phi^{\odot} \in D(A^*)$ be a corresponding eigenvector of A^*. Without loss of generality we may assume that $\langle \phi, \phi^{\odot} \rangle = 1$. Let $P^{\odot}$ and $P^{\odot\star}$ be the associated spectral projections on $X^{\odot}$ and $X^{\odot\star}$, respectively. We set out to evaluate $\langle \phi^{\odot}, \phi^{\odot\star} \rangle$ where $\phi^{\odot\star} = (y,0) \in Y \times \{0\} \subseteq X^{\odot\star}$ is given, but $\phi^{\odot}$ is unknown. Since the range of $P^{\odot\star}$ is spanned by $j\phi$ we have $P^{\odot\star}\phi^{\odot\star} = \kappa j\phi$ for a certain $\kappa \in \mathbb{C}$. In fact, by (4.9) it follows that

$$\langle \phi^{\odot}, \phi^{\odot\star} \rangle = \langle P^{\odot}\phi^{\odot}, \phi^{\odot\star} \rangle = \langle \phi^{\odot}, P^{\odot\star}\phi^{\odot\star} \rangle = \kappa \langle \phi^{\odot}, j\phi \rangle = \kappa \tag{4.77}$$

so κ is to be determined. This may be done as follows. From the Cauchy integral representation [107, §5.8] for $P_{\lambda}^{\odot\star}$ we infer that

$$P^{\odot\star}\phi^{\odot\star} = \frac{1}{2\pi i} \oint_{\partial C_\lambda} R(z, A^{\odot\star})\phi^{\odot\star}\, dz = \kappa j\phi \tag{4.78}$$

where C_λ is any open disk centered at λ such that $\overline{C}_{\lambda,0} \subseteq \rho(A)$ where $C_{\lambda,0} := C_\lambda \setminus \{\lambda\}$ and ∂C_λ is its boundary. Since $\phi^{\odot\star} \in Y \times \{0\}$ the integrand in (4.78) may be calculated using Lemma 4.36. Specifically, for $z \in \partial C_\lambda$ we have

$$R(z, A^{\odot\star})\phi^{\odot\star} = j(\varepsilon_z \otimes \Delta(z)^{-1}y) = \begin{bmatrix} \Delta(z)^{-1}y \\ \varepsilon_z \otimes \Delta(z)^{-1}y \end{bmatrix}$$

Since $j\phi = \phi(0)$ we may restrict our attention to the first component to infer that

$$\frac{1}{2\pi i} \oint_{\partial C_\lambda} \Delta(z)^{-1}y\, dz = \kappa\phi(0) \tag{4.79}$$

We note that the integral is Y-valued and (4.79) is an identity in Y. The integrand may be evaluated using the results of §4.3.4. Indeed, for each $z \in \partial C_\lambda$ it is necessary to solve a system of the type (4.54), but with $S_z\phi$ replaced by y.

For this purpose we may apply Theorem 4.30 as follows. Let us assume that λ is a root of the characteristic equation (4.52) on the imaginary axis, $\lambda \notin \mathscr{S}$, the roots $\pm\rho_i(\lambda)$ of the polynomial (4.46) are all distinct and (4.49) holds. Suppose it has also been verified that the matrix $T(\lambda)$ is invertible. By choosing the radius of C_λ sufficiently small, we guarantee that for every $z \in C_\lambda$ it holds that $z \neq -\alpha$, $z \notin \mathscr{S}$, the roots $\pm\rho_i(z)$ are all distinct, (4.49) is satisfied (with z instead of λ) and $T(z)$ is invertible. Furthermore, in this way we may

also ensure that $z \in \rho(A)$ for every $z \in C_{\lambda,0}$. In particular, all the maps

$$C_\lambda \ni z \mapsto \pm\rho_i(z) \in \mathbb{C} \qquad (i = 1,\dots,N)$$

are analytic. By (4.59) and (4.60) (with y in place of h_z) this implies that

$$C_\lambda \ni z \mapsto \hat{\Gamma}_z(x) \in \mathbb{C}^{2N}$$

is analytic for all $x \in \overline{\Omega}$. Hence by (4.62) (with y instead of h_z) we have, for every $x \in \overline{\Omega}$,

$$\begin{aligned}\oint_{\partial C_\lambda} [\Delta(z)^{-1}y](x)\,dz &= \oint_{\partial C_\lambda} \frac{y(x)}{z+\alpha} + \sum_{i=1}^{N} \left[\gamma_{i,z}(x)e^{\rho_i(z)x} + \gamma_{-i,z}(x)e^{-\rho_i(z)x}\right] dz \\ &= \sum_{i=1}^{N} \left[e^{\rho_i(\lambda)x} \oint_{\partial C_\lambda} [\Gamma_{0,z}]_i\,dz + e^{\rho_{-i}(\lambda)x} \oint_{\partial C_\lambda} [\Gamma_{0,z}]_{-i}\,dz \right] \end{aligned} \tag{4.80}$$

where $\Gamma_{0,z}$ is as in (4.61). Since $\Gamma_{0,z}$ involves $S(z)^{-1}$, the maps

$$C_\lambda \ni z \mapsto [\Gamma_{0,z}]_{\pm i} \in \mathbb{C} \qquad (i = 1,\dots,N)$$

cannot be expected to be analytic and (4.80) may not be reduced further.

In summary, (4.80) provides a way to evaluate (4.79) by numerical integration. It suffices to parametrise ∂C_λ and apply a quadrature rule to compute the $\mathbb{C}$-valued contour integrals

$$\oint_{\partial C_\lambda} [\Gamma_{0,z}]_{\pm i}\,dz \qquad (i = 1,\dots,N)$$

which are independent of $x \in \overline{\Omega}$. We then verify that $\frac{1}{2\pi i}$ times (4.80) and $\phi(0)$ are indeed proportional to each other as functions of $x \in \overline{\Omega}$. The value of $\langle \phi^\odot, \phi^{\odot\star} \rangle$ in (4.77) then equals the corresponding proportionality constant κ.

4.5 Numerical calculations

In §4.3.3 we derived a characteristic equation for problem (4.24) under the assumption that J is a finite linear combination of exponentials. The main result was formulated in Theorem 4.28. Subsequently, in §4.3.4 we obtained a closed expression for the associated resolvent operator. In the present section we apply these findings together with the theory from §4.4 to a concrete example. For reasons that will become apparent later, we assume that the connectivity function has a bi-exponential form,

$$J(x,r) = \hat{c}_1 e^{-\mu_1|x-r|} + \hat{c}_2 e^{-\mu_2|x-r|} \qquad \forall x, r \in \overline{\Omega} \tag{4.81}$$

and we choose the activation function S as in [50],

$$S(V) = \frac{1}{1+e^{-rV}} - \frac{1}{2} \qquad \forall V \in \mathbb{R}$$

Since $S(0) = 0$ it follows that (NF) admits the trivial steady state $V \equiv 0$ on which we will focus from now on. Here we have $S'(0) = \frac{r}{4}$ and hence $c_i = \frac{r}{4}\hat{c}_i$ for $i = 1,2$.

Let us continue by expressing the characteristic equation for this example and discussing a naive approach for finding its roots. Thereafter we compare these results with a more traditional approach which discretises the spatial domain $\overline{\Omega}$. Such a discretisation can be studied using techniques and software that are already available. We conclude with a normal form analysis of a Hopf bifurcation and a double Hopf bifurcation to illustrate the potential of the results from §4.4.

4.5.1 Spectral calculations

In order to apply Theorem 4.28, we start by considering the characteristic polynomial $\mathscr{P}$ from (4.46), which presently takes the form

$$\begin{aligned}\mathscr{P}(\rho) = \frac{e^{\lambda\tau_0}(\lambda+\alpha)}{2}&(\rho^2-(\lambda+\mu_1)^2)(\rho^2-(\lambda+\mu_2)^2)\\ &+c_1(\lambda+\mu_1)(\rho^2-(\lambda+\mu_2)^2)+c_2(\lambda+\mu_2)(\rho^2-(\lambda+\mu_1)^2)\end{aligned}$$

This is a second order polynomial in ρ^2. We apply a Newton algorithm to the mapping $\lambda \mapsto \det S(\lambda)$ to find the solutions of the characteristic equation (4.52). At each root $\hat{\lambda}$ we need to verify that $\hat{\lambda} \notin \mathscr{S}$, the numbers $\pm\rho_{1,2}(\hat{\lambda})$ are all distinct and (4.49) is satisfied. (Note that both of these are *open* conditions.) Passing this test we may conclude that $\hat{\lambda}$ is indeed an eigenvalue.

4.5.2 Discretisation

Derivation [50]

An approximate solution to the neural field equation can be obtained by discretising (NF). This reduces the state space from $C([-h,0];Y)$ to $C([-h,0];\mathbb{R}^{m+1})$ for some $m \in \mathbb{N}$. Hence the theory of 'classical' DDE can be applied to analyse the approximate system.

We heuristically derive the discretised system following [50] but we make a few minor corrections. Consider the original equation (4.1):

$$\frac{\partial V}{\partial t}(t,x) = -\alpha V(t,x) + \sum_{i=1}^{m} \int_{x_{i-1}}^{x_i} J(x,r)S(V(t-\tau(x,r),r))\,dr$$

for some partition $-1 = x_0 < x_1 < \ldots < x_m = 1$. We approximate every single integral with a two-point trapezoid rule evaluated at the end points of the integration interval,

$$\frac{\partial V}{\partial t}(t,x) \approx -\alpha V(t,x) + \sum_{i=1}^{m} \frac{x_i - x_{i-1}}{2} \big[J(x,x_{i-1}) S(V(t-\tau(x,x_{i-1}),x_{i-1})) + J(x,x_i) S(V(t-\tau(x,x_i),x_i)) \big]$$

By writing $V_j(t) = V(t,x_j)$, we obtain for $j = 0,1,\ldots,m$,

$$\frac{dV_j}{dt}(t) = -\alpha V_j(t) + \sum_{i=1}^{m} \frac{x_i - x_{i-1}}{2} \big[J(x_j,x_{i-1}) S(V_{i-1}(t-\tau(x_j,x_{i-1}))) + J(x_j,x_i) S(V_i(t-\tau(x_j,x_i))) \big]$$

As in (4.34) we take $\tau(x,r) = \tau_0 + |x-r|$. Also, with some abuse of notation we write $J(|x-r|)$ for $J(x,r)$, since the dependence in the right-hand side of (4.81) on x,r is only via $|x-r|$. By restriction to an equidistant mesh of size $\delta = x_i - x_{i-1} = \frac{2}{m}$, we obtain

$$\frac{dV_j}{dt}(t) = -\alpha V_j(t) + \frac{2}{m} \sum_{i=1}^{m} \frac{1}{2} \big[J(\delta|i-j-1|) S(V_{i-1}(t-\tau_0-\delta|i-j-1|)) + J(\delta|i-j|) S(V_i(t-\tau_0-\delta|i-j|)) \big]$$

Defining

$$w_i = \begin{cases} \frac{1}{2} & \text{if } i \in \{0,m\} \\ 1 & \text{if } i \in \{1,2,\ldots,m-1\} \end{cases}$$

enables us to telescope the summation, arriving at

$$\frac{dV_j}{dt}(t) = -\alpha V_j(t) + \frac{2}{m} \sum_{i=0}^{m} w_i J(\delta|i-j|) S(V_i(t-\tau_0-\delta|i-j|)) \qquad \text{(DNF)}$$

for all $j = 0,1,\ldots,m$. We refer to (DNF) as the *discretisation* of (NF) or (4.1). Note that (DNF) indeed is a classical DDE, albeit with many delays, which may be implemented in `MATLAB` to perform forward-time simulations using the `dde23` scheme. In particular, the software package `DDE-BIFTOOL` [46] allows us to determine the spectrum of the discretised system. At the end of this section we consider two examples in which we use both our analytic results and these numerical tools to study critical points in neural fields.

Convergence of discretisation

In order to 'validate' the above discretisation procedure, we generate discretisations with different resolutions and compare their spectra with the spectral values obtained by using the methods from §4.3.3. This is illustrated in Figure 4.1. The black arrows indicate four

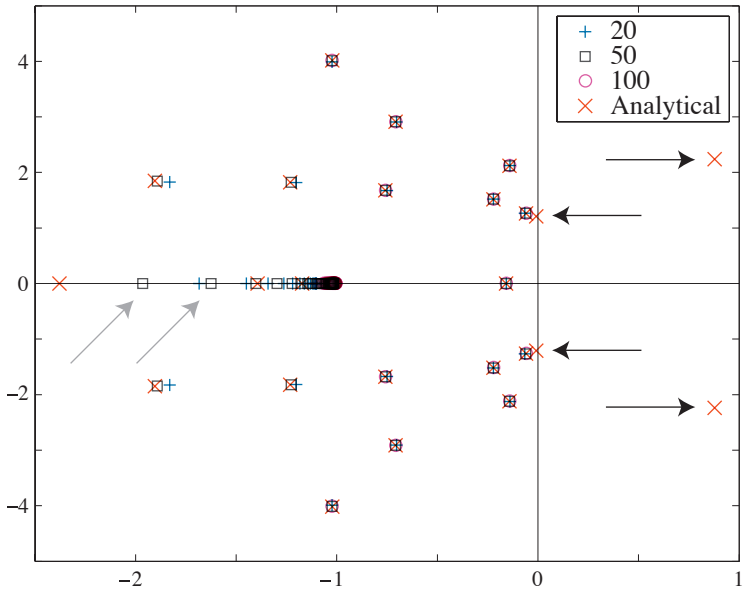

Fig. 4.1 Comparison between spectra of the discretised system for $m = 20, 50, 100$ and roots of the characteristic equation. The four black arrows indicate four roots which are not in the spectrum and the grey arrows point out distinct values which are not found. See text for a more elaborate description of these points. $\alpha = 1, \tau_0 = 1, c_1 = -5, c_2 = 2, \mu_1 = 2, \mu_2 = 0$.

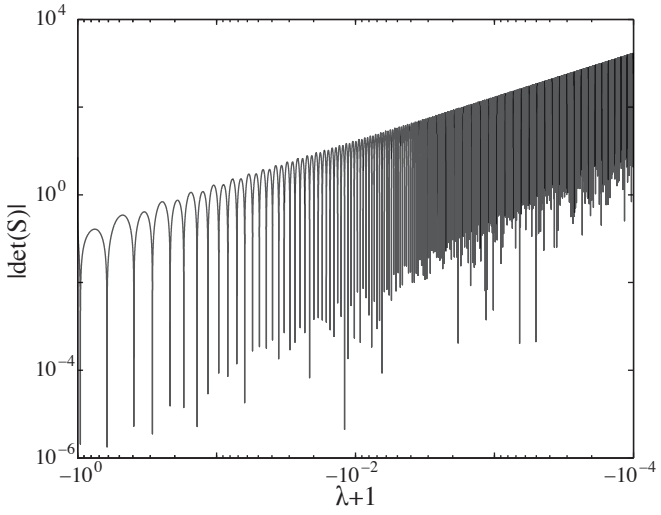

Fig. 4.2 Detail of the accumulation of eigenvalues along the real line near $\lambda = -1$: $|\det(S)|$ is plotted near the accumulation point and downward peaks correspond to roots of the characteristic equation.

roots of the characteristic equation which do not satisfy all conditions stated in Theorem 4.28: these points do satisfy (4.52), but also $\rho_1(\hat{\lambda}) = \rho_2(\hat{\lambda})$. Therefore they are to be rejected as eigenvalues. Furthermore, the grey arrows indicate eigenvalues which are not found using the algorithm of §4.5.1. These eigenvalues all lie in the 'accumulation region' near the point $-\alpha$.

We proceed by studying this accumulation of eigenvalues more closely. For $\lambda \uparrow -1$ along the real axis the absolute value of $\det S(\lambda)$ is plotted in Figure 4.2 on log-log scale. Every downward peak corresponds to a root of the characteristic equation. For λ close to $-\alpha$ the numerical accuracy drops causing the peaks to be less pronounced. This shows that, while these are not located by the root finder algorithm, the characteristic equation does have accumulating roots near the essential spectrum $\{-\alpha\}$ as is suggested by the spectrum of the discretisation, cf. Figure 4.1. However, due to both the high frequency oscillations and numerical errors, the Newton algorithm is unable to locate these roots.

Finally we observe that spectra corresponding to finer meshes converge to the analytic spectrum. However, it appears that for increasing resolutions `DDE-BIFTOOL` focuses on roots near $-\alpha$ instead of eigenvalues located further away. This is clearly seen when $m = 100$, in which case no spectral values λ are found with $\operatorname{Re}\lambda > -1.2$. For that reason we have chosen $m = 50$ in the following examples.

4.5.3 Hopf bifurcation

Rhythms and oscillations are important features of nervous tissue that could be studied with neural field models. For that reason Hopf bifurcations play a key role in the analysis of neural field equations. In this subsection we study a concrete example of a Hopf bifurcation, both analytically and numerically. We also compare the results of both methods.

Initially we focus on a connectivity of the 'inverted wizard hat'-type. Similarly as in [50] we consider the steepness parameter r of the activation function as bifurcation parameter.

Spectrum

The characteristic equation (4.52) is used to determine the point spectrum for a range of parameters. For the values shown in Table 4.1 there exists a purely imaginary pair of simple eigenvalues. The corresponding spectrum is displayed in Figure 4.3. The figure also shows the spectrum as calculated by `DDE-BIFTOOL` for a discretisation of $m = 50$ intervals. From the graph it is obvious that the solution algorithm of §4.5.1 is unable to locate eigenvalues near the accumulation point $-\alpha = -1$. We discuss this phenomenon

Table 4.1 Parameters corresponding to Hopf bifurcation

parameter	α	τ_0	r	$\hat{c}_1$	$\hat{c}_2$	μ_1	μ_2
value	1.0	1.0	4.220214885988226	3.0	−5.5	0.5	1.0

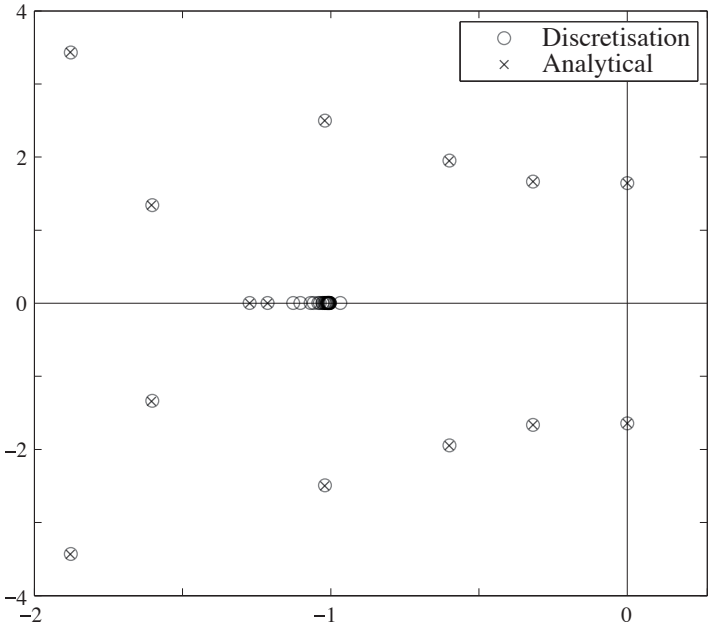

Fig. 4.3 Spectrum at a Hopf bifurcation. Comparison between analytic approach and discretised system ($m = 50$).

below. Apart from that, the numerical approximation seems to be very close to the analytic solution. Only in the far left half-plane an error can be observed. From a dynamical point of view such an error is of course rather innocuous.

First Lyapunov coefficient

In order to determine analytically the type of Hopf bifurcation (i.e. sub- or supercritical), the first Lyapunov coefficient has to be determined. Before the result of §4.4.2 can be applied, the eigenfunction corresponding to the eigenvalues at criticality has to be determined. Application of Theorem 4.28 yields

$$\phi(t,x) = e^{\lambda t}\left[\gamma_1(e^{\rho_1 x} + e^{-\rho_1 x}) + \gamma_2(e^{\rho_2 x} + e^{-\rho_2 x})\right] \qquad \forall t \in [-h,0], \forall x \in \overline{\Omega}$$

with

$$\rho_1 = 0.321607348361597 - 0.880461478656249i$$
$$\rho_2 = 0.110838003673357 - 2.312123026384049i$$
$$\gamma_1 = -0.191821747840362 - 0.172140605861736i$$
$$\gamma_2 = -0.080160108888561$$

corresponding to $\lambda = 1.644003102046893i$. (Note that in the present example with τ_0 as in Table 4.2 and $\overline{\Omega} = [-1,1]$ the delay interval equals $[-h,0] = [-3,0]$.) Since the activation function S is odd, its second derivative vanishes and the critical normal form coefficient g_{21} in (4.72) significantly simplifies to

$$g_{21} = \frac{1}{2}\langle \phi^{\odot}, D^3 R(0)(\phi,\phi,\overline{\phi})\rangle$$

The pairing is expressed as a contour integral around λ which we evaluate numerically, see §4.4.4. We find $g_{21} \approx -0.326 + 0.0389i$ and hence the first Lyapunov coefficient is $l_1 \approx -0.198$. The negative sign of l_1 indicates a *supercritical* Hopf bifurcation. Therefore stable periodic solutions are expected to emerge from the bifurcating steady state.

Simulations

We choose $r = 6$ which is beyond the critical parameter value of Table 4.1. For the initial condition $V(t,x) = \varepsilon = 0.01$ for $t \in [-h,0]$ with $h = 3$ and $x \in [-1,1]$ the simulation result is shown in Figure 4.4. After a transient time, the system approaches its stable periodic attractor. The convergence to stable periodic motion is consistent with the sign of the first Lyapunov coefficient. Furthermore, both the shape and period of this attractor match with the eigenfunction and eigenvalue respectively.

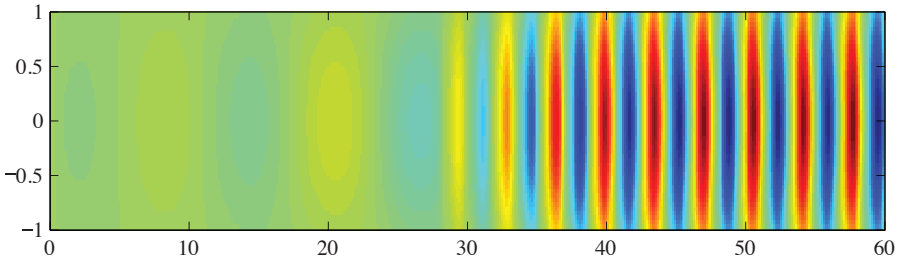

Fig. 4.4 Forward time simulation of discretised system ($m = 50$) for $r = 6$ beyond a Hopf bifurcation. A long transient is observed before the solution approaches the limit cycle.

4.5.4 Double Hopf bifurcation

The spectrum at the Hopf point studied in §4.5.3 consists mainly of complex pairs of eigenvalues. Therefore it is to be expected that system parameters can be tuned such that a second pair of complex eigenvalues arrives at the imaginary axis, giving rise to a double Hopf bifurcation. In this subsection we show that this is indeed possible and we study this bifurcation both analytically and numerically.

Spectrum

Table 4.2 Parameters corresponding to double Hopf bifurcation.

parameter	α	τ_0	r	$\hat{c}_1$	$\hat{c}_2$	μ_1	μ_2
value	1.0	1.0	4.828749714457348	3.0	-5.5	0.0	0.999592391420082

Table 4.3 Values of λ and corresponding ρ

λ	$\rho(\lambda)$
$2.030930500644927i$	$0.454550410967142-1.057267648955222i$
	$0.054136932895367-3.495632804443535i$
$1.299147304907829i$	$1.075429529957343-0.717519976488838i$
	$1.128716151852882-2.306528729845143i$

Parameters for which the system has two complex pairs of eigenvalues on the imaginary axis and no eigenvalues in the positive right half-plane are identified, see Table 4.2. The corresponding spectrum is depicted in Figure 4.5 while Table 4.3 lists the values of λ at this critical point. As with the regular Hopf bifurcation, we observe that the root finding algorithm misses most eigenvalues near the essential spectrum at $-\alpha = -1$.

Next we compute the eigenfunctions corresponding to the critical eigenvalues. For this purpose Theorem 4.28 may be applied using the data in Table 4.3. Modulus and argument of both eigenfunctions are depicted in Figure 4.6.

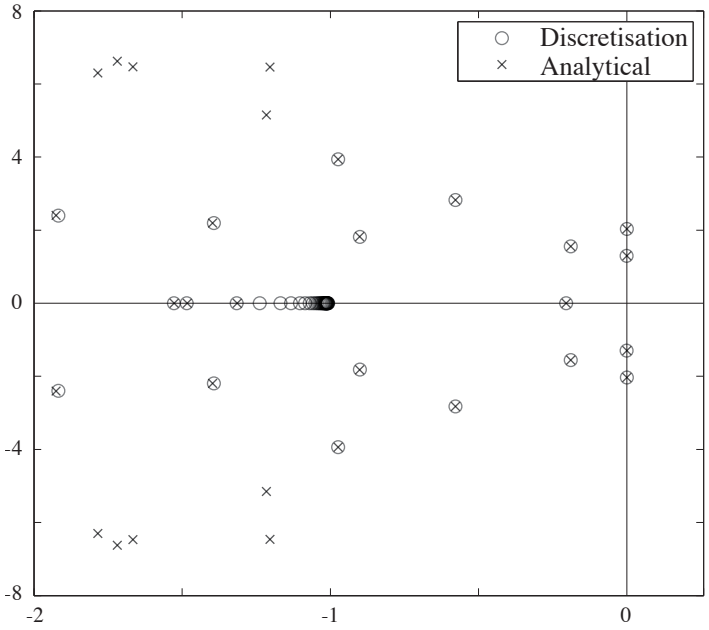

Fig. 4.5 Spectrum at a double Hopf bifurcation. Comparison between analytic approach and discretised system ($m = 50$).

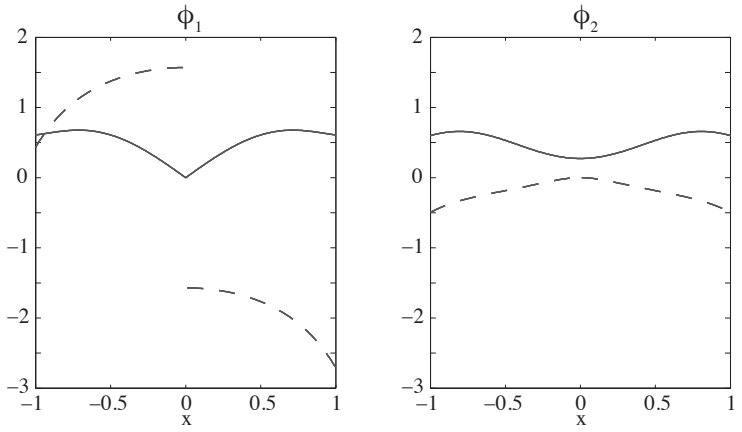

Fig. 4.6 Eigenfunctions corresponding to the critical eigenvalues. $\lambda = i1.299...$ is shown left and $\lambda = i2.030...$ on the right. Solid lines depict the modulus and dashed lines the argument.

Normal form coefficients

With this information available, the normal form coefficients of the double Hopf bifurcation may be evaluated. The coefficients g_{2100}, g_{1011}, g_{1110}, and g_{0021} from §4.4.3 are found as in §4.5.3, which results in the matrix

$$\begin{bmatrix} p_{11} & p_{12} \\ p_{21} & p_{22} \end{bmatrix} = \begin{bmatrix} -8.822 & -3.367 \\ -13.79 & -1.310 \end{bmatrix}$$

Since $p_{11}p_{22} > 0$, we conclude that this double Hopf bifurcation is of the 'simple' type, see [74, §8.6.2]. Defining $\theta := \frac{p_{12}}{p_{22}} \approx 2.57$ and $\delta := \frac{p_{21}}{p_{11}} \approx 1.56$, we find that $\theta\delta > 1$ and therefore this 'simple' bifurcation has sub-type I [74]. The key feature of this sub-type is the presence of a regime in parameter space for which two distinct stable periodic solutions exist.

Simulations

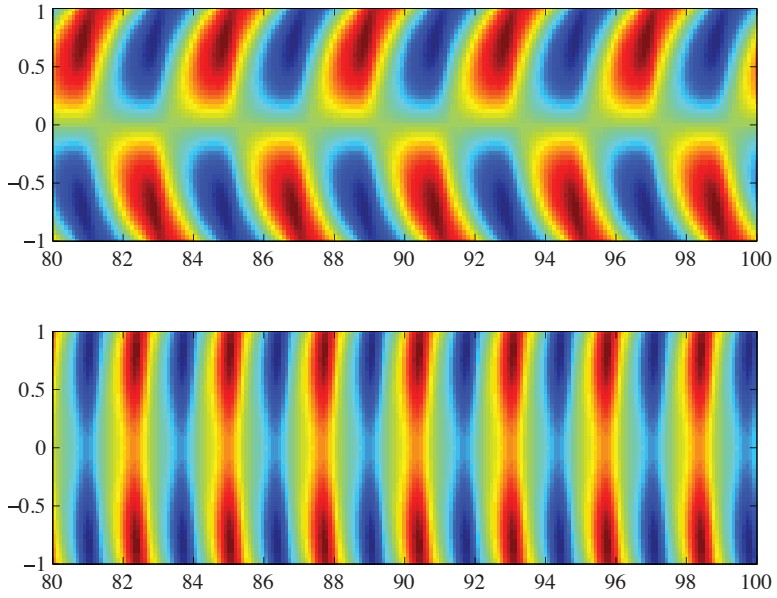

Fig. 4.7 Bi-stability near double Hopf bifurcation: for $r = 6$ and $\mu_2 = 1$ the time evolution is shown for different initial conditions ($m = 50$). Top and bottom diagrams correspond to (4.82a) and (4.82b) respectively.

The parameters are adjusted slightly, such that both pairs of complex eigenvalues have a positive real part. More specifically we choose $r = 6$ and $\mu_2 = 1$ while keeping other

parameters as in Table 4.2. For the following two initial conditions

$$V(t,x) = \varepsilon x \tag{4.82a}$$

$$V(t,x) = \varepsilon \tag{4.82b}$$

with $\varepsilon = 0.01$, the discretised system ($m = 50$) is integrated forwards in time, see Figure 4.7.

For the chosen parameters the system has two stable periodic attractors and the asymptotic behaviour is determined by their initial conditions. This result is consistent with the predictions of the normal form computation. Furthermore we observe, since the system is close to the double Hopf bifurcation, that both the shape and period of the periodic solutions are fairly well approximated by the critical eigenfunctions (c.f. Figure 4.6). Indeed, the moduli of the eigenfunctions correspond to the amplitude of the asymptotic solution. For either of the solutions the extrema are located near the borders of the domain. The antiphasic solutions in the upper panel are indicated by the jump of size π in the argument of the first eigenfunction, see Figure 4.6 on the left.

4.6 Discussion

We have demonstrated that neural field equations with transmission delay fit well into the sun-star framework for delay equations. As a consequence, standard results from dynamical systems theory, such as the principle of linearised (in)stability, center manifold reduction and normal form computation, are readily available. These, in turn, open the possibility for a systematic study of codimension one and two local bifurcations, w.r.t. parameters in the connectivity and activation functions. This facilitates an understanding of the effect of parameters in terms of biological quantities.

In §4.5 we analysed the dynamics of a one population model with the inverted *wizard* hat as connectivity function. The choice of an inverted *Mexican* hat is biologically more plausible, as pyramidal cells are surrounded by a cloud of interneurons, while long range connections are by and large excitatory. We have chosen the inverted wizard hat mainly for mathematical convenience. Indeed, in §4.3.3 an analytic formula for the location of the eigenvalues was derived. It is well known that the combination of an inverted Mexican hat connectivity with a transmission delay leads to dynamic instabilities [14, 67]. In [28] Turing instabilities were shown to occur for the inverted wizard hat connectivity.

We have seen that the stationary spatially homogeneous state destabilises upon increasing the steepness (gain) of the activation function. This is in line with other findings indicating that the activation function strongly influences dynamical behaviour, see for instance [48, 29].

It is mathematically challenging to consider neural field equations on unbounded spatial domains, leading to infinite delays, although such is of less importance from a biological viewpoint. Our main goal for the near future is to develop tools for numerical bifurcation analysis for the class of equations studied in this paper. Normal form computation is a first prerequisite for this task. Hence we are on our way.

Chapter 5
Spatially extended neurons as extension to neural fields

Abstract Recent development of new mathematical tools for studying lumped models with a spatial component, i.e. neural fields, allows for the incorporation of features that were previously excluded for they made the mathematical analysis intractable; e.g. distance dependent transmission delays. Now that traditional neural fields, requiring extensive simplifications of both the single cell dynamics and the network architecture, are about to be fully characterized, the time seems right to consider more involved formulations of neural fields. Here we propose an extension to the prevalent framework of neural fields that facilitates the inclusion of relevant spiking behaviors observed in single neurons, e.g. tonically bursting and rebound spikes/bursts; features surmised to be incompatible for lumping. This new setting is dependent on the firing rate reduction of a single neuron, i.e. a model that reproduces the rate at which spikes are generated rather than the generation of individual spikes. Results are consistent with traditional reductions based on integrate-and-fire neurons both with and without spike frequency adaptation, but the main outcome is the formulation of a neural field based on Izhikevich neurons. Although we show a clear correspondence between the original network and the reduction, the reduction still needs refinements; both on the level of modeling as well as the mathematical analysis.

5.1 Introduction

Lumped models of neural tissue provide a concise description for the collective action of many neurons which can be analyzed thoroughly with, for example, dynamical systems, and stochastic processes. Despite the fact that models of this type describe the neural dynamics at a much coarser level, such that fine structures of the underlying network of spiking neurons are lost, it is, on the other hand, advantageous that lumped models characterize the network at a scale comparable to prevalent imaging techniques, like EEG, ECoG and MEG in a clinical environment, and calcium imaging and LFP in an experimental

setup. For that reason, these models are helpful for interpreting the results and relating them to physiological mechanisms underlying the observations.

Depending on the goals one might have in mind, a preference could be given to study a certain class of models using a certain tool. Theory of stochastic processes and results from quantum mechanics have been used to derive lumped models from first principles: global behavior of a population neurons, which fires spikes unpredictably (e.g. a Poisson process) to given input, can be expressed as a stochastic differential equation [18, 11]. The deterministic part of the SDE obtained in this manner can be studied methodically using dynamical systems theory: identification of bifurcations and multistability give a description of the possible states and transitions the model might exhibit, which are considered relevant for some cases of epilepsy [81, 100, 125]. Although steady states are deemed mundane from a dynamical systems' point of view, they have seem to play a critical role in the clinical relevance of the model. Indeed, the brain is sometimes viewed as a filter, characterized by the dynamical system, that processes a certain noisy input, representing, for instance, sensory input from thalamus. In this case, Laplace and Fourier transforms can be used to determine to frequency response of the model, which is shown comparable to the power spectrum of electrical neural activity [82, 98, 80].

Lumped models which have a spatial component, often refered to as neural fields[1], are less suitable for the latter type of analysis, for the simple reason that input and output are poorly defined for a spatial arrangement. While neural fields often have a concise formulation, analysis from a dynamical systems' point of view is in most cases far for trivial. Already from the earliest incarnations of such fields, analysis was performed numerically [133] or additional assumptions were required for tractability; a common one being the (almost) binary activation of neural tissue (first introduced by Amari [2]). Over the past years, several novel techniques have been proposed which offer new ways for studying neural fields. For instance, the stability and dynamics of pulses and waves can be studied with Evans functions [71], the evolution of a contour of an active region in a neural field is given in [31] and the dynamics of neural fields with distance-dependent transmission delays are in full detail characterized in [118].

Now that such new analytic tools enable us to comprehend the complex behavior of neural fields, one might wonder whether the prevalent neural field equations can be extended. Although many variants exist for the reduction of the dendrites, the synapses and the network architecture — of which an excellent overview is given in [16], — a careful reduction of the spiking dynamics of individual neurons is typically amiss. Although in some reductions take spike frequency adaptation (SFA) into account, more complex

[1] Although the brain is a three-dimensional structure, the terminology "field," suggesting a two-dimensional organization, is still accurate: the brain's predominant structure is the cortical sheet which can be seen as a collection of two-dimensional layers.

neural dynamics, like instrinsic bursting and rebound spikes/bursts, are still thought to be incompatible for lumping.

Here we propose a novel framework, based on existing lumping procedures, that enables the inclusion of a wider class of spiking behaviors. Essentially, the state space of a single neuron is split in two regimes: subthreshold and spiking. By leaving the model's behavior unaltered in the subthreshold regime, processes responsible for "advanced" dynamics, e.g. shunting inhibition and slow calcium currents, remain intact, allowing an accurate manifestation of slow currents. Instead, only the fast dynamics responsible for the spike generation are simplified: we replace them with a slowly varying variable that accurately describes the firing rate of the neuron, which might be dependent on the current state of the slow variables. Furthermore, the firing rate itself can, if necessary, also be used to estimate the contribution to the slow variables due to spiking, e.g. inflow of calcium ions. Next, the reduced model is extended across space and common techniques are used to simplify the network connectivity in order to obtain a closed neural field formulation.

The procedure is illustrated using three examples: the first two are used to obtain the prevalent neural field equations with and without adaptation, while the third example considers the Izhikevich neuron, c.f. [68]. A neural field formulation which relates to this popular model of a spiking neuron is novel and might provide an additional tool in studying networks of this type of neuron.

The outline of this text is as follows. We begin by describing the lumping of one population of spiking neurons by first smoothing the dynamics of each neuron over time and, thereafter, we simplify the spatial structure of the connections, upon which the neural field equations readily appear. The equations found in this manner are dependent on the firing rate reduction of a single neuron, i.e. a model which does not produce individual spikes but one that mimics the rate at which spikes are generated. Although trivial in some cases, no general or rigurous procedure exists for this reduction; hence we illustrate what such reduction might look like for concrete models. Finally we compare simulation results of both the detailed model and the spiking neuron network to assess the quality of the reduction.

5.2 Generalized neural field reduction

5.2.1 One population of spiking neurons

For clarity, a neural field of only one type of neurons, whose connections are dependent on the separation between two cells, is considered first. Thereafter, the results obtained from one population are easily extended to multiple interacting populations which might have different properties.

By assuming that the interaction between neurons occurs exclusively unidirectional via synapses (thereby neglecting gap junctions, diffusion of ions, etc.), it suffices to consider the spike times of neurons only. For a given neuron let $T(t) := \{\hat{t}_i, i = 1,\dots,n | 0 < \hat{t}_1 < \dots < \hat{t}_n \leq t\}$ be the (possibly empty) set of all its spike times up to and including time t. If it is assumed that each spike arriving at a synaptic terminal results in an identical response of the synapse, the synaptic activation can be considered a linear process. Letting s denote the synaptic activity, its value at time t is given by

$$s(t) = \sum_{\hat{t} \in T(t)} q(t - \hat{t}) \tag{5.1}$$

where q is given activation function corresponding to a single spike. This assumption, however, forces us to neglect slow processes at the synaptic sites, for example synaptic depression and potentiation. In order to ensure causality, such that synapses do not anticipate to events that did not occur yet, one requires $q(t) = 0$ for $t < 0$. From the biological point of view, it is natural to assume that the synaptic activation is bounded from above and decays over time. Hence, $q(t) \leq Ce^{-\alpha t}$ for all $t \geq 0$ and some $C, \alpha > 0$.

Furthermore, q is considered as the impulse response of a linear operator $Q : \mathscr{D}' \mapsto \mathscr{D}'$, i.e.

$$Qq = \delta$$

where δ is the Dirac delta mass centered at 0 and equality holds in the sense of distributions. Now the synaptic activation (5.1) takes the form:

$$Qs(t) = \sum_{\hat{t} \in T(t)} \delta(t - \hat{t}) \tag{5.2}$$

where the linearity of Q is used and equality holds in the sense of distributions.

Next, the interactions for a population of neurons are described. For a population of N neurons let s_i denote the synaptic activation for $i = 1,\dots,N$ and T_i the corresponding spike times. The linear operator Q, however, is identical for all neurons in the population. Let $z_i(t)$ be the total synaptic activation of synapses onto neuron i, then z_i is given by:

$$z_i(t) = \sum_{j=1}^{N} w_{ij} s_j(t - \tau_{ij}) \tag{5.3}$$

where the synaptic weight w_{ij} represents the strength of connections from neuron j to i and τ_{ij} is the corresponding transmission delay due to a finite propagation speed. For $x_i : \mathbb{R} \mapsto \mathbb{R}^n$, $x_i(t)$ represents the state of neuron i at time t. Since some single-cell models are based on reset mechanisms which allow jumps in the state-space, the time course of x_i needs not be continuous. Therefore, x_i is taken *càdlàg*, i.e. right continuous with left limits. Away from the spike times $\hat{t}_{i,k}$, for $k = 1,2,\dots$ and $\hat{t}_{i,0} = 0$, the state of the neuron satisfies the differential equation:

$$\dot{x}_i(t) = g(x_i(t), z_i(t)), \qquad x_i(0) = x_{i,0}, \qquad t \in [\hat{t}_{i,k-1}, \hat{t}_{i,k}), k = 1, 2, \ldots \tag{5.4}$$

where g is a model for the dynamics of the neuron. Furthermore, we assume that any finite time interval only contains finitely many spikes.

Now, the full neural network is given by cellular dynamics (5.4), communicating via synapses as in (5.2), which are connected according to (5.3).

5.2.2 Reduction

The network of spiking neurons can be lumped in several ways. Here is chosen to first obliterate the spikes of the individual neurons, which is refered to as *temporal averaging* because it smooths the spike trains produced by neurons. Thereafter, upon making additional assumptions on the spatial structure of the network, the connectivity between the cells can be condensed — this is called *spatial averaging*.

5.2.2.1 Temporal averaging

Time coarse-graining serves two main purposes. Omitting individual spikes of the neurons reduces the amount of bookkeeping. Secondly, possible discontinuities of the underlying dynamical system are smoothed, such that the remaining vectorfield is Lipschitz continuous. Let us consider each of the arguments in more detail below.

Disregarding the spike times of a neuron implies that the neurons within the population interact with each other with rate encoding, rather than spike encoding. In other words, the time-varying rate at which spikes are generated is of greater interest than the precise times at which the individual spikes are generated. This is typically the case for neurons reaching high spiking frequencies, or neurons with relatively slow synapses.

As in many other cases, much can be learned from the system when it is reduced *ad absurdum*. If it is assumed that a neuron generates spikes at a rate $\lambda(t)$, independent of any spikes produced before time t, the spike train of a neuron can be considered as a realization of an inhomogeneous Poisson process [34, §3.1.ii]. Clearly, the memorylessness of the neuron is an unrealistic premise, since neurons do not only have a refractory period, they also tend to almost periodic behavior when firing at high frequencies — in which case spike times are strongly dependent on preceding spikes. Let $\tilde{T}(t;\lambda)$ be the set of spike times generated by an inhomogeneous Poisson process with rate $\lambda(t)$, then the synaptic activation, now a stochastic process denoted by $\tilde{s}(t)$, is again of the form:

$$\tilde{s}(t) = \sum_{\hat{t} \in \tilde{T}(t;\lambda)} q(t - \hat{t}).$$

The process $\tilde{s}$ is called a shot noise process [34, §5.6.ii], whose expectation and variance are given by:

$$\varsigma(t) := \mathbb{E}[\tilde{s}(t)] = \int_0^t \lambda(\tau) q(t-\tau)\, d\tau \qquad \mathrm{Var}[\tilde{s}(t)] = \int_0^t \lambda(\tau) q^2(t-\tau)\, d\tau$$

The expectation ς satisfies the inhomogeneous ODE:

$$Q\varsigma = \lambda,$$

where we imposed the initial conditions $\varsigma^{(k)}(0) = 0$ for all $k = 0, 1, 2, \ldots$.

Similarly as in the original model a network is built of these time-averaged neurons and subscripts are used to specify the synaptic activation, firing rate, etc. for the corresponding neuron. From the expected synaptic activation of a single neuron, one readily arrives, analogous to (5.3), at the expected total synaptic activation onto cell i, denoted by $\zeta_i(t)$:

$$\zeta_i(t) = \sum_{j=1}^{N} w_{ij} \varsigma_j(t - \tau_{ij}). \tag{5.5}$$

Disregarding spikes has a major consequence for the neural models which incorporate spike-dependent reset mechanisms, such as integrate-and-fire neurons and variations thereof. Models of this type have to be adjusted such that:

- the reduced model is independent of spike times, and
- the reduced model yields a firing rate which accurately reproduces the rate of the original model.

The first objective is required in order to obtain a dynamical system which functions in the abscence of spikes times, while the second objective ensures that the synaptic variable can be mimiced adequately. Although the identification of this reduced model is in some special cases straightforward, there does not seem to exist a general procedure for this reduction. In section 5.3 the reduction is performed for three different models: the IF neuron, IF neuron with SFA, and the Izhikevich neuron. The latter is treated in great detail because its reduction is novel and its result convincing.

For now it suffices to assume that such a firing rate reduction exists, characterized by some $\gamma : \mathbb{R}^\nu \times \mathbb{R} \mapsto \mathbb{R}^\nu$ and $f : \mathbb{R}^\nu \times \mathbb{R} \mapsto \mathbb{R}$ such that the rate of change of state $\chi_i(t)$ of the i-th neuron at time t, with $\chi_i \in C^1(\mathbb{R}, \mathbb{R}^\nu)$, satisfies:

$$\dot{\chi}_i(t) = \gamma(\chi_i(t), \zeta_i(t)).$$

Here $\zeta_i(t)$ represents the total synaptic activation on cell i at time t. Furthermore, the instanteneous firing rate f_i of the neuron at time t is given by:

$$f_i(t) = f(\chi_i(t), \zeta_i(t)).$$

which yields the corresponding synaptic activation

$$Q\varsigma_i = f_i.$$

The above three equations, together with (5.5), lead to the temporally averaged model network model.

5.2.2.2 Spatial averaging

Whenever a network has a spatial structure of some sort, it can be considered for spatial averaging. In this section the reduction is performed and the required assumptions are given and discussed.

First of all, a distinction is made between *network structure* and *network connectivity* or *realization*: the former is a prescription, possibly based on physiology, for the generation of connections in the network, which typically involves a random process of some sort. A realization of this process is now called a *connectivity*. Due to the stochastic nature of the connections, one can define the expected weight of a connection: $\bar{w}_{ij} = \mathbb{E}w_{ij}$. Upon denoting the position of the ith neuron by $r_i \in \Omega$, where Ω is a bounded open region of $\mathbb{R}^n$, the expected weight from neuron j to neuron i is expressed as:

$$W(r_i, r_j) = \bar{w}_{ij} = \mathbb{E}w_{ij}$$

The biological background of the model makes it natural to assume that $W : \Omega \times \Omega \mapsto \mathbb{R}$ is continuous. Note, however, that this continuity only applies to the expected value: a realization of the network will almost surely violate this property.

From the synaptic weights, the expected time averaged synaptic activation arriving at a neuron with position r is given by:

$$Z(t, r; r_1, \ldots, r_N) = \sum_{j=1}^{N} W(r, r_j)\varsigma_j(t - \tau(r, r_j)) \tag{5.6}$$

with $\tau(r, r') \in C(\Omega \times \Omega; \mathbb{R}^+)$ denoting the transmission delay from a neuron with position r' to one at r. Have h denote the maximum delay in the system:

$$h = \sup_{r,r' \in \Omega} \tau(r, r')$$

Since $Z(t, r; r_1, \ldots, r_N)$ is continuous, nearby neurons are expected to receive almost identical input. In the abscence of multistability and away from bifurcations, it seems natural to assume that neurons receiving similar input will also spike at a comparable rate. Implications and complications arising from this assumption will be discussed later in more detail, but for now we assume it holds. In this case, the function $F : \mathbb{R} \times \Omega \mapsto \mathbb{R}$, representing the

instantaneous firing rate of a neuron at position r at time t, is continuous too. Likewise, the expected synaptic activation $S(t,r)$, resulting from the equation

$$QS(\cdot,r) = F(\cdot,r)$$

is continuous if and only if its initial value S_0 is so on $[-h,0]\times\Omega$.

By setting $S(t,r_i) = \varsigma_i(t)$ equation 5.6 takes the form:

$$Z(t,r;r_1,\ldots,r_N) = \sum_{j=1}^{N} W(r,r_j)S(t-\tau(r,r_j),r_j).$$

Considering that $Z(t,r;r_1,\ldots,r_N)$ is the expected synaptic input conditioned to the neuron positions r_i, the unconditional expectation might be more valuable. Henceforth, it is assumed that positions $r_1,\ldots,r_N$ are independently and uniformly distributed on Ω. This yields:

$$\begin{aligned}\bar{Z}(t,r) &= \mathbb{E}[Z(t,r;r_1,\ldots,r_N)] \\ &= \frac{N}{|\Omega|}\int_\Omega W(r,r')S(t-\tau(r,r'),r')\,dr'\end{aligned}$$

where $|\Omega| = \int_\Omega dr'$ denotes the size of the domain. By defining the density $\rho = \frac{N}{|\Omega|}$, and dropping the bar, one obtains:

$$Z(t,r) = \rho\int_\Omega W(r,r')S(t-\tau(r,r'),r')\,dr', \tag{5.7}$$

where the neuron density ρ will from now on be included in the weight function W.

The last remaining unknown, which has to be determined before the spatial averaging is completed, is the firing rate $F(t,r)$. Analogous to the previous steps in the procedure, the result of the temporal averaged system is extended to the domain Ω. Hence, the rate of change of the state of a neuron with position r at time t is given by $X(t,r)$, such that:

$$\frac{\partial X}{\partial t}(t,r) = \gamma(X(t,r),Z(t,r)).$$

Similarly, the firing rate is determined by:

$$F(t,r) = f(X(t,r),Z(t,r)).$$

By substition of (5.7) one readily arrives at the neural field formulation:

$$QS(t,r) = f\left(X(t,r),\int_\Omega W(r,r')S(t-\tau(r,r'),r')\,dr'\right) \tag{5.8a}$$

$$\frac{\partial X}{\partial t}(t,r) = \gamma\left(X(t,r),\int_\Omega W(r,r')S(t-\tau(r,r'),r')\,dr'\right) \tag{5.8b}$$

where notation is abused such that $QS(t,r)$ refers to $\big[QS(\cdot,r)\big](t)$.

At this point, the terminology *spatially extended neuron* has become clear, for the structure of the system (5.8) is as follows: The neural field is obtained by essentially extending a single neuron model to space and combining it with a relevant interaction, which has a spatial dependency.

5.2.3 Multiple populations

The derivation presented so far in this section has focused on the reduction of only one population of neurons. Since neural tissue clearly consists of multiple types of neurons, for instance excitory and inhibitory, it appears mandatory to discuss the extension of the neural field (5.8) to multiple populations of cells. Instead of starting with a network of multiple types of spiking neurons and more or less repeating the procdure followed for a single populations, the extended model is put forward without derivation. The same method can be applied, but the notation becomes too convoluted to provide any new insights.

Now, let N denote the number of different populations in the network. Let the neurons in population i be located in a bounded open connected subspace $\Omega_i \subset \mathbb{R}^n$ and suppose they have a synaptic response characterized by Q_i. Furthermore, the states of the neurons underlying population i are given by $X_i : \mathbb{R} \times \Omega_i \mapsto \mathbb{R}^{\nu_i}$ with ν_i representing the dimension of the temporally averaged cell model corresponding to population i. With $S_i : \mathbb{R} \times \Omega_i \mapsto \mathbb{R}$ representing the synaptic activity of neurons in population i, the input $Z_{ij}(t,r)$ from all neurons in population j arriving at neuron of population i with position r at time t is given by:

$$Z_{ij}(t,r) = \int_{\Omega_j} W_{ij}(r,r') S_j(t - \tau_{ij}(r,r'), r')\, dr', \quad r \in \Omega_i$$

with $\tau_{ij} : \Omega_i \times \Omega_j \mapsto \mathbb{R}^+$ the transmission delay from a neuron in population j at position r' to a neuron in population i at position r and $W_{ij} : \Omega_i \times \Omega_j \mapsto \mathbb{R}$ the corresponding weight.

Since synaptic activity arriving at a cell can activate different processes on the receiving neuron, the inputs from different populations are not summed to provide the total input at a neuron, instead they are provided as separate arguments. This allows, for instance, to distinguish between shunting and hyperpolarizing inhibition, or model the effect of a channel which is both ligand- and voltage-sensitive, like the NMDA receptor. By including such features into the time averaging procedure, one obtains for each population i a $\gamma_i : \mathbb{R}^{\nu_i} \times \underbrace{\mathbb{R} \times \ldots \times \mathbb{R}}_{\times N} \mapsto \mathbb{R}^{\nu_i}$ and a $f_i : \mathbb{R}^{\nu_i} \times \underbrace{\mathbb{R} \times \ldots \times \mathbb{R}}_{\times N} \mapsto \mathbb{R}$ such that for $r \in \Omega_i$:

$$Q_i S_i(t,r) = f_i\left(X_i(t,r), Z_{i1}(t,r), \ldots, Z_{iN}(t,r)\right)$$
$$\frac{\partial X_i}{\partial t}(t,r) = \gamma_i\left(X_i(t,r), Z_{i1}(t,r), \ldots, Z_{iN}(t,r)\right)$$

which, for $i = 1, \ldots, N$, completes the mean field formulation for N populations.

5.3 Temporal averaging of specific models

In the previous section, the time-course smoothing procedure has focused particularly on the smoothing of spike trains with respect to network dynamics. The reductions obtained in that manner are dependent on the reduction of a single cell, characterized by $f : \mathbb{R}^\nu \times \mathbb{R} \mapsto \mathbb{R}$ and $\gamma : \mathbb{R}^\nu \times \mathbb{R} \mapsto \mathbb{R}^\nu$ on some reduced state space $\mathbb{R}^\nu$. This step, however, is crucial since the final lumped model inherits all properties of this reduced model, including the flaws the reduction might have. Here, three examples are provided to illustrate how this procedure can be performed for different models.

5.3.1 IF neuron

The first example is the simplest type of an integrate-and-fire neuron. Let $\phi(t) \in [0,1)$ denote the phase of the neuron at time t and have:

$$\dot{\phi}(t) = f(I(t)), \quad \phi \bmod 1, \quad \phi(0) = \phi_0$$

in which $f \in C(\mathbb{R}, \mathbb{R})$ is a non-negative Lipschitz-continuous function denoting the neuron's response to an input current $I(t)$. The neuron generates a spike at time $\hat{t}$ when

$$\lim_{t \nearrow \hat{t}} \phi(t) = 1.$$

From here it is obvious that $f(I(t))$ represents the instantaneous firing rate of the neuron at time t and that there is no need for additional state variables; henceforth ν is set to 0. Whenever the input current I is chosen as the total synaptic input Z, the resulting system is of the form:

$$QS(t,r) = f\left(\int_\Omega W(r,r') S(t - \tau(r,r'), r')\, dr'\right), \quad r \in \Omega \tag{5.9}$$

which, for $Q = \frac{\partial}{\partial t} + \alpha$, yields the most traditional formulation of a neural field.

5.3.2 IF neuron with adaptation

To enrich the dynamics of the integrate-and-fire neuron, the model can be extended with a slow hyperpolarizing current, which activates whenever the neuron generates a spike. The resulting neuron will have spike frequency adaption (SFA), i.e. upon depolarizing stimuli the neuron will spike at a rate which decreases slowly over time. In some cases, the adaptation might even (temporarily) prevent the neuron from spiking. Denoting the slow current with u, the model is of the form:

$$\begin{aligned} &\dot{\phi}(t) = f(I(t) - u(t)), && \phi \bmod 1, \\ &\dot{u}(t) = -\mu u(t), && u(\hat{t}^+) = u(\hat{t}^-) + \psi \text{ for } \hat{t} \text{ a spike time} \end{aligned}$$

for positive μ and ψ.

Similarly as in the IF model without SFA, the firing rate is readily avaible from the equation for the phase ϕ. Since spike frequency is solely dependent on the slow variable and the input current, we consider u as an additional state variable in the reduced model, hence we set $\nu = 1$. As the original dynamics of u are dependent on the spike times of the neuron itself, we have to average the discrete increments over time; resulting a time coarse-grained current $\bar{u}$. For slowly varying firing rates, the current u is expected to increase with ψ every $\frac{1}{f}$ units of time. Hence, the expected increase per unit of time is given ψf, yielding:

$$\dot{\bar{u}}(t) = -\mu \bar{u}(t) + \psi f(I(t) - \bar{u}(t)).$$

By dropping the bar and choosing the input current I to equal the synaptic activation s, one obtains the neural field with SFA:

$$\begin{aligned} QS(t,r) &= f\left(\int_\Omega W(r,r')S(t-\tau(r,r'),r')\,dr' - u(t,r)\right), \\ \frac{\partial u}{\partial t}(t,r) &= -\mu u(t,r) + \psi f\left(\int_\Omega W(r,r')S(t-\tau(r,r'),r')\,dr' - u(t,r)\right) \end{aligned}$$

for $r \in \Omega$.

5.3.3 Izhikevich neuron

The Izhikevich neuron is a popular model in computational neuroscience because it has rich dynamics whilst being computationally tractable:

$$\begin{cases} \dot{V} = 0.04V^2 + 5V + 140 - u + I_{\text{ext}}(t) \\ \dot{u} = a(bV - u) \end{cases}, \qquad V(t^-) = 30 \Rightarrow \begin{cases} V(t^+) = c \\ u(t^+) = u(t^-) + d \end{cases} \tag{5.10}$$

Indeed, with four parameters the model is able to reproduce many of the key features observed in real neural tissue, e.g. intrinsic spiking/bursting, spike-frequency adaptation, and rebound spikes/bursts. Due to a clever reset process, as in all other integrate-and-fire models, the model does not require a fast recovery variable relating to a resonating current. Hence, the variable u is often seen as a slow variable within the neuron, e.g. Calcium concentration.

5.3.3.1 Izhikevich neuron in the phase plane

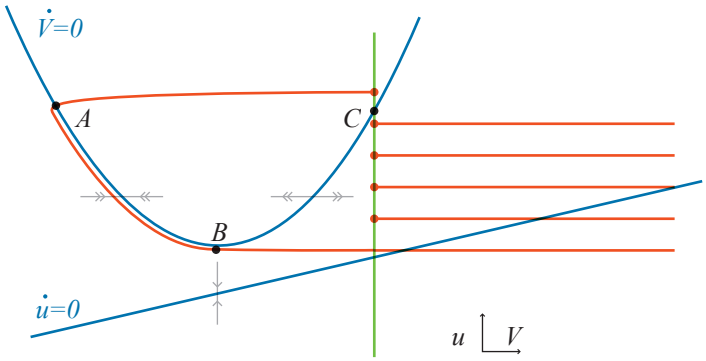

Fig. 5.1 $V-u$ phase plane of the Izhikevich neuron. (Blue) nullclines of V and u, (green) reset value c, and (red) periodic solution of the system. The red dots correspond with resets. See text for description of the points A, B, and C.

Since the Izhikevich model has two variables, phase plane analysis is a natural starting point for characterizing the model. Figure 5.1 depicts the phase portrait of an intrinsically bursting neuron: Starting on the V-nullcline at point A, the dynamics are exclusively governed by the u component which are, in this case, directed downwards. As u decreases slowly, the fast dynamics in the V direction push the system towards the V-nullcline, causing the orbit to closely follow the quadratic V-nullcline. After passing point B, V increases fast until the threshold $V = 30$ is reached and V is reset onto the green line with increased u. As long as the system's reset point is right of the unstable branch of the V-nullcline, another spike is generated. Note that this condition is equivalent to the resets points lying below point C: the intersection point of the V-nullcline and the reset line $V = c$ (in green).

Upon being reset above C, the dynamics in the V-direction are pointing towards the left and the system evolves in that direction until the limit cycle is completed when hitting A.

From this phase plane several key features are chosen, which are to be preserved by the reduced model:

- The right branch of the V-nullcline determines the firing threshold.
- The left branch of the V-nullcline characterizes the dynamics in the subthreshold regime.
- The u-nullcline left of the firing threshold determines the slow dynamics in the subthreshold regime.
- Point B corresponds to the entrance of the bursting regime.
- Point C corresponds to the exit of the bursting regime.
- Point A corresponds to the undershoot after burst termination.
- The firing rate or the reciprocal of the interspike interval.

Furthermore, the Izhikevich neuron also has features which are to be excluded in the reduced model:

- Spiking dynamics and reset.
- The dynamic contribution to u during a spike.

An interpretation of these criteria, expressed as a set of ODEs, is as follows.

5.3.3.2 Realization

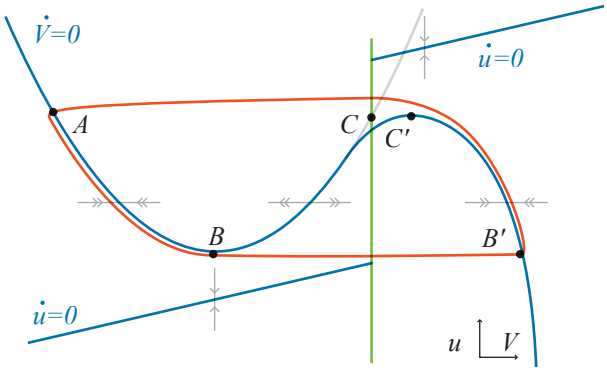

Fig. 5.2 $V-u$ phase plane of the reduced model. (Blue) nullclines of V and u, (green) reset value c, and (red) periodic solution of the system. See text for description of the points A, B, C, and C'.

First, the model's ability to produce spikes, i.e. V quickly reaches 30mV, is taken away by adding another branch to the V-nullcline, see Figure 5.2. Orbits close to this addi-

tional branch correspond with a neuron being in burst-state and, since the condition (non-)bursting is binary, the precise shape and position of this artificial branch are of little importance.

In the bursting regime, the time between consecutive spikes is approximated as follows. Assuming that $J = -u + I_{\text{ext}}(t)$ varies sufficiently slow to be considered as a constant parameter for V, the reduced membrane potential v satisfies:

$$\dot{v} = 0.04v^2 + 5v + 140 + J, \quad v(0) = c \tag{5.11}$$

where the fact is used that v is reset to c after each spike. Albeit nonlinear, this equation has an analytic solution $v(t;J,c)$ which is used to find the time-to-spike T_s for which $v(T_s;J,c) = 30$:

$$T_s(J;c) = T(\sqrt{65-4J};30) - T(\sqrt{65-4J};c),$$

with function T given by:

$$T(j;v) = \frac{5}{j}\left[\ln\left(\frac{25}{2} + \frac{v}{5} - \frac{j}{2}\right) - \ln\left(\frac{25}{2} + \frac{v}{5} + \frac{j}{2}\right)\right]$$

Here it is noted that j is allowed to be complex, in which case the complex logarithm is used. In order to have $T_s(J;c)$ positive and real-valued, it is necessary (and sufficient) that

$$\text{Re}\left(\frac{25}{2} + \frac{c}{5} - \frac{\sqrt{65-4J}}{2}\right) > 0.$$

Hence,

$$0.04c^2 + 5c + 140 + J > 0, \tag{5.12}$$

which is equivalent to (5.11) having a positive right hand side at the initial value.

Inside the bursting regime the instantaneous firing rate is now readily determined as the reciprocal of the inter spike times. Since, by definition, a burst is a brief period during which the neuron fires at high rates, this proposed definition of the firing rate is troublesome, for it might take arbitrary low values. Hence, the firing rate inside the bursting regime is capped at a minimal value:

$$f_b(J;c) = \begin{cases} \max\left(\frac{1}{T_s(J;c)}, f_{\min}\right) & 0.04c^2 + 5c + 140 + J > 0, \\ f_{\min} & \text{otherwise} \end{cases}$$

In order to distinguish between bursting or non-bursting regime, the actual firing rate is set to:

$$f(V,J;c) = H_\omega(V-c) f_b(J;c) \tag{5.13}$$

with H_ω a smooth approximation to the Heaviside step function with steepness-parameter ω. The step function aligned at the reset value now distinguishes between the bursting and non-bursting regimes of the neuron.

This firing rate is not only the main output variable of the neuron, but it is also finds its way back into in the dynamical system. Namely, everytime a spike is generated, the recovery variable is increased by d, which yields an time-averaged increase rate of fd in the reduced model. Hence, the recovery variable in the reduced model takes the form:

$$\dot{u_r} = a(bV_r - u_r) + d \cdot f(V_r, -u_r + I; c).$$

Although the precise position and shape of the additional branch are insignificant, the local maximum at C' is not. Since at this point the stability of the slow manifold, i.e. V-nullcline, changes due to a fold bifurcation, it corresponds with the termination of the burst. For that reason it is important that this maximum is in line with the original termination point C, such that the undershoot at A is preserved accurately. Taking into account the requirement that subthreshold behavior should not be modified too much, the new branch is conveniently introduced by an exponential. In this case, the full reduced system takes the form:

$$\begin{cases} \dot{V}_r = 0.04V_r^2 + 5V_r + 140 - u_r + I_{\text{ext}}(t) - \xi \exp(\eta(V - c)) \\ \dot{u}_r = a(bV_r - u_r) + d \cdot f(V_r, -u_r + I_{\text{ext}}(t); c) \end{cases} \tag{5.14}$$

with η and ξ parameters characterizing the additional branch. Appropriate values for these parameters can be determined as follows: Have $u = n_v(V)$ depict the V-nullcline of the original Izhikevich model, then the level of point C in Figure 5.2 is given by $n_v(c)$. For $u = n_{vr}(V_r) = n_v - \xi \exp(\eta(V - c))$ the V_r-nullcline of the reduced model, the following equations should hold to have point C' at the same level as C:

$$\begin{aligned} n_{vr}(c + \kappa) &= n_v(c) \\ n'_{vr}(c + \kappa) &= 0 \end{aligned}$$

with κ representing the horizontal separation between C and C'. Solving the equations results in:

$$\eta = \frac{n'_v(c + \kappa)}{n_v(c + \kappa) - n_v(c)} \qquad \xi = \frac{n_v(c + \kappa) - n_v(c)}{e^{\eta \kappa}}.$$

It is undesirable to choose low values of κ since the additional branch will be very steep and the stiffness of the dynamical system increases unnecessarily. Large values, on the contrary, will result in a branch which is too gradual, such that both the timing and the subthreshold behavior are affected. Here κ is chosen as 0.8.

5.3.3.3 Single cell comparison

In order to assess the quality of the proposed reduction (5.14), simulations are performed for different parameters of the model. Not only the membrane potentials and recovery variables of both models, also the output firing rate of the reduced model is matched with the discrete spikes of the original model. For that, define:

$$N(t) := \text{number of spikes in } [0,t] \tag{5.15a}$$

$$N_r(t) := \int_0^t f(V_r(\tau), -u_r(\tau) + I_{\text{ext}}(\tau))\, d\tau \tag{5.15b}$$

for the Izhikevich and the reduced model respectively.

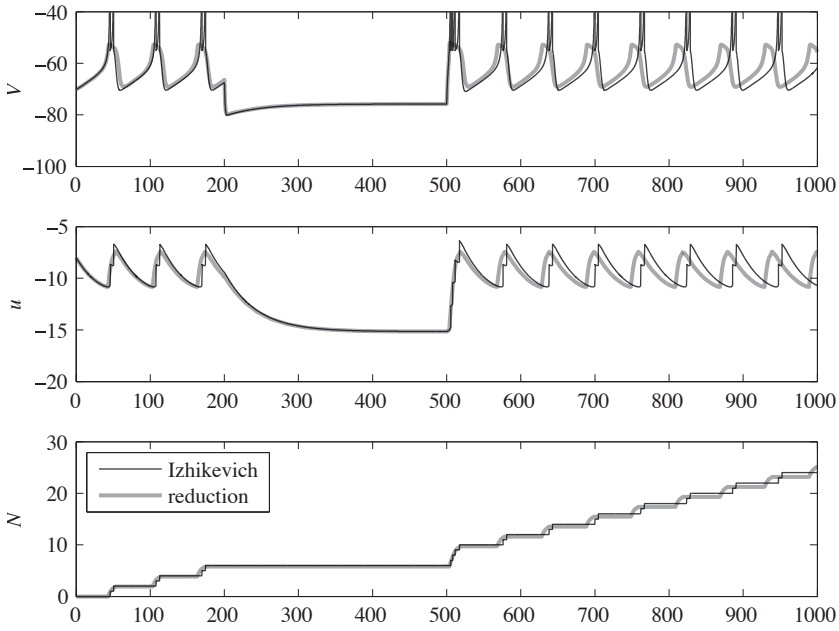

Fig. 5.3 Tonic bursting neuron, which is suppressed with a negative current. Top, middle, and bottom diagrams correspong with V, u and N (c.f. (5.15)) respectively. Parameters as follows: $a = 0.02$, $b = 0.2$, $c = -55$, $d = 2$, $\kappa = 0.8$, and $f_{\min} = 0.1$. Furthermore, a background current I_0 is given of magnitude 6, which is set to -6 between 200–500ms, resulting in a suppression of the bursting pattern.

Figure 5.3 shows a typical comparison of two tonically bursting neurons. The general impression is that the reduction very successful in mimicing the original Izhikevich model. Although in the latter half of the simulation the inter-burst frequency of the reduced model

is higher, which results in a phase difference between both models, the average spiking behavior, on the other hand, is accurately preserved by the reduction.

An overview of other types of spiking behavior is given in Appendix B.

5.3.3.4 Neural field formulation

For completeness we state the full neural field formulation:

$$QS(t,r) = f\left(V(t,r), I(t,r)\right), \tag{5.16a}$$

$$\frac{\partial V}{\partial t}(t,r) = 0.04V^2(t,r) + 5V(t,r) + 140 + I(t,r) - \xi \exp(\eta(V(t,r) - c)), \tag{5.16b}$$

$$\frac{\partial u}{\partial t}(t,r) = a(bV(t,r) - u(t,r)) + d \cdot f\left(V(t,r), I(t,r)\right) \tag{5.16c}$$

where f is given by (5.13) and $I(t,r)$ by

$$I(t,r) = -u(t,r) + I_0 + \int_\Omega W(r,r')S(t - \tau(r,r'), r')\, dr' \tag{5.16d}$$

with I_0 representing a constant applied background current.

5.4 Comparison

Now that we discussed the general derivation of neural fields and described how this formulation is dependent on the type of spiking neuron of which the network consists, we study how well the proposed neural fields corresponds to the network of spiking neurons they represent. Simulations of the neural field and the detailed model are performed for all three cases discussed in the previous section, i.e. integrate-and-fire, integrate-and-fire with SFA, and the Izhikevich neuron.

Here, only the dynamics of a single population of merely identical neurons are considered, since we are primarily interested in the quantitative and qualitative comparison of both formulations. As we are limited to only a single population, we cannot make a distinction between excitatory and inhibitory neurons. Instead, narrowing our interest strictly to the mathematical formulation and correctness of neural fields, we violate the biological premise by allowing neurons to make both excitatory and inhibitory connections. Although the physiological relevance of these simulations is contrived, successes obtained in this setting will certainly assist in understanding models which are physiologically relevant.

Setup

To start, we only consider one-dimensional networks on the interval $\Omega = [-1,1]$ and exponential synapses with a decay rate α are chosen for all connections in all network, i.e. $q(t) = e^{-\alpha t}$ for $t \geq 0$ and hence:

$$Q := \frac{d}{dt} + \alpha$$

Furthermore, in the spiking neuron network we set p_{con} as the probability for one neuron to make a connection to another. The synaptic weight of this connection will be dependent on the distance between the neurons with position r and r':

$$w(r,r') = \hat{c}_1 e^{-\mu_1|r-r'|} + \hat{c}_2 e^{-\mu_2|r-r'|}.$$

The expected weight for a connection, which takes in account the neural density $\rho = \frac{|\Omega|}{N}$, is now given by:

$$W(r,r') = p_{\text{con}} \frac{2}{N} \left(\hat{c}_1 e^{-\mu_1|r-r'|} + \hat{c}_2 e^{-\mu_2|r-r'|} \right).$$

This is equivalent to setting:

$$W(r,r') = c_1 e^{-\mu_1|r-r'|} + c_2 e^{-\mu_2|r-r'|}, \qquad c_i := \hat{c}_i p_{\text{con}} \frac{2}{N}, \quad i = 1,2$$

Furthermore, we choose time lags of the form $\tau(r,r') = \tau_0 + \frac{1}{v}|r-r'|$ with τ_0 representing the onset delay of synapses and v the conduction velocity of action potentials. Now, both the form of W and τ are in accordance with [118].

Next to the inhomogeneties introduced in the spiking neuron network, due to the random generation of connection, we slightly randomize the parameters of the individual cells, too. This type of perturbation will ensure that the synchronization patterns we observe are caused due to the network interactions, rather than to intrinsic properties of the neurons. Within the neural field formulation, the expected value of each of these parameters is used.

Finally a word on the initial conditions: as delays are present in the synaptic variable S, it is required to define its history up to the maximal delay in the system. We choose for the case in which no action potentials have taken place before $t = 0$ and hence $S(t,r) = 0$ for $t \leq 0$. For the models which include a slow variable, i.e. u in the IF with SFA and Izhikevich models, a small linear gradient across space is applied at $t = 0$, such that the system starts in an asymmetric state.

Simulations

Simulations of the spiking neuron network are performed with Norns — Neural Network Studio [124]: a dedicated C++ simulation tool with an intiutive Matlab interface. We distribute the total number of neurons equidistant on the domain Ω and generate the connections as described above. The spike trains obtained from Norns are post-processed within Matlab, which we discuss in detail below. All simulations with the spiking neuron network are performed for $N = 400$.

The neural field reduction is discretized on an equidistant mesh, as proposed by [50], such that the resulting system is a finite system of delay differential equations with a finite number of delays. This discretization is then evaluated using solvers for DDEs, like `dde23` in Matlab or, when the system is stiff, RADAR5 in Fortran [57]. Except where noted, simulations are run on a mesh of 60 elements.

Comparison

To assess the comparison between both models, it is desirable to compare the same physical quantities within both models. In this light, the synaptic activation S appears to be the best choice: it can be determined from individual spike trains and it is the key variable in the neural field formulations.

For the neural fields, S is readily available from the spatial discretization which is used to perform the simulations. In the network of spiking neurons, we reconstruct the synaptic activation of all neurons by convolving the spike train with the template q. Since this is essentially temporal averaging of the spike trains, we will also perform a type of spatial averaging on the spike data in order to assist in a better comparison with the lumped model. To that, we divide the neurons among groups of ten, i.e. the cell numbers 1–10, 11–20, etc., and we determine the average synaptic activation of every group. This characterization of the network activity has a comparable resolution in both space and time as the discretization of the neural field, such that comparing both models should be natural.

5.4.1 IF model

The integrate-and-fire neuron is studied for the sigmoidal activation function f:

$$f(I) = \frac{a}{1+e^{-2(I-b)}}$$
$$a \sim N(0.2, 0.02), \qquad b \sim N(0.2, 0.1)$$

Results of the model are depicted in 5.4 for an “inverted wizard hat”-type connectivity.

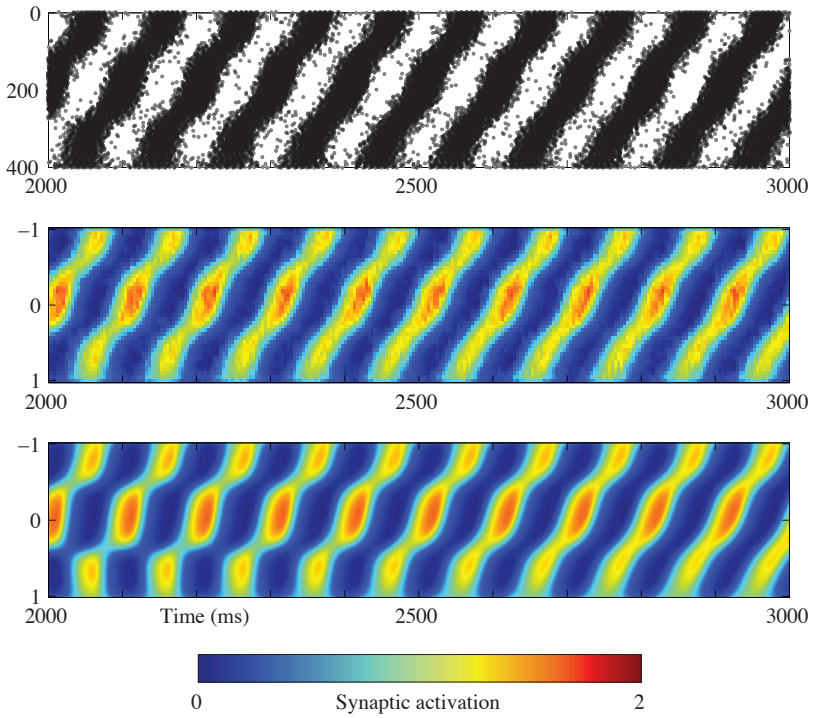

Fig. 5.4 Comparison of a network of integrate-and-fire neurons with the corresponding neural field. (Top) shows raster plot of all spikes of the individual neurons in the network, (middle) shows the coarse-grained synaptic activation of the spiking neuron network, (bottom) depicts the matched neural field. Time along the horizontal axis is measured in ms, while space is depicted along the vertical axis. Parameters as follows: $\alpha = 10$, $p_{\text{con}} = 0.9$, $c_1 = 9$, $c_2 = -18$, $\mu_1 = 2$, $\mu_2 = 5$, $\tau_0 = 40$, $v = 10^{-1}$. Note that the domain is *not* periodic, one wavefront is generated while another deceases.

There is an obvious similarity between both models: not only the qualitative behavior of the traveling pulse is captured by the neural field, it does so quantitatively:

- The period of the oscillations is accurately mimiced.
- The intensity of the synaptic activation at certain time matches in both models.
- Subtle features due to transient behavior are preserved as the model approaches its limiting attractor at $t = 3000$, in particular the block-like structure seen close to $t = 2000$.

Even though small inhomogeneties are present in the spiking neuron network, the neural field is able to mimic the underlying network very accurate. Simulations for a lower probability, as low as $p_{\text{con}} = 0.2$, still show a striking correspondence

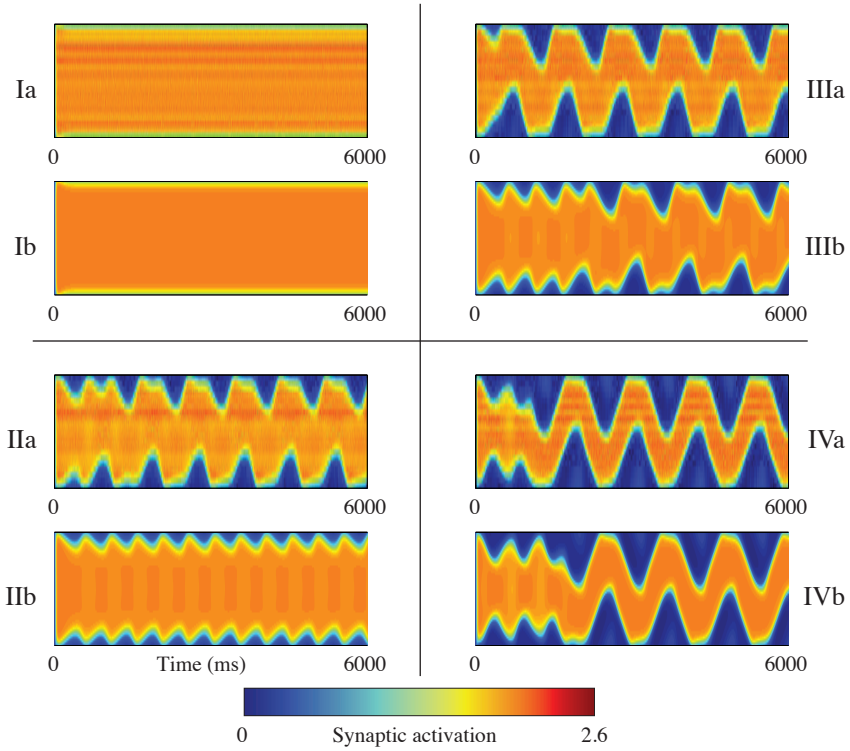

Fig. 5.5 (I)-(IV) showing simulations for decreasing width parameter μ_1 of lateral inhibition in a network of IF neurons with SFA (a), combined with the corresponding neural field (b). The neural field (IIa) corresponds with a breather. See text for a detailed description of the behavior and comparison. Parameters: $\alpha = 10$, $p_{\text{con}} = 0.75$, $c_1 = -5$, $c_2 = 10$, $\mu_2 = 4$, $\tau_0 = 10$, $v = 5^{-1}$, $\mu = 100^{-1}$ (adaptation) and $\psi = 0.05$; $\mu_1 = [2.6, 2.32, 2.3, 2.2]$ for (I)-(IV) respectively.

5.4.2 IF model with adaptation

More complicated dynamics are expected to be seen in the neural fields with adaptation. In the absence of delays, a common phenomenon occuring in these fields is the so-called *breather* [52]: a localized spot of increased activity whose width changes periodically over time. They are typically found in systems with local excitation and lateral inhibtion, combined with a rather steep firing rate curve f. Here we focus on this type of behavior as well and, in particular, how well the spiking neuron network is able to exhibit the same behavior.

A series of simulation for a decreasing width parameter μ_1 of the lateral inhibition is performed. For this series, we enhance the steepness of the firing rate function, such that we obtain:

$$f(I) = \frac{a}{1+e^{-4(I-b)}}$$
$$a \sim N(0.2, 0.02), \qquad b \sim N(0.2, 0.1)$$

Figure 5.5 depicts how the neural field transitions from a stationary "bump"-solution (Ib) to a breather (IIb). Although the underlying spiking neuron network reproduces the bump (Ia), a breather is not to be seen in (IIa). Instead, the network exhibits a spot of activity which travels periodically along the full domain, at a frequency which is close to half of the breather (IIb). The origin of this type of behavior may be explained by (IIIb): a small change in the parameter μ_1 (i.e. from 2.32 to 2.3) results in what appears to be a symmetry-breaking period doubling bifurcation of the periodic breather solution. The spiking neuron network, on its turn, accurately mimics this type of behavior in (IIIa), apart for a phase-shift. This type of behavior continues to exist in (IV) for another decrement of the parameter.

Returning to the fact that no breather is seen in the spiking neuron network, we speculate the following: Indeed, the neural field is able to exhibit breather behavior, but its regime in parameter-space is rather small. It seems, therefore, most likely that the inhomogeneties in the detailed model interfere with the expression of this delicate behavior. Yet another reason might come from the fact that additional simulations in the same parameter regime, which are not shown here, suggest that a more complex bifurcation structure is present. If this is the case, then the discrepancy between (IIa) with respect to (IIb) could be due to presence of multiple attractors in the system or due transient behavior. In the latter case, one should keep in mind the inhomogenities of the underlying network; very delicate structures are not expected to be reproduced in the presence of random perturbations.

A dissimilarity between both models is also found the other way around, i.e. the spiking neuron network exhibits multistability while the neural field captures only one of these solutions. Figure 5.6 depicts how for different initial conditions the network of spiking neurons can exhibit two different solutions (top and middle). Independent of the initial conditions chosen, however, the neural field would always result in a limiting behavior shown in the bottom diagram.

Similarly as in the other case, where the neural field exhibited a type of behavior not captured by the detailed model, it is possible that a bifurcation is nearby. Inhomogenities in the spiking neuron network "soften" the definite nature of bifurcations, suggesting that a bifurcation is imminent when a parameter is altered.

5.4.3 Izhikevich model

We compare a network of intrinsically bursting Izhikevich neurons to the derived neural field (5.16). The discretization of the neural field appears to be a stiff problem, as we

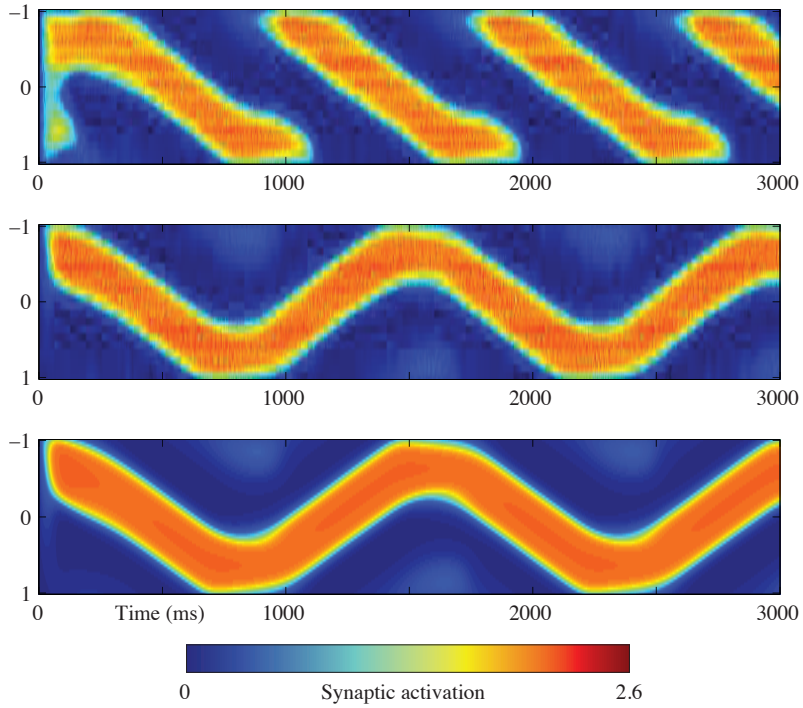

Fig. 5.6 Bistability in a network of IF neurons with SFA (top and middle) is not reproduced by the neural field (bottom). See text for a more detailed description. Parameters: $\alpha = 10$, $p_{\text{con}} = 0.75$, $c_1 = -5$, $c_2 = 10$, $\mu_1 = 2$, $\mu_2 = 4$, $\tau_0 = 10$, $\nu = 5^{-1}$, $\mu = 100^{-1}$ (adaptation) and $\psi = 0.05$.

will discuss in more detail below, hence the simulations of this model are performed with RADAR5.

A typical result related to a weak lateral inhibtion type connectivity is depicted in Figure 5.7. The figure shows both the start of the simulations and a fragment further into the simulation.

In the beginning of the simulations the neural field is able to capture the key features of the spiking neuron network, in particular the synaptic activation (i.e. left middle and bottom). Indeed, both the frequency and the very slight curvature of the wave fronts (the latter one is most clear by comparing the first and last wave front in the bottom left corner) are conserved by the neural field. On the other hand, by comparing the synaptic activation with the raster plot, i.e. left middle and top, we observe a notable discrepancy, too. That is: the spiking neuron network has subtle traits which are not, or barely, captured by the synaptic acitivity of the network. In particular, the black arrows indicate the 'echoing' of wave fronts, during which a subset of neurons fires collective at a marked point later in

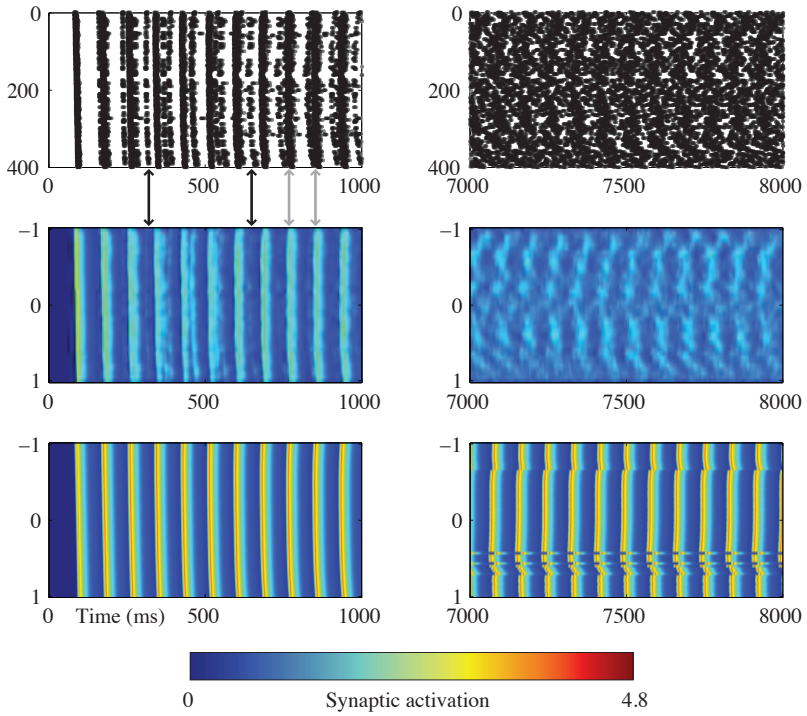

Fig. 5.7 Comparison of a network of Izhikevich neurons (top two rows) and the corresponding neural field (bottom row). At the beginning of the simulation, the raster plot (top left) reveals some features of the network which are barely seen in the synaptic activation (middle left). These include, indicated with black arrows, 'echoing:' a portion of neurons fires coherently some time after the majority has fired. Gray arrows represent 'widening,' i.e. a less synchronous wave front. The right diagrams depict a later moment in the simulation, where a notable dyscrepancy is seen between the spiking neuron network (right middle) and the neural field (right bottom). Parameters: $\alpha = 30$, $p_{\text{con}} = 0.8$, $c_1 = 0.6$, $c_2 = -0.2$, $\mu_1 = 3$, $\mu_2 = 0.5$, $\tau_0 = 10$, $v = 5^{-1}$, $a = 0.02$, $b = 0.2$, $c \sim N(-50, 1)$, $d = 2$, $I_0 = 6$.

time. Also, the 'broadening' of wave fronts occurs, where neurons fire less coherently, as is designated by the gray arrows, None of these effects are seen in the neural field model.

The discrepancy between both models is more apparent at a later point in time, c.f. the right column of diagrams in Figure 5.7. While the dominant frequency of the waves is preserved, the shape has become quite different. The neural field is dominated by rather clear wave fronts, whereas the spiking neuron network appears less structured. A subtle feature of the wave fronts is preserved though: the broken wave fronts at the top and bottom the network, which are distinctly visible in the neural field, are, at closer inspectation, also present in the spiking neuron network.

Finally we comment on the fracturing of the wave fronts in the neural field. The fact that the wave fronts fall apart suggests that the spatial resolution of the discretization is

insufficient. Whereas the low resolution will play an important role in this effect, another reason should be considered too. At closer inspection, the proposed Izhikevich reduction is essentially an oscillator of the relaxation type, i.e. its limit cycle arises due an interplay of bifurcations of the *layer problem* with respect to the slow variable. Fenichel theory prescribes that the limit cycles are particularly sensitive to perturbations whenever the orbit is near one of these bifurcations [51]. Since the discretization of the neural field is essentially a finite collection of relaxation oscillators, it is to be expected that the system will, at some points in time, be more sensitive to perturbations than at other moments. This might explain why the fragmentation is particularly observed at a point later in time rather than at the beginning: after more periods have passed, it has become more likely that two neigboring oscillators received a slightly different input while their orbits were close to a critical point.

Another pair of simulations is depicted in Figure 5.8, this time with an "inverted wizard hat" type of connectivity. Furthermore, the spatial discretization now incorparates 120 mesh elements, compared to 60 in all other simulations.

At first glance we note that the correspondence between both models is much better than in the previous case, particularly because of the wave fronts which have remained well defined over the course of time. Furthermore it is seen that at the beginning of the simulation the neural field is able to capture some of the key features of the spiking neuron network, in particular the phase advancing of the lower half of the network and one position at which the wave front tends to break. Later in the simulation, i.e. right column of diagrams, we observe that the wave front of the neural field has broken several times already, and that another breakline is imminent just below the middle line (indicated with arrow). Although the simulation is performed at an increased resolution, the wave front is still deteriorated, suggesting that wave breaking is independent of resolution. Indeed, this idea is strengthened by the fact that the spiking neuron network also seems to have a broken wave front. Hence, we conclude that wave breaking is a systemic feature of the system and it should therefore not be obliterated from the analysis.

Therefore, we focus on the breaking of waves more detailedly: first a qualitative description of the phenomonon and consequently we speculate on the possible underlying mechanism. Figure 5.9 depicts the phase difference θ of a wave front with respect to some global oscillation of the system. The horizontal axis of each diagram represents a subinterval of the one dimensional domain Ω. Here (I) shows an 'intact' wave front, i.e. a wave front which has not broken until a specific moment, and hence, the phase difference θ is merely constant. At a certain point in time, one part of the wave advances its phase faster than the remaining part, such that two distinct wave fronts arise, c.f. (II). Since, due to the formulation of the system, continuity is preserved, a *breakline* appears, i.e. an interval where the phase of the wave front takes intermediate values: this region is marked gray. Note that if this region is small, the spatial discretization might not be able to capture this

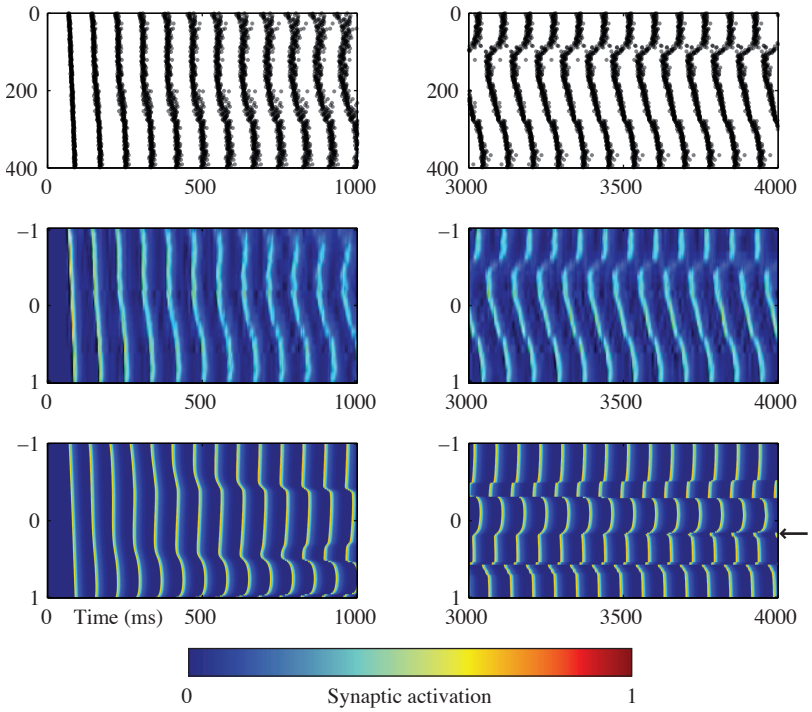

Fig. 5.8 Comparison of a network of Izhikevich neurons (top two rows) and the corresponding neural field (bottom row). At the beginning of the simulation (left diagrams) both networks show qualitative comparable behavior: in particular the phase advancement of the wave front near $x = 0.8$. Later in the simulation (right diagrams) the comparison is less clear, especialy since the wave front in the neural field (right bottom) has broken several times already. The black arrow indicates a position where the temporal evolution of a breakline is shown. However, the spiking neuron network (right top and middle) suggest that wave breaking also occurs naturally in the detailed model. Parameters: $\alpha = 10$, $p_{\text{con}} = 0.9$, $c_1 = 12.5$, $c_2 = -25$, $\mu_1 = 2$, $\mu_2 = 5$, $\tau_0 = 40$, $v = 10^{-1}$, $a = 0.01$, $b = 0.2$, $c \sim N(-55,1)$, $d \sim N(8,0.1)$, $I_0 \sim N(10,0.1)$. The number of mesh points of the neural field was set 120.

region and, hence, the breaking appears as a discontinuity in the simulations. The part of the wave front which advanced with repest to the remaining part, can move ahead one half or one full phase allowing both wave fronts to synchronize again, c.f. (II)-(IV), apart from the breakline. Furthermore, we typically observe that the width of the breakline diminishes as the phase difference between the wave fronts decreases: see (IV) and (V). This suggests that at some point in time the width of the breakline might become negligible, such that the states (I) and (V) are almost identical. Hence, another wave break could be initiate, of which the result is depicted in (VI). This illustrates that, when this phenomenon occurs recurrently, absolute continuity of the solution might be lost.

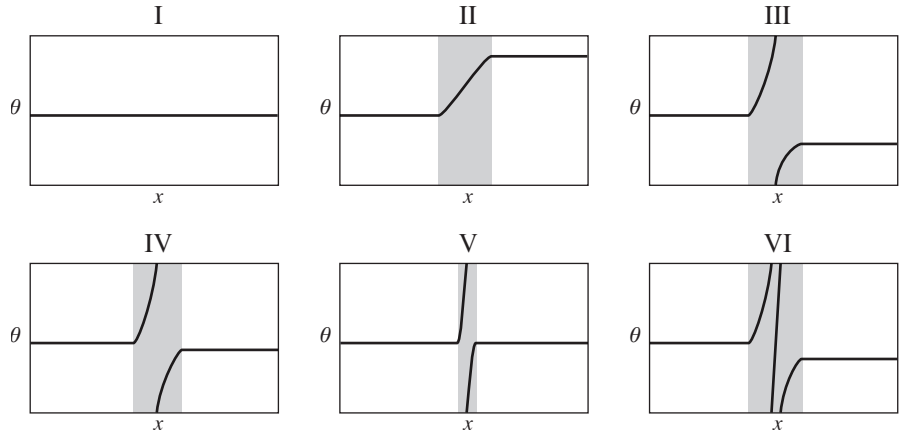

Fig. 5.9 Caricature illustrating a possible mechanism for wave breaking. The local phase difference θ of the wave front, with respect to some global oscillation, is plotted for an subinterval of Ω. (I)-(V) shows how the phase differences might evolve when a wave breaks, gets ahead half period and synchronizes again with the remaining part of the wave front. (VI) illustrates that this phenomenon can be recurrent, which might eventually lead to a loss of absolute continuity. Whenever the breakline (i.e. marked region) is narrow, the effect might appear as a discontinuity when discretized. See text for a more detailed description of the processes playing a role in the phenomenon. Note that the phase difference θ remains, despite the jumps seen in the diagrams, continuous since it is considered on the cylinder, i.e. modulo π.

The mechanisms that underly the wave breaking are not clear at this point and further analysis is required to characterize the phenomenon in more detail. Instead we hint on a particular process: first of all, it appears that the formation of wave fronts is global property of the system. This follows not only form the fact that wave fronts continue to exist for extended periods of time (as opposed to desynchronized activity in which neurons fire seemingly uncorrelated), but it is strengened by the observation that broken wave fronts have the tendency to restore their synchrony, either in-phase or anti-phase, at a global scale — apart from a negliable the breakline. But as the orbit approaches a synchronous solutions, it appears that other mechanisms come into play which are in favor of wave breaking. In this respect, wave breaking and, consequently, the restoration of broken fronts show correspondence with a homoclinic orbit: a particular state might attract nearby solutions, but as orbits near this state, they are repelled into a another direction.

5.5 Discussion

We have demonstrated that the prevalent procedures for condensing a network of spiking neurons to a neural field, such as [133, 2, 99, 98, 80, 15, 16], can be expanded to more general single cell models than the commonly assumed (leaky) integrators. The proposed

method consists of two distinct procedures: first temporal averaging is performed such that we, for each neuron, specify the rate at which action potentials are generated rather than the precise timing of each spike. Secondly, spatial averaging can be applied when the network has a particular spatial structure.

No general procedure exists for temporal averaging of a single cell model, but we show by example that is not necessarily limited to leaky integrators. Indeed, we show that the firing rate of an Izhikevich neuron [68] can be accurately mimiced by a dynamical system that leaves the subthreshold dynamics intact. The reduction matches quantitatively with the original model and it is able to capture more advanced types of spiking behavior, such as bursting and rebound spikes/bursts.

Such a single cell firing rate reduction can be extended across a spatial domain to represent a population of neurons. The connectivity between the neurons can be in some cases be condensed due to spatial averaging. Therefore it is required that the network is a random graph: the probability of having a connection between two neurons is independent of any other connections in the network and, furthermore, it depends only on the position of the source and target neuron, in a continuously differentiable manner. Similarly, the synaptic weights of each connection are also assumed to be independent random variables which only depend smoothly on the positions of two connecting neurons. These particular assumptions exclude the possibility to condense networks whose structure is not entirely random, e.g. small-world and scale-free networks: both of which arise in prevalent detailed models [92].

Next to describing the general assumptions and premises of the lumping procedure, we also show how well the proposed reductions relate to the underlying spiking neuron network. This is primarily done by comparing simulation results of both models. It is first shown that the reduction for integrate-and-fire neurons in very accurate: not only the asymptotic spatiotemporal pattern is reproduced, but subtle features of the transient behavior too.

Extended with spike frequency adaptation, neural fields are capable of generating breathers [52]. Indeed, we are able to replicate this pattern in the current setting, which also incorporates space dependent delays. We find that for our particular choice of the parameter regime that the region in which the breather exists is fairly small. Therefore, this particular solution is not observed in the corresponding spiking neuron network. Other attractors, on the contrary, such as a stationary bump and an assymmetric breather are genuinely reproduced.

Although the firing rate reduction of a single Izhikevich neuron is accurate, the corresponding neural field is less so. Wave fronts formed by synchronously bursting neurons can break or otherwise deteriorate in both the spiking neuron network and the neural field. The breaking of wave fronts has been reported before with respect to a discrete chain of weakly coupled relaxation oscillators [104]. Since the reduced Izhikevich model is indeed

an oscillators of the relaxation type, it appears that this phenomenon is related to this kind of oscillators. Hence, further mathematical analysis of spatial networks of these oscillators is required in order to understand the processes involved in the breaking of wave fronts. Consequently, this analysis will be valuable for improving the neural field formulation with exhibit wave breaking.

Indeed, the framework rooted on sun-star calculus, as proposed in [118], appears to be a convenient setting for characterizing the phenomenon. Based on empirical findings, however, we suggest the possibility that recurrent breaking of wave fronts can result in a loss of absolute continuity. In this particular case, the asymptotic solution might contain a fractal structure of some sort, which is likely to hinder its analysis.

Hence we can conclude that neural fields have the potential to capture more realistic types of spiking behavior, such as exhibited by the Izhikevich neuron. In pursuit of a suitable neural field reduction, which is accurate as well as workable, this work offers promising explorative results. We show that it is required to refine the aspects of both modeling and mathematical analysis in order to achieve such a reduction.

Chapter 6
Conclusions and outlook

No single model would be able to capture all processes in the brain at once, since its interactions are too numerous and too complex. Therefore, a sensible understanding of the complex brain network can, due to its multiscale nature, only be attained by setting up an entire hierarchy of models. In this hierarchy, each model is dedicated to a particular phenomenon of the system, such that it provides an insightful and workable description of that phenomenon. Ideally, every model has a close connection with others, in the sense that it is based on currently existing models and that it can be validated using others. In this light, it is common practice to apply some sort of averaging, or lumping, in order to relate processes occuring at a smaller or faster scale to a coarser or slower scale. However, it appears that not all models are combined in a straightforward manner, especially not those involving many scales. The work presented in this thesis focuses on a particular class of models which has revealed itself as being challenging to fit into the multiscale framework: namely the emergent behavior of networks of neurons.

Since, until now, no generic procedure exists for reducing an arbitrary network of spiking neurons to an insightful description for their collective action, an *ad hoc* approach is often chosen, which emphasizes particular features of the network at hand. Indeed, in chapters 2 and 3 it is shown that such an approach can be highly convincing: the behavioral changes due to variations in two parameters matched qualitatively with the original detailed model. For such reductions, however, since they are based on imprecise assumptions, it is generally not clear for what regions in parameter space they are legitimate and, hence, it is required to routinely validate the reduced model with the original network. Yet, these types of reductions are still valuable to determine 'points of interest' at which the behavior of the underlying spiking neuron network can be studied in more detail.

Clearly, the development of a more general framework, which facilitates the lumping of networks of spiking neurons, is desirable in the near future. Chapter 4, therefore, focuses on the establishment of a functional analytic setting for neural fields incorporating transmission delay, showing that mathematical analysis of stability and bifurcations wi-

htin these models is indeed tractable. Consequently, in Chapter 5, attention is given to the formulation and derivation of such models from a network of spiking neurons. Explicitly stating all assumptions made in the reduction, the framework is shown to facilitate the inclusion of more complex cell dynamics.

While the preliminary results presented here are promising, there is a lot room for improvements and extensions. With respect to the abstract setting of the neural fields, for instance, essential questions remain about the spectral properties as well as — more pragmatically — the identification of a characteristic equation at spatially non-homogeneous steady states. Furthermore, the proposed field of Izhikivich neurons should be studied more analytically and, in particular, the phenomenon of wave breaking. On the side of model formulation and derivation, it is highly recommendend to take into account stochastic components within the derivation of lumped models. Such stochasticity might not only accommodate for the unobserved processes in the network but also, with a proper correlation structure, allow the reduction of networks with a particular structure, e.g. small-world or scale-free.

Finally a word on the applicability of the work in this dissertation. Indeed, the majority of the presented results relates to conceptual and simplistic networks of spiking neurons, but, with a proper understanding of these fundamental networks, the functioning of more complex models might readily be explained. Both the application of dynamical system's theory, allowing identification of multistability and behavioral transitions, and the utilization of elementary networks, which are only able to capture coarse features of the network's dynamics, encourage the modeling of epileptic seizures. This idea is further strengthened by the observation that the spatial scale of the studied networks (approximately 1mm–10mm) coincides with the typical size of epileptic foci.

Appendix A
Proof of Proposition 4.26

We use the same notation as in Lemma 4.23 and its proof. We recall that the vector $Z = [\zeta_0, \zeta_1, \ldots, \zeta_{N-1}, 1]$ is chosen such that the vector $\beta = [\beta_0, \beta_1, \ldots, \beta_N]$, whose elements are the coefficients of the characteristic polynomial $\mathscr{P}$, is given by $\beta = M^T Z$. Introducing $r := [1, \rho^2, \rho^4, \ldots, \rho^{2N}]$ we see that

$$\mathscr{P}(\rho) = r^T M^T Z \tag{A.1}$$

First we determine the vector Z, thereafter we split M, and we conclude the proof by determining how Z acts on each factor in this decomposition.

Although Z can be obtained by applying the inverse of the Vandermonde matrix W, we will proceed in a different manner. We start by rewriting (4.42) as

$$\begin{bmatrix} 1 & k_1^2 & k_1^4 & \ldots & k_1^{2N-2} & 0 \\ 1 & k_2^2 & k_2^4 & \ldots & k_2^{2N-2} & 0 \\ \vdots & \vdots & \vdots & & \vdots & \vdots \\ 1 & k_N^2 & k_N^4 & \ldots & k_N^{2N-2} & 0 \\ 0 & 0 & 0 & \ldots & 0 & 1 \end{bmatrix} \begin{bmatrix} \zeta_0 \\ \zeta_1 \\ \vdots \\ \zeta_{N-1} \\ 1 \end{bmatrix} = \begin{bmatrix} -k_1^{2N} \\ -k_2^{2N} \\ \vdots \\ -k_N^{2N} \\ 1 \end{bmatrix} \tag{A.2}$$

For $m \in \mathbb{N}$ we define $P_m := [p_1, p_2, \ldots, p_m]$ with $p_i \in \{0,1\}$ for $i = 1, \ldots, m$. We set $|P_m| = \sum_{i=1}^m p_i$ equal to the number of 1's in P_m. Using Gaussian elimination the solution of (A.2) is found to be

$$Z = \begin{bmatrix} (-1)^{N-0} \sum_{|P_N|=N-0} k_1^{2p_1} k_2^{2p_2} \ldots k_N^{2p_N} \\ (-1)^{N-1} \sum_{|P_N|=N-1} k_1^{2p_1} k_2^{2p_2} \ldots k_N^{2p_N} \\ \vdots \\ (-1)^{1} \sum_{|P_N|=1} k_1^{2p_1} k_2^{2p_2} \ldots k_N^{2p_N} \\ 1 \end{bmatrix}$$

From the proof of Lemma 4.23 we recall the decomposition

$$M^T = e^{\lambda\tau_0}(\lambda+\alpha)I + 2\Xi \tag{A.3}$$

where I is the $(N+1)\times(N+1)$ identity matrix and Ξ was defined in the proof of Lemma 4.23. Expanding the bilinear forms in the matrix Ξ and moving the summation in front of the matrix yields

$$\Xi = \sum_{i=1}^{N} c_i k_i \Xi_i, \qquad \Xi_i := \begin{bmatrix} 0 & 1 & k_i^2 & \dots & k_i^{2(N-1)} \\ 0 & 0 & 1 & \dots & k_i^{2(N-2)} \\ \vdots & & \ddots & \ddots & \vdots \\ 0 & & & 0 & 1 \\ 0 & \dots & \dots & \dots & 0 \end{bmatrix} \tag{A.4}$$

Now substitute (A.3) with (A.4) into (A.1) to obtain

$$\begin{aligned} \mathscr{P}(\rho) &= r^T \left[e^{\lambda\tau_0}(\lambda+\alpha)I + 2\sum_{i=1}^{N} c_i k_i \Xi_i \right] Z \\ &= e^{\lambda\tau_0}(\lambda+\alpha)\left[1 \;\; \rho^2 \;\; \rho^4 \;\; \dots \;\; \rho^{2N}\right] Z + 2r^T \sum_{i=1}^{N} c_i k_i \Xi_i Z \end{aligned} \tag{A.5}$$

We observe that on the one hand,

$$e^{\lambda\tau_0}(\lambda+\alpha)\left[1 \;\; \rho^2 \;\; \rho^4 \;\; \dots \;\; \rho^{2N}\right] Z = e^{\lambda\tau_0}(\lambda+\alpha)\prod_{i=1}^{N}(\rho^2 - k_i^2)$$

while on the other hand,

$$r^T \sum_{i=1}^{N} c_i k_i \Xi_i Z =$$

$$\sum_{i=1}^{N} c_i k_i \left[1 \;\; \rho^2 \;\; \rho^4 \;\; \dots \;\; \rho^{2N}\right] \begin{bmatrix} (-1)^{N-1}\sum_{|P_{N-1}|=N-1} k_1^{2p_1} k_2^{2p_2} \dots k_{i-1}^{2p_{i-1}} k_{i+1}^{2p_i} \dots k_N^{2p_{N-1}} \\ (-1)^{N-2}\sum_{|P_{N-1}|=N-2} k_1^{2p_1} k_2^{2p_2} \dots k_{i-1}^{2p_{i-1}} k_{i+1}^{2p_i} \dots k_N^{2p_{N-1}} \\ \vdots \\ (-1)^{1}\sum_{|P_{N-1}|=1} k_1^{2p_1} k_2^{2p_2} \dots k_{i-1}^{2p_{i-1}} k_{i+1}^{2p_i} \dots k_N^{2p_{N-1}} \\ 1 \\ 0 \end{bmatrix}$$

Hence by (A.5) it follows that

$$\mathscr{P}(\rho) = e^{\lambda\tau_0}(\lambda+\alpha)\prod_{j=1}^{N}(\rho^2 - k_j^2) + 2\sum_{i=1}^{N} c_i k_i \prod_{\substack{j=1 \\ j\neq i}}^{N}(\rho^2 - k_j^2)$$

which is equivalent to (4.46), in the sense that the two polynomials have identical roots. Hence the proof is complete.

Appendix B
Comparison of Izhikevich model

Similar to the comparison described in section 5.3.3.3 An overview of the parameters used in the following simulations is provided in Table B.1. Furthermore, $\kappa = 0.8$, $f_{\min} = 0.1$, and

$$I_{\text{ext}}(t) = I_0 + I_s(H_\infty(t-200) - H_\infty(t-500))$$

such that, next to a background current I_0, an additional current of size I_s is applied for $200 < t < 500$. Remarks relating to specific simulations are given in the captions of the corresponding figures.

Table B.1 Parameter values by simulation number

#	a	b	c	d	I_0	I_s
1	0.02	0.2	−55	2	6	−12
2	0.02	0.2	−50	8	4	4
3	0.02	0.2	−55	4	10	20
4	0.03	0.25	−52	2	0	−10

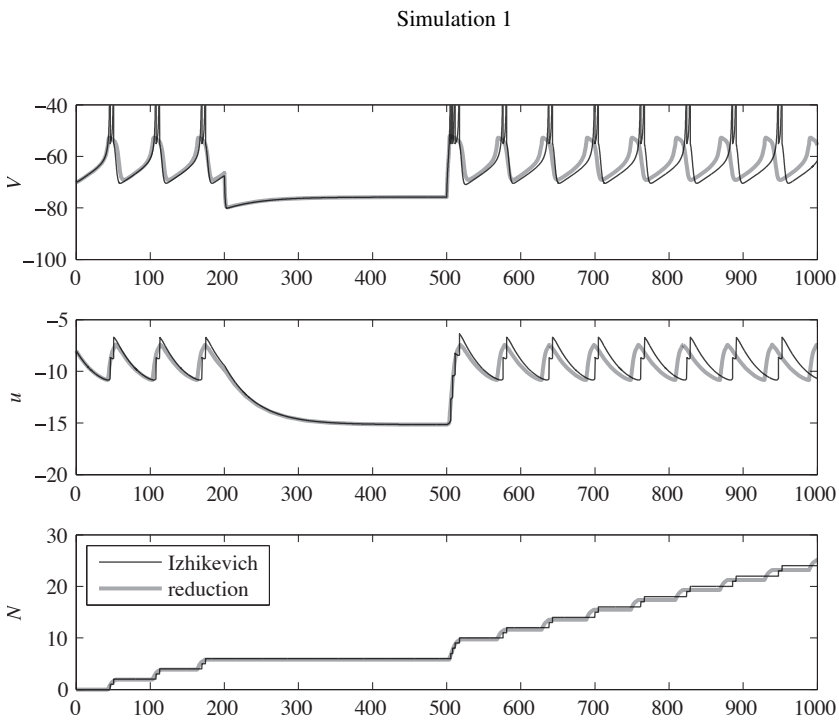

Fig. B.1 Tonic bursting neuron, which is suppressed with a negative current. In the latter half of the simulation the inter-burst frequency of the reduced model is higher, which results in a phase difference between both models. The average spiking behavior, however, is still preserved by the reduction.

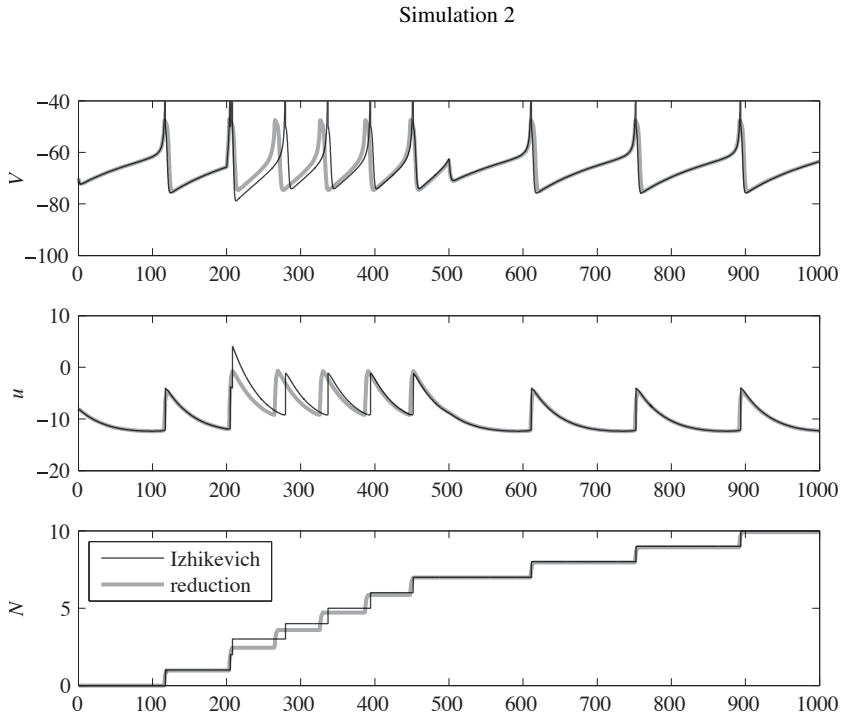

Fig. B.2 Tonic spiking neuron receiving a positive current. At the onset of the stimulus the reduction is quite off, in particular the undershoot is smaller. This results in the number of spikes being estimated wrongfully. Furthermore, one sees that during the stimilus the frequency of the reduced model is lower than the original model. This is contrary to the frequency without stimilus.

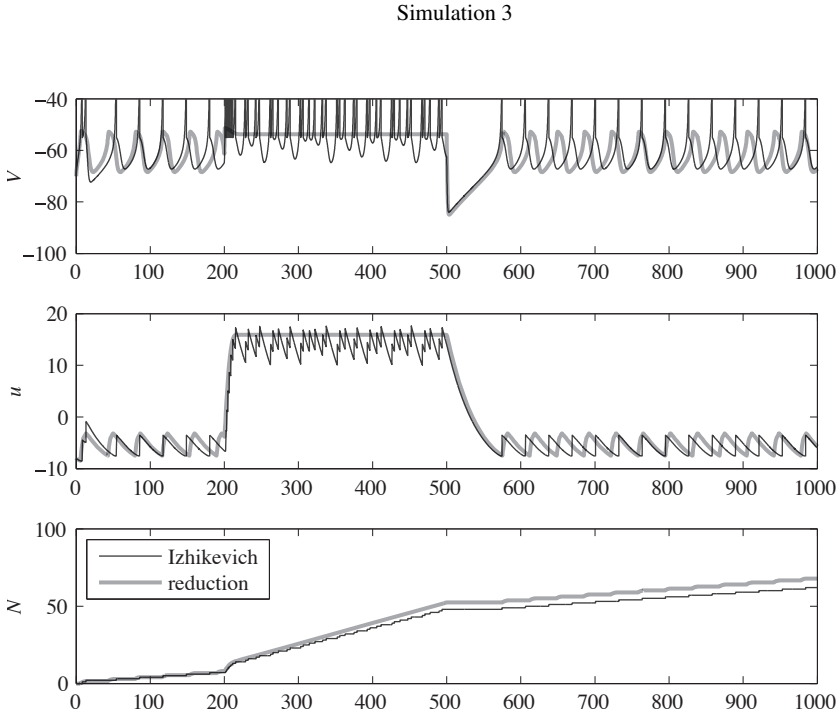

Fig. B.3 Mixed mode oscillations: switching from tonic spiking to chaotic upon input. Despite the chaotic nature of the original model the average firing rate is accurately reproduced by the reduction. Although the intrinsic frequency differs a lot, as can be seen by the large phase shifts, the spike number is still accurate.

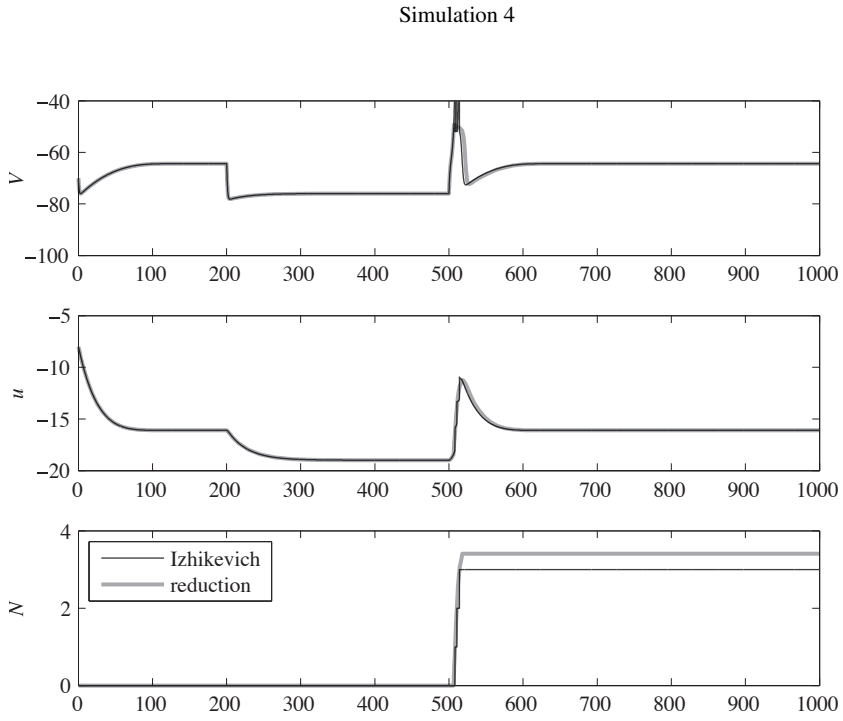

Fig. B.4 Rebound burst after hyperpolarization. The timing, subthreshold behavior and spike count are all very accurate.

References

1. R.A. Adams, *Sobolev Spaces*, Academic Press, New York-London, 1975, Pure and Applied Mathematics, Vol. 65.
2. S. Amari, *Dynamics of pattern formation in lateral-inhibition type neural fields*, Biological cybernetics **27** (1977), no. 2, 77–87.
3. D.K.F. Angeles, *Proposal for revised clinical and electroencephalographic classification of epileptic seizures*, Epilepsia **22489** (1981), no. 501.
4. T. Arbogast and J.L. Bona, *Methods of Applied Mathematics*, Department of Mathematics, University of Texas, 1999-2008, available from the first author's homepage.
5. W. Arendt, C.J.K. Batty, M. Hieber, and F. Neubrander, *Vector-Valued Laplace Transforms and Cauchy Problems*, Monographs in Mathematics, vol. 96, Birkhäuser Verlag, Basel, 2001.
6. O. Arino and E. Sánchez, *A theory of linear delay differential equations in infinite dimensional spaces*, Delay Differential Equations and Applications, NATO Sci. Ser. II Math. Phys. Chem., vol. 205, Springer, 2006, pp. 285–346.
7. P. Baldi and A.F. Atiya, *How delays affect neural dynamics and learning*, Neural Networks, IEEE Transactions on **5** (1994), no. 4, 612 –621.
8. M. Bazhenov, N.F. Rulkov, and I. Timofeev, *Effect of synaptic connectivity on long-range synchronization of fast cortical oscillations*, Journal of neurophysiology **100** (2008), no. 3, 1562–1575.
9. J. Bélair and S.A. Campbell, *Stability and bifurcations of equilibria in a multiple-delayed differential equation*, SIAM J. Appl. Math. **54** (1994), 1402–1424.
10. R. Bellman and K.L. Cooke, *Differential-difference equations*, Academic Press, 1963.
11. M. Benayoun, J.D. Cowan, W. Van Drongelen, and E. Wallace, *Avalanches in a stochastic model of spiking neurons*, PLoS computational biology **6** (2010), no. 7, e1000846.
12. J.M. Bower and D. Beeman, *The book of genesis (2nd ed.): exploring realistic neural models with the general neural simulation system*, Springer-Verlag, New York, NY, USA, 1998.
13. M. Breakspear, J.A. Roberts, J.R. Terry, S. Rodrigues, N. Mahant, and P.A. Robinson, *A unifying explanation of primary generalized seizures through nonlinear brain modeling and bifurcation analysis.*, Cereb Cortex **16** (2006), 1296–1313.
14. P.C. Bressloff, *New mechanism for neural pattern formation*, Physical Review Letters **76** (1996), no. 24, 4644–4647.
15. ———, *Stochastic neural field theory and the system-size expansion*, SIAM Journal on Applied Mathematics **70** (2009), no. 5, 1488–1521.
16. ———, *Spatiotemporal dynamics of continuum neural fields*, Journal of Physics A: Mathematical and Theoretical **45** (2011), no. 3, 033001.

17. F.E. Browder, *On the spectral theory of elliptic differential operators. I*, Math. Ann. **142** (1961), 22–130.
18. M.A. Buice and J.D. Cowan, *Field-theoretic approach to fluctuation effects in neural networks*, Physical Review E **75** (2007), no. 5, 051919.
19. S.A. Campbell, R. Edwards, and P. Van den Driessche, *Delayed coupling between two neural network loops*, SIAM Journal on Applied Mathematics **65** (2004), no. 1, pp. 316–335.
20. S.A. Campbell, I. Ncube, and J. Wu, *Multistability and stable asynchronous periodic oscillations in a multiple-delayed neural system*, Physica D: Nonlinear Phenomena **214** (2006), no. 2, 101 – 119.
21. S.A. Campbell, Y. Yuan, and S.D. Bungay, *Equivariant hopf bifurcation in a ring of identical cells with delayed coupling*, Nonlinearity **18** (2005), 2827–2846(20).
22. Y. Chen and J. Wu, *Minimal instability and unstable set of a phase-locked periodic orbit in a delayed neural network*, Physica D: Nonlinear Phenomena **134** (1999), no. 2, 185 – 199.
23. P.S. Churchland and T.J. Sejnowski, *The computational brain*, MIT Press, Cambridge, MA, USA, 1999.
24. Ph. Clément, O. Diekmann, M. Gyllenberg, H.J.A.M. Heijmans, and H.R. Thieme, *Perturbation theory for dual semigroups. I. The sun-reflexive case*, Math. Ann. **277** (1987), no. 4, 709–725.
25. ———, *Perturbation theory for dual semigroups. II. Time-dependent perturbations in the sun-reflexive case*, Proc. Roy. Soc. Edinburgh Sect. A **109** (1988), no. 1-2, 145–172.
26. ———, *Perturbation theory for dual semigroups. III. Nonlinear Lipschitz continuous perturbations in the sun-reflexive case*, Volterra integrodifferential equations in Banach spaces and applications (Trento, 1987), Pitman Res. Notes Math. Ser., vol. 190, Longman Sci. Tech., Harlow, 1989, pp. 67–89.
27. ———, *Perturbation theory for dual semigroups. IV. The intertwining formula and the canonical pairing*, Semigroup Theory and Applications (Trieste, 1987), Lecture Notes in Pure and Appl. Math., vol. 116, Dekker, New York, 1989, pp. 95–116.
28. S. Coombes, *Waves, bumps, and patterns in neural field theories*, Biological Cybernetics **93** (2005), no. 2, 91–108.
29. ———, *Large-scale neural dynamics: simple and complex.*, NeuroImage **52** (2010), no. 3, 731.
30. S. Coombes and C. Laing, *Delays in activity-based neural networks*, Royal Society of London Philosophical Transactions Series A **367** (2009), 1117–1129.
31. S. Coombes, H. Schmidt, and I. Bojak, *Interface dynamics in planar neural field models*, Journal of mathematical neuroscience (2012).
32. S. Coombes, N.A. Venkov, L. Shiau, I. Bojak, D.T.J. Liley, and C.R. Laing, *Modeling electrocortical activity through improved local approximations of integral neural field equations*, Physical Review E **76** (2007), no. 5, 051901.
33. P.H. Coullet and E.A. Spiegel, *Amplitude equations for systems with competing instabilities*, SIAM J. Appl. Math. **43** (1983), no. 4, 776–821.
34. D.R. Cox and V. Isham, *Point processes*, vol. 12, Chapman & Hall/CRC, 1980.
35. O. Devinsky, *Patients with refractory seizures*, New England Journal of Medicine **340** (1999), no. 20, 1565–1570.
36. A. Dhooge, W. Govaerts, and Yu.A. Kuznetsov, *MATCONT: a MATLAB package for numerical bifurcation analysis of ODEs*, ACM Trans. Math. Software **29** (2003), no. 2, 141–164.
37. O. Diekmann, P. Getto, and M. Gyllenberg, *Stability and bifurcation analysis of Volterra functional equations in the light of suns and stars*, SIAM Journal on Mathematical Analysis **39** (2007), no. 4, 1023–1069.
38. O. Diekmann and M. Gyllenberg, *Abstract delay equations inspired by population dynamics*, Functional analysis and evolution equations, Birkhäuser, Basel, 2008, pp. 187–200.

39. _____, *Equations with infinite delay: Blending the abstract and the concrete*, Journal of Differential Equations **252** (2012), no. 2, 819 – 851.
40. O. Diekmann, M. Gyllenberg, and H.R. Thieme, *Perturbation theory for dual semigroups. V. Variation of constants formulas*, Semigroup Theory and Evolution Equations (Delft, 1989), Lecture Notes in Pure and Appl. Math., vol. 135, Dekker, New York, 1991, pp. 107–123.
41. O. Diekmann, S.A. van Gils, S.M. Verduyn Lunel, and H.-O. Walther, *Delay equations: Functional-, complex-, and nonlinear analysis*, Applied Mathematical Sciences, vol. 110, Springer Verlag, 1995.
42. A. Draguhn, R.D. Traub, D. Schmitz, and J.G.R. Jefferys, *Electrical coupling underlies high-frequency oscillations in the hippocampus in vitro*, Nature **394** (1998), no. 6689, 189–192.
43. J. Engel, *Concepts of epilepsy*, Epilepsia **36** (1995), 23–29.
44. _____, *Report of the ilae classification core group*, Epilepsia **47** (2006), no. 9, 1558–1568.
45. K.-J. Engel and R. Nagel, *One-Parameter Semigroups for Linear Evolution Equations*, Graduate Texts in Mathematics, vol. 194, Springer-Verlag, New York, 2000.
46. K. Engelborghs, T. Luzyanina, and D. Roose, *Numerical bifurcation analysis of delay differential equations using dde-biftool*, ACM Trans. Math. Softw. **28** (2002), 1–21.
47. G.B. Ermentrout and J.D. Cowan, *Large scale spatially organized activity in neural nets*, SIAM Journal on Applied Mathematics (1980), 1–21.
48. G.B. Ermentrout, J.Z. Jalics, and J.E. Rubin, *Stimulus-driven traveling solutions in continuum neuronal models with a general smooth firing rate function*, SIAM Journal of Applied Mathematics **70** (2010), no. 8, 3039–3064.
49. T. Faria, *On a planar system modelling a neuron network with memory*, Journal of Differential Equations **168** (2000), no. 1, 129 – 149.
50. G. Faye and O. Faugeras, *Some theoretical and numerical results for delayed neural field equations*, Physica D: Nonlinear Phenomena **239** (2010), no. 9, 561–578.
51. N. Fenichel, *Geometric singular perturbation theory for ordinary differential equations*, Journal of Differential Equations **31** (1979), no. 1, 53–98.
52. S.E. Folias and P.C. Bressloff, *Breathing pulses in an excitatory neural network*, SIAM Journal on Applied Dynamical Systems **3** (2004), no. 3, 378–407.
53. W.J. Freeman, *Mass action in the nervous system*, Academic Press New York, 1975.
54. W. Govaerts, R. Khoshsiar Ghaziani, Yu.A. Kuznetsov, and H.G.E. Meijer, *Numerical methods for two-parameter local bifurcation analysis of maps*, SIAM J. Sci. Comput. **29** (2007), no. 6, 2644–2667.
55. R.S. Greenwood, *Adverse effects of antiepileptic drugs*, Epilepsia **41** (2005), no. s2, S42–S52.
56. G. Greiner and J.M.A.M. van Neerven, *Adjoints of semigroups acting on vector-valued function spaces*, Israel J. Math. **77** (1992), no. 3, 305–333.
57. N. Guglielmi and E. Hairer, *Users' guide for the code RADAR5*, University of Geneva, Version 2.1.
58. S. Guo, Y. Chen, and J. Wu, *Two-parameter bifurcations in a network of two neurons with multiple delays*, Journal of Differential Equations **244** (2008), no. 2, 444 – 486.
59. S. Guo and L. Huang, *Hopf bifurcating periodic orbits in a ring of neurons with delays*, Physica D: Nonlinear Phenomena **183** (2003), no. 1-2, 19 – 44.
60. J. Hale, *Functional differential equations*, Analytic Theory of Differential Equations (P. Hsieh and A. Stoddart, eds.), Lecture Notes in Mathematics, vol. 183, Springer Berlin / Heidelberg, 1971, 10.1007/BFb0060406.
61. J.K. Hale, *Theory of Functional Differential Equations*, second ed., Springer-Verlag, 1977.
62. A.R. Houweling, M. Bazhenov, I. Timofeev, M. Steriade, and T.J. Sejnowski, *Homeostatic synaptic plasticity can explain post-traumatic epileptogenesis in chronically isolated neocortex*, Cerebral Cortex **15** (2005), 834–845.

63. L. Huang and J. Wu, *Nonlinear waves in networks of neurons with delayed feedback: Pattern formation and continuation*, SIAM Journal on Mathematical Analysis **34** (2003), no. 4, 836–860.
64. A. Hutt, *Local excitation-lateral inhibition interaction yields oscillatory instabilities in nonlocally interacting systems involving finite propagation delay*, Physics Letters A **372** (2008), no. 5, 541–546.
65. A. Hutt and F.M. Atay, *Analysis of nonlocal neural fields for both general and gamma-distributed connectivities*, Physica D: Nonlinear Phenomena **203** (2005), no. 1, 30–54.
66. _____, *Spontaneous and evoked activity in extended neural populations with gamma-distributed spatial interactions and transmission delay*, Chaos, Solitons & Fractals **32** (2007), no. 2, 547–560.
67. A. Hutt, M. Bestehorn, T. Wennekers, et al., *Pattern formation in intracortical neuronal fields*, Network Computation in Neural Systems **14** (2003), no. 2, 351–368.
68. E.M. Izhikevich, *Simple model of spiking neurons.*, IEEE Trans Neural Netw **14** (2003), 1569–1572.
69. E.M. Izhikevich and G.M. Edelman, *Large-scale model of mammalian thalamocortical systems.*, Proc Natl Acad Sci U S A **105** (2008), 3593–3598.
70. S.G. Janssens, Yu.A. Kuznetsov, and O Diekmann, *A normalization technique for codimension two bifurcations of equilibria in delay equations (in preparation)*, Tech. report, Mathematical Institute, Utrecht University, 2011.
71. T. Kapitula, N. Kutz, and B. Sandstede, *The evans function for nonlocal equations*, Indiana University mathematics journal **53** (2004), no. 2004.
72. T. Kato, *Perturbation Theory for Linear Operators*, Die Grundlehren der mathematischen Wissenschaften, Band 132, Springer-Verlag New York, 1966.
73. Yu.A. Kuznetsov, *Numerical normalization techniques for all codim* 2 *bifurcations of equilibria in ODE's*, SIAM J. Numer. Anal. **36** (1999), no. 4, 1104–1124.
74. _____, *Elements of applied bifurcation theory*, 3rd ed., Springer, 2004.
75. Yu.A. Kuznetsov and V.V. Levitin, *CONTENT: Integrated environment for the analysis of dynamical systems*, Tech. report, Centrum voor Wiskunde en Informatica (CWI), Kruislaan 413, 1098 SJ Amsterdam, The Netherlands, 1997, Version 1.5.
76. Yu.A. Kuznetsov and H.G.E. Meijer, *Numerical normal forms for codim 2 bifurcations of fixed points with at most two critical eigenvalues*, SIAM J. Sci. Comput. **26** (2005), no. 6, 1932–1954.
77. P. Kwan and M.J. Brodie, *Early identification of refractory epilepsy*, N Engl J Med **342** (2000), 314–319.
78. W.G. Lennox, *Epilepsy and related disorders*, vol. 2, Little, Brown, 1960.
79. D.T.J. Liley and I. Bojak, *Understanding the transition to seizure by modeling the epileptiform activity of general anesthetic agents*, Journal of Clinical Neurophysiology **22** (2005), no. 5, 300–313.
80. D.T.J. Liley, P.J. Cadusch, and M.P. Dafilis, *A spatially continuous mean field theory of electrocortical activity*, Network: Computation in Neural Systems **13** (2002), no. 1, 67–113.
81. F.H. Lopes da Silva, W. Blanes, S.N. Kalitzin, J. Parra, P. Suffczynski, and D.N. Velis, *Epilepsies as dynamical diseases of brain systems: basic models of the transition between normal and epileptic activity.*, Epilepsia **44 Suppl 12** (2003), 72–83.
82. F.H. Lopes da Silva, A. Hoeks, H. Smits, and L.H. Zetterberg, *Model of brain rhythmic activity*, Biological Cybernetics **15** (1974), 27–37, 10.1007/BF00270757.
83. H. Lu, *Chaotic attractors in delayed neural networks*, Physics Letters A **298** (2002), no. 2-3, 109 – 116.
84. W.W. Lytton, *Computer modelling of epilepsy*, Nat Rev Neurosci **9** (2008), 626–637.
85. J.M. Mahaffy, P.J. Zak, and K.M. Joiner, *A geometric analysis of stability regions for a linear differential equation with two delays*, International Journal of Bifurcation and Chaos **5** (1995), no. 3, 779.
86. H. Markram, *The blue brain project.*, Nat Rev Neurosci **7** (2006), 153–160.

87. R.H. Mattson, J.A. Cramer, J.F. Collins, D.B. Smith, A.V. Delgado-Escueta, T.R. Browne, P.D. Williamson, D.M. Treiman, J.O. McNamara, and C.B. McCutchen, *Comparison of carbamazepine, phenobarbital, phenytoin, and primidone in partial and secondarily generalized tonic-clonic seizures.*, N Engl J Med **313** (1985), 145–151.
88. H.G.E. Meijer, *Codimension 2 Bifurcations of Iterated Maps*, Ph.D. thesis, Utrecht University, 2006.
89. R. Miller, *What is the contribution of axonal conduction delay to temporal structure in brain dynamics?*, Oscillatory event-related brain dynamics, 1994, pp. 53–57.
90. J. Milton and D. Black, *Dynamic diseases in neurology and psychiatry*, Chaos: An Interdisciplinary Journal of Nonlinear Science **5** (1995), no. 1, 8–13.
91. J. Milton and P. Jung, *Epilepsy as a dynamic disease*, Springer, 2003.
92. R.J. Morgan and I. Soltesz, *Nonrandom connectivity of the epileptic dentate gyrus predicts a major role for neuronal hubs in seizures*, Proceedings of the National Academy of Sciences **105** (2008), no. 16, 6179–6184.
93. E. Munro and C. Börgers, *Mechanisms of very fast oscillations in networks of axons coupled by gap junctions*, Journal of computational neuroscience **28** (2010), no. 3, 539–555.
94. P.L. Nunez, *The brain wave equation: A model for the EEG*, Mathematical Biosciences **21** (1974), no. 3-4, 279–297.
95. P.L. Nunez and R. Srinivasan, *Electric fields of the brain: The neurophysics of eeg*, 2nd ed., Oxford University Press, 2005.
96. L. Olien and J. Bélair, *Bifurcations, stability, and monotonicity properties of a delayed neural network model*, Physica D: Nonlinear Phenomena **102** (1997), no. 3-4, 349 – 363.
97. P.A. Robinson, C.J. Rennie, and J.J. Wright, *Propagation and stability of waves of electrical activity in the cerebral cortex*, Physical Review E **56** (1997), no. 1, 826.
98. P.A. Robinson, C.J. Rennie, J.J. Wright, H. Bahramali, E. Gordon, and D.L. Rowe, *Prediction of electroencephalographic spectra from neurophysiology*, Phys. Rev. E **63** (2001), 021903.
99. PA Robinson, JJ Wright, and CJ Rennie, *Synchronous oscillations in the cerebral cortex*, Physical Review E **57** (1998), no. 4, 4578.
100. S. Rodrigues, D. Barton, R. Szalai, O. Benjamin, M.P. Richardson, and J.R. Terry, *Transitions to spike-wave oscillations and epileptic dynamics in a human cortico-thalamic mean-field model.*, J Comput Neurosci **27** (2009), 507–526.
101. D. Roose and R. Szalai, *Continuation and bifurcation analysis of delay differential equations*, Numerical Continuation Methods for Dynamical Systems: Path following and boundary value problems, Springer-Canopus, 2007, pp. 359–399.
102. A. Roxin, N. Brunel, and D. Hansel, *Role of delays in shaping spatiotemporal dynamics of neuronal activity in large networks*, Physical review letters **94** (2005), no. 23, 238103.
103. L.P. Shayer and S.A. Campbell, *Stability, bifurcation, and multistability in a system of two coupled neurons with multiple time delays*, SIAM Journal on Applied Mathematics **61** (2000), 673–700.
104. D. Somers and N. Kopell, *Waves and synchrony in networks of oscillators of relaxation and non-relaxation type*, Physica D: Nonlinear Phenomena **89** (1995), no. 1, 169–183.
105. Y. Song, V.A. Makarov, and M.G. Velarde, *Stability switches, oscillatory multistability, and spatio-temporal patterns of nonlinear oscillations in recurrently delay coupled neural networks*, Biol. Cybern. **101** (2009), 147–167.
106. S. Spencer and L. Huh, *Outcomes of epilepsy surgery in adults and children*, The Lancet Neurology **7** (2008), no. 6, 525–537.
107. A.E. Taylor, *Introduction to Functional Analysis*, John Wiley & Sons Inc., New York, 1958.
108. I. Timofeev, M. Bazhenov, S. Avramescu, and D.A. Nita, *Posttraumatic epilepsy: the roles of synaptic plasticity*, The Neuroscientist **16** (2010), no. 1, 19–27.

109. I. Timofeev, F. Grenier, M. Bazhenov, T.J. Sejnowski, and M. Steriade, *Origin of cortical oscillations in deafferented cortical slabs*, Cerebral Cortex **10** (2000), 1185–1199.
110. R.D. Traub, D. Contreras, M.O. Cunningham, H. Murray, F.E.N. LeBeau, A. Roopun, A. Bibbig, W.B. Wilent, M.J. Higley, and M.A. Whittington, *Single-column thalamocortical network model exhibiting gamma oscillations, sleep spindles, and epileptogenic bursts.*, J Neurophysiol **93** (2005), 2194–2232.
111. R.D. Traub, M.A. Whittington, E.H. Buhl, F.E. LeBeau, A. Bibbig, S. Boyd, H. Cross, and T. Baldeweg, *A possible role for gap junctions in generation of very fast eeg oscillations preceding the onset of, and perhaps initiating, seizures.*, Epilepsia **42** (2001), no. 2, 153.
112. W. Van Drongelen, H. Koch, F.P. Elsen, H.C. Lee, A. Mrejeru, E. Doren, C.J. Marcuccilli, M. Hereld, R.L. Stevens, and J.-M. Ramirez, *Role of persistent sodium current in bursting activity of mouse neocortical networks in vitro.*, J Neurophysiol **96** (2006), 2564–2577.
113. W. Van Drongelen, H.C. Lee, M. Hereld, Z. Chen, F.P. Elsen, and R.L. Stevens, *Emergent epileptiform activity in neural networks with weak excitatory synapses.*, IEEE Trans Neural Syst Rehabil Eng **13** (2005), 236–241.
114. W. van Drongelen, H.C. Lee, M. Hereld, D. Jones, M. Cohoon, F. Elsen, M.E. Papka, and R.L. Stevens, *Simulation of neocortical epileptiform activity using parallel computing*, Neurocomputing **58** (2004), 1203–1209.
115. ———, *Simulation of neocortical epileptiform activity using parallel computing*, Neurocomputing **58-60** (2004), 1203 – 1209, Computational Neuroscience: Trends in Research 2004.
116. S.A. Van Gils, *On a formula for the direction of Hopf bifurcation*, Tech. Report TW/225, Center for Mathematics and Computer Science, 1984.
117. S.A. Van Gils and S.G. Janssens, *A class of abstract delay differential equations in the light of suns and stars (in preparation)*, Tech. report, Department of Mathematics, University of Twente, 2012.
118. S.A. Van Gils, S.G. Janssens, Yu.A. Kuznetsov, and S. Visser, *On local bifurcations in neural field models with transmission delays*, Journal of Mathematical Biology.
119. R. Veltz, *An analytical method for computing Hopf bifurcation curves in neural field networks with space-dependent delays*, C. R. Math. Acad. Sci. Paris **349** (2011), no. 13-14, 749–752.
120. R. Veltz and O. Faugeras, *Local/global analysis of the stationary solutions of some neural field equations*, SIAM J. Applied Dynamical Systems **9 (3)** (2010), 954–998.
121. ———, *Stability of the stationary solutions of neural field equations with propagation delays*, J. Math. Neurosci. **1** (2011), Art. 1, 25.
122. ———, *A center manifold result for delayed neural fields equations*, electronic preprint, available from the first author's homepage (2012), 44p.
123. N.A. Venkov, S. Coombes, and P.C. Matthews, *Dynamic instabilities in scalar neural field equations with space-dependent delays*, Physica D: Nonlinear Phenomena **232** (2007), no. 1, 1–15.
124. S. Visser, `http://www.math.utwente.nl/~visser/skuld`, 5 dec 2011.
125. S. Visser, H.C. Lee, H.G.E. Meijer, W. van Drongelen, M.J.A.M. van Putten, and S.A. van Gils, *Comparing epileptiform behavior of meso-scale detailed models and populations models of neocortex*, Journal of Clinical Neurophysiology **27** (2010), 471–478.
126. J. Von Neumann, *Probabilistic logics and the synthesis of reliable organisms from unreliable components*, Automata studies **34** (1956), 43–98.
127. J.J. Wei and S. Ruan, *Stability and bifurcation in a neural network model with two delays*, Physica D: Nonlinear Phenomena **130** (1999), no. 3-4, 255 – 272.
128. J.J. Wei and M.G. Velarde, *Bifurcation analysis and existence of periodic solutions in a simple neural network with delays*, Chaos: An Interdisciplinary Journal of Nonlinear Science **14** (2004), no. 3, 940–953.

129. U.P. Wen, K.M. Lan, and H.S. Shih, *A review of hopfield neural networks for solving mathematical programming problems*, European Journal of Operational Research **198** (2009), no. 3, 675 – 687.
130. F. Wendling, F. Bartolomei, J.J. Bellanger, and P. Chauvel, *Epileptic fast activity can be explained by a model of impaired gabaergic dendritic inhibition.*, Eur J Neurosci **15** (2002), 1499–1508.
131. H.S. White, *Comparative anticonvulsant and mechanistic profile of the established and newer antiepileptic drugs*, Epilepsia **40** (2005), no. s5, s2–s10.
132. H.R. Wilson and J.D. Cowan, *Excitatory and inhibitory interactions in localized populations of model neurons*, Biophysical Journal **12** (1972), 1–24.
133. ———, *A mathematical theory of the functional dynamics of cortical and thalamic nervous tissue.*, Kybernetik **13** (1973), 55–80.
134. J. Wu, T. Faria, and Y.S. Huang, *Synchronization and stable phase-locking in a network of neurons with memory*, Mathematical and Computer Modelling **30** (1999), no. 1-2, 117 – 138.
135. K. Yosida, *Functional Analysis*, 6 ed., Grundlehren der Mathematischen Wissenschaften, vol. 123, Springer-Verlag, Berlin, 1980.
136. Y. Yuan, *Dynamics in a delayed-neural network*, Chaos, Solitons & Fractals **33** (2007), no. 2, 443 – 454.
137. Y. Yuan and S.A. Campbell, *Stability and Synchronization of a Ring of Identical Cells with Delayed Coupling*, Journal of Dynamics and Differential Equations **16** (2004), 709–744.

Summary

No single model would be able to capture all processes in the brain at once, since its interactions are too numerous and too complex. Therefore, it is common practice to simplify the parts of the system. Typically, the goal is to describe the collective action of many underlying processes, without studying each individually. The work presented here analyzes a particular class of models which has revealed itself as being challenging for such simplifications: neural networks.

As no generic procedure exists for reducing an arbitrary network of spiking neurons, an ad hoc approach is often chosen, which emphasizes particular features of the network. In the first part of thesis, it is illustrated that such approaches can be convincing by showing that the reduced model matches the original complicated model. Being based on imprecise assumptions, it is essential to routinely validate the reduced model with the original network, reducing the effectiveness.

Therefore it is desirable to develop a more general framework, to facilitate the lumping of networks of spiking neurons. The second half of this thesis focuses on the establishment of a functional analytic setting for neural fields with transmission delay, showing that their behavior can be characterized in full detail. Consequently, attention is given to the formulation of such models from a neural network. Explicitly stating all assumptions made in the reduction, the framework is shown to facilitate the inclusion of complex cell dynamics.

Although the majority of the presented results relates to conceptual and simplistic networks of spiking neurons, it is proposed that a clinical application towards epilepsy is within reach. During seizures the majority of the neurons behaves very coherently, such that elementary networks would be able to captures these dynamics adequately. In this setting, the mathematical framework offers an effective setting for a complete characterization of the insult.

Samenvatting

Omdat de processen in het brein talloos en complex zijn, is het niet mogelijk om deze met slechts één model te beschrijven. Daarom is het gebruikelijk afzonderlijke delen van het systeem in kaart te brengen, hetgeen doorgaans wordt bewerkstelligd door het gezamenlijke gedrag van een groot aantal onderliggende processen te bestuderen — dit in tegenstelling tot een aanpak waarbij alle processen individueel worden bestudeerd. Het werk beschreven in deze dissertatie focust op een bepaalde klasse modellen waarvan is gebleken dat ze moeilijk te vereenvoudigen zijn: neurale netwerken.

Aangezien er geen algemene methode bestaat om een willekeurig netwerk te vereenvoudigen, is het doorgaans gebruiken om voor een *ad hoc* benadering te kiezen, zoals beschreven is in het eerste deel van dit werk. Omdat een dergelijke vereenvoudiging bepaalde eigenschappen van het netwerk uitbuit, kunnen deze modellen op overtuigende wijze overeenstemmen met het oorspronkelijke, complexe model. De gemaakte aannames zijn echter ondoorzichtig, zodat het noodzakelijk is om het vereenvoudigde model routinematig te valideren, hetgeen de voorgestelde effectiviteit tenietdoet.

Zodoende lijkt het wenselijk om een algemenere methode te ontwikkelen die het vereenvoudigen van neurale netwerken mogelijk maakt. In het tweede deel van deze thesis wordt eerst een abstracte basis gelegd voor de analyse van neurale velden die reistijd van pulsen in acht nemen. Vervolgens wordt de afleiding van dergelijke modellen zorgvuldig bestudeerd, waaruit blijkt dat, na opsommen van alle aannames, het mogelijkheid is om cellen met een complexe dynamica in het model op te nemen.

Ondanks dat een groot deel van de gepresenteerde resultaten gebaseerd zijn op elementaire neurale netwerken, zijn er genoeg mogelijkheden voor een toepassing. Tijdens een epilepstische aanval is gedrag van de meeste neuronen namelijk zeer samenhangend, zodat dit fenomeen inderdaad gevat kan worden met een rudimentair model. Onder deze omstandigheden staat de eerder gelegde wiskundige basis toe dat deze modellen tot in detail worden begrepen.

Acknowledgements

The work presented here would never have been accomplished without the support and involvement of many others, to whom I owe an expression of gratitude.

First of all, I am grateful to my promotors, whose inspiration, energy, and open-mindedness have always encouraged me to formulate and pursue my own ideas. Stephan: during our casual meetings on an almost daily basis you taught me many intriguing details about mathematics, its applications, and academia in general. Michel: I frequently found myself enthralled by your fascination for the human brain and its disorders.

Secondly, I would like to thank Wim van Drongelen at The University of Chicago, who always welcomed me in his lab. Here, students and collaborators created a stimulating environment and I was introduced to a variety of clinical, experimental, and theoretical aspects of neuroscience. Similar hospitality was found at the Mathematical Institute at Universiteit Utrecht thanks to Odo Diekmann, Sebastiaan Janssens, and Yuri Kuznetsov.

The staff and students of the Department of Applied Mathematics at Universiteit Twente provided a peaceful and friendly working climate. In this respect I would like to mention particularly Bernard, Gerard, Hil, Antonios and the group's secretaries Mariëlle and Linda. Additionally, I enjoyed the contact, group outings and Sinterklaas with the staff from and relating to the chair of Clinical Neurophysiology: Jessica, Esther, Floor, Marleen, Jeannette, Shaun, Regina, Chin, Cecile, and Bas-Jan. The company of my office mates Marcel, Julia and Bettina has been unrivaled: epochs of serious work alternated briefly with periods of fun and laughter. Our lunch walks, with joined forces of Nastya, Bob, and Alef, were always relaxing and refreshing.

Furthermore, I would like to thank my close friends Mathijs, Gea, and Tom for the countless dinners and the unwinding of many days. Finally, I am grateful to the dear members of my family, Sigrid, Bruno, Sima, Koko, and PeeWee, for their unconditional support and encouragement, especially during strenuous times.

February 2013

About the author

Sid Visser was born on July 13th 1987 in Amsterdam, the Netherlands. After he graduated from Utrecht's Stedelijk Gymnasium in 2004, he started his studies in Applied Mathematics at the University of Twente, Enschede, the Netherlands. Sid obtained his bachelor's degree, with a minor in Imaging and Computer Vision, in 2007 and continued studying for master's Applied Mathematics. As part of this program, he visited The University of Chicago in fall 2008, where he developed a C++ environment for the simulation of detailed neural networks. He graduated in 2009, with the thesis entitled "Synchronization-based Parameter Estimation of Neuronal Networks."

In 2009 Sid started his Ph.D. under supervision of Prof. dr. S.A. van Gils and Prof. dr. ir. M.J.A.M. van Putten at the University of Twente. The work done during this project has been presented at conferences in Amsterdam, Berlin, Chicago, Stockholm, and Toronto. He obtained his Ph.D. in 2013 and he continued his research in the field of mathematical neuroscience as a postdoctoral researcher at the University of Nottingham, Nottingham, United Kingdom.

In his spare time, Sid is often found listening to a variety of music, taking pictures, or constructing Lego apparati.


9 789036 535083

STELLINGEN

bij het proefschrift

From spiking neurons to brain waves

van

Sid Visser

1. Van de in hoofdstuk 4 genoemde voorwaarden voor het bestaan van de resolvente (Theorem 4.30, blz. 76), namelijk

   - $z \notin \mathcal{S}$,
   - het karakteristieke polynoom $\mathcal{P}_z$ heeft $2N$ verschillende nulpunten,
   - $k_j \neq \pm\rho_i$ voor alle $i, j \in \{1, 2, \ldots, N\}$ en
   - de matrix $T(z)$ is inverteerbaar,

   zijn de laatste twee redundant.

2. Neurale veldvergelijkingen die langzame tijdschalen en 'bursting' cellen in acht nemen, zoals bijvoorbeeld beschreven in hoofdstuk 5, zijn bijzonder geschikt om de stapsgewijze uitbreiding, welke typerend is voor een Jacksons insult[1], te karakteriseren.

3. De oorspronkelijke Wilson-Cowan vergelijkingen[2] komen voort uit integraalvergelijkingen welke, in het geval van één excitatoire populatie, reduceren tot

$$E(t+\tau) = \left(1 - \int_{t-r}^{t} E(s)ds\right) S\left(\int_0^t \alpha(t-s)[cE(s) + P(s)]ds\right)$$

   Hier representeert $E(t)$ de ratio van actieve cellen op tijd t, r de refractaire periode, S een sigmoidale functie, α de impuls respons van synapsen, c de sterkte van recurrente excitatoire verbindingen en P de externe input.

   Op dit punt in de afleiding heeft parameter τ nog geen fysische interpretatie afgezien dat ze klein doch positief is, hetgeen suggereert dat de opvolgende Taylor-expansie van $E(t+\tau)$ rond $E(t)$ legitiem is. Echter zal deze laatste stap de bijbehorende karakteristieke vergelijking kwalitatief veranderen, waardoor men zich oprecht dient af te vragen of het vereenvoudigde model nog wel aansluit bij het oorspronkelijke.

[1] A.J. Trevelyan, D. Sussillo, B.O. Watson and R. Yuste, *Modular propagation of epileptiform activity: evidence for an inhibitory veto in neocortex*, The Journal of Neuroscience **26** (2006), 12447–12455.

[2] H.R. Wilson and J.D. Cowan, *Excitatory and inhibitory interactions in localized populations of model neurons*, Biophysical Journal **12** (1972), 1–24.

4. Corticale netwerken met sterke laterale inhibitie, oftewel netwerken waarin de lange horizontale verbindingen voornamelijk inhibitoir zijn, zullen ten gevolge van schade aan het netwerk eerder geneigd zijn hyperexciteerbaar te worden dan netwerken zonder laterale inhibitie.

5. Netwerken van stochastische neuronen en de approximatie dezer, door middel van de Fokker–Planck vergelijking[3], lijken een veelbelovende methode om de onzekerheid van, danwel het gebrek aan waarnemingen te modelleren. Echter wordt in deze afleidingen de coefficient van de lineaire ruis overschat omdat de postsynaptische processen in het netwerk, nodeloos, als stochastisch worden verondersteld.

6. Zij K een kubus met ribbe 1, dan is de afstand r tussen twee punten, elk liggend op overstaande zijden van K, verdeeld met dichtheid $f(r)$

$$f(r) = \begin{cases} 2r\left(r^2 + \pi - 1 - 4\sqrt{r^2-1}\right) & 1 \leq r \leq \sqrt{2} \\ 2r\left(-r^2 - 1 + 4\sqrt{r^2-2} - 2\arcsin\frac{r^2-3}{r^2-1}\right) & \sqrt{2} < r \leq \sqrt{3} \\ 0 & \text{elders} \end{cases}$$

7. In acht nemend dat bepaalde netwerken van spoorwegen Turing-compleet zijn[4], in combinatie met het bijbehorende stop-probleem, kan men nooit met zekerheid stellen dat hun trein überhaupt ooit zal aankomen.

8. To be with Art is all we ask...
   Gilbert and George (1970)

[3] E. Wallace, M. Benayoun, W. van Drongelen and J.D. Cowan, *Emergent oscillations in networks of stochastic spiking neurons*, PLoS ONE **6** (2011), no. 5, e14804.

[4] I. Stewart, *The magical maze: seeing the world through mathematical eyes*, Phoenix, 1998.